COMPUTATIONAL HYDRODYNAMIC AND HEAT TRANSFER ANALYSIS OF MAGNETOHYDRODYNAMIC INTERNAL FLOW

A DISSERTATION SUBMITTED TO
THE GRADUATE SCHOOL OF NATURAL AND APPLIED SCIENCES OF
KARABUK UNIVERSITY

BY

Selcuk SELIMLI

IN PARTIAL FULFILLMENT OF THE REQUIREMENTS FOR THE
DEGREE OF DOCTOR OF MECHANICAL ENGINEERING

JUNE 2015

I certify that the dissertation is submitted by Selcuk SELIMLI entitled as "COMPUTATIONAL HYDRODYNAMIC AND HEAT TRANSFER ANALYSIS OF MAGNETOHYDRODYNAMIC INTERNAL FLOW" is fully adequate in scope and quality as a dissertation for the degree of Doctor of Philosophy in Mechanical Engineering.

Prof. Dr. Erol ARCAKLIOGLU ....

Dissertation Advisor, Mechanical Engineering Department

Prof. Dr. Ziyaddin RECEBLI ....

Dissertation Advisor, Energy Systems Engineering Department

This study is unanimously accepted by the examining committee as a dissertation for the degree of Doctor of Philosophy in Mechanical Engineering. June 15, 2015.

Title, Name SURNAME (Institution)	Signature
Chairman : Prof. Dr. Erol ARCAKLIOGLU (KBU)	....
Member : Prof. Dr. Ziyaddin RECEBLI (KBU)	....
Member : Prof. Dr. Adnan SOZEN (GU)	....
Member : Prof. Dr. Mehmet OZKAYMAK (KBU)	....
Member : Assoc. Prof. Dr. Kurtulus BORAN (GU)	....
Member : Assoc. Prof. Dr. Mehmet OZALP (KBU)	....
Member : Assoc. Prof. Dr. Kamil ARSLAN (KBU)	....

……….….., 2015

The degree of Doctor of Philosophy in Mechanical Engineering is approved for the submitted dissertation by the Administrative Board of the Graduate School of Natural and Applied Sciences, Karabuk University.

Prof. Dr. Nevin AYTEMIZ ....

Head of Graduate School of Natural and Applied Sciences

I hereby declare that this dissertation and the work reported herein was composed by and originated entirely by me. Information derived from the published and unpublished work of others has been acknowledged in the text and references are given in the list of sources.

Selcuk SELIMLI

ABSTRACT

Ph.D. Dissertation

COMPUTATIONAL HYDRODYNAMIC AND HEAT TRANSFER ANALYSIS OF MAGNETOHYDRODYNAMIC INTERNAL FLOW

Selcuk SELIMLI

Karabuk University
Graduate School of Natural and Applied Science
Department of Mechanical Engineering

Dissertation Advisors
Prof. Dr. Erol ARCAKLIOGLU
Prof. Dr. Ziyaddin RECEBLI
June 2015, 167

Magnetohydrodynamic (MHD) is a branch of fluid science which investigates the dynamic behaviours of electrically conductive fluids under the magnetic forces. In this dissertation, effects of externally applied magnetic field and also electrical field together with the magnetic field on liquid lithium hydrodynamic, thermophysical flow parameters and heat transfer were investigated numerically in case of steady state flow in a cylindrical pipe and a rectangular duct. Reason of studying the combined effect of magnetic and electrical field is that practically magnetic field creation is restricted because of the limited potential of the metals magnetization. So, magnetic field effect on electrically conductive fluids could be improved by the combined application of magnetic and electrical field. Analyses were done by Navier-Stokes, continuity and energy equations base for constant surface temperature boundary condition. Numerical analyses were occurred by ANSYS Fluent 15.0

software MHD module. Studied models were meshed in hexahedral type and optimum mesh size was determined by mesh studies. Evaluated results showed that increase in applied magnetic field which is on liquid lithium laminar flow decreases flow velocity and dynamic pressure, but also static pressure, skin friction coefficient, wall shear stress, central temperature, local temperature and Nusselt number and so heat transfer increases. Increase in positive directional electrical field (E^+) which is applied together with magnetic field supports the effect of magnetic field and so flow velocity and dynamic pressure decreases more, but also static pressure, skin friction coefficient, wall shear stress, central temperature, local temperature and Nusselt number and so heat transfer increases more. Increase in applied negative directional electrical field (E^-) together with magnetic field weaken the effect of magnetic field and so flow velocity and dynamic pressure increases more, but also static pressure, skin friction coefficient, wall shear stress, central temperature, local temperature and Nusselt number and so heat transfer decreases more. In the case of turbulent flow condition, increase in applied magnetic field increases static pressure, but also flow velocity, dynamic pressure, skin friction coefficient, wall shear stress, central temperature, local temperature and Nusselt number and so heat transfer decreases. Increase in positive directional electrical field (E^+) applied together with magnetic field supported the effect of magnetic field and so static pressure increases more, flow velocity, dynamic pressure, skin friction coefficient, wall shear stress, central temperature, local temperature and Nusselt number and so heat transfer decreases more. Increase in negative directional electrical field (E^-) applied together with magnetic field weaken the effect of magnetic field and so static pressure decreases, but also flow velocity, dynamic pressure, skin friction coefficient, wall shear stress, central temperature, local temperature and Nusselt number and so heat transfer increases.

Keywords : MHD, liquid metals, laminar and turbulent flow, hydrodynamic and thermophysical properties, magnetic and electrical field.

Scientific Code : 914.1.065

ÖZET

Doktora Tezi

MANYETOHİDRODİNAMİK İÇ AKIŞIN HESAPLAMALI HİDRODİNAMİK VE ISI TRANSFER ANALİZİ

Selçuk SELİMLİ

Karabük Üniversitesi
Fen Bilimleri Enstitüsü
Makine Mühendisliği Anabilim Dalı

Tez Danışmanları
Prof. Dr. Erol ARCAKLIOĞLU
Prof. Dr. Ziyaddin RECEBLİ
Haziran 2015, 167

Manyetohidrodinamik, akışkanlar bilim alanının elektriksel iletken akışkanların manyetik kuvvetler altında dinamik davranışlarını inceleyen bilim dalıdır. Bu tez çalışmasında, sıvı lityumun silindirik boru ve dikdörtgen kanal içerisinde kararlı akışında hidrodinamik, termofiziksel akışkan parametreleri ve ısı transferi üzerine dışardan uygulanan manyetik alan ve birlikte uygulanan elektrik ve manyetik alanların etkileri sayısal olarak incelenmiştir. Manyetik ve elektrik alanın birlikte uygulanması durumunun çalışılmasının sebebi, pratikte manyetik alan oluşturmadaki kısıtlılıktır. Bu duruma sebep ise metallerin manyetikleşmelerindeki sınırlılıktır. Böylece, elektriksel iletken akışkanlar üzerindeki manyetik alan etkisi manyetik ve elektrik alanın birlikte uygulanması ile geliştirilebilir. Çözümlemeler sabit yüzey sıcaklığı sınır şartı için Navier-Stokes, süreklilik ve enerji denklemleri tabanlı olarak yapılmıştır. Sayısal analizleme ANSYS Fluent 15.0 yazılımı MHD modülü kullanılarak gerçekleştirilmiştir. Çalışılan modeller hexahedral hücre yapılı ağ yapısı ile oluşturulmuş ve optimum ağ hücre boyutu ağ yapısı çalışmaları ile belirlenmiştir. Değerlendirilen sonuçlar uygulanan manyetik alan indüksiyonunun artması ile sıvı lityumun laminar akışında, akış hızı ve dinamik basıncın azaldığını, aynı zamanda statik basınç, yüzey sürtünme katsayısı, kayma gerilmesi, merkezcil sıcaklık, lokal sıcaklık ve Nusselt sayısının dolayısı ile ısı geçişinin arttığını göstermiştir. Manyetik alan ile birlikte uygulanan pozitif yönlü elektrik alan şiddetinin (E^+) artması ile manyetik alan etkinin güçlendirildiği ve böylece akış hızının ve dinamik basıncın daha da azaldığı, aynı zamanda statik basınç, yüzey sürtünme katsayısı, kayma gerilmesi, merkezcil sıcaklık, lokal sıcaklık ve Nusselt sayısının dolayısı ile ısı geçişinin daha da arttığı belirlenmiştir. Manyetik alan ile birlikte uygulanan negatif yönlü elektrik alan şiddetinin (E^-) artması ile manyetik alan etkinin zayıflatıldığı ve böylece akış hızının ve dinamik basıncın daha da arttığı, aynı zamanda statik basınç, yüzey sürtünme katsayısı, kayma gerilmesi, merkezcil sıcaklık, lokal sıcaklık ve Nusselt sayısının dolayısı ile ısı geçişinin daha da azaldığı tespit edilmiştir. Türbülans akış durumunda ise uygulanan manyetik alan şiddetinin artması ile statik basıncın arttığı, fakat bunun yanında akış hızı, dinamik basınç, yüzey sürtünme katsayısı, kayma gerilmesi, merkezcil sıcaklık, lokal sıcaklık ve Nusselt sayısının dolayısı ile ısı geçişinin azaldığı belirlendi. Manyetik alan ile birlikte uygulanan pozitif yönlü elektrik alan şiddetinin (E^+) artması ile manyetik alan etkinin güçlendirildiği ve böylece akış statik basıncın daha da arttığı, fakat bunun yanında akış hızının, dinamik basıncın, yüzey sürtünme katsayısının, kayma gerilmesinin, merkezcil sıcaklığın, lokal sıcaklığın ve Nusselt sayısının dolayısı ile ısı geçişinin daha da azalttığı tespit edilmiştir. Manyetik alan ile birlikte uygulanan negatif yönlü elektrik alan şiddetinin (E^-) artması ile manyetik alan etkinin zayıflatıldığı ve böylece statik basıncın azaldığı, fakat bunun yanında akış hızının, dinamik basıncın, yüzey sürtünme katsayısının, kayma gerilmesinin, merkezcil sıcaklığın, lokal sıcaklığın ve Nusselt sayısının dolayısı ile ısı geçişinin arttığı belirlenmiştir.

Anahtar Sözcükler : MHD, sıvı metaller, laminar ve türbülans akış, hidrodinamik ve termofiziksel parametreler, manyetik ve elektrik alan.

Bilim Kodu : 914.1.065

ACKNOWLEDGEMENTS

I would like to express my sincerely thanks to my advisors are Prof. Dr. Erol ARCAKLIOGLU and Prof. Dr. Ziyaddin RECEBLI. I am indebted to their advices, supports and pushing ideas to the full development, writing and presenting results in an engaging manner.

I would like to thank to Prof. Dr. Mehmet OZKAYMAK, and Assoc. Prof. Dr. Mehmet OZALP, for their valuable comments and suggestions to the progress of the studies.

I would like to express my special thanks to my parents who are Fatma and Husnu SELIMLI to their priceless efforts to my educational life. Also, to my two brothers who are Samed Mustafa and Ahmet SELIMLI to their motivational supports.

CONTENTS

Pages

LIST OF FIGURES

Pages

Pages

Pages

LIST OF TABLES

Pages

SYMBOLS AND ABBREVIATIONS INDEX

SYMBOLS

B	: Magnetic field induction, (T)
c_p	: Specific heat, (J/kgK)
D	: Diameter, (m)
D_h	: Hydraulic diameter, (m)
E	: Electrical field intensity (V/m)
E^+	: Applied electrical field intensity which is in the same direction with $(\vec{U}x\vec{B})$ vectorial multiplication (V/m)
E^-	: Applied electrical field intensity which is in the opposite direction with $(\vec{U}x\vec{B})$ vectorial multiplication (V/m)
F	: Lorentz force (N)
F_x, F_y, F_z	: Lorentz force components in Cartesian coordinates, (N)
F_r, F_φ, F_z	: Lorentz force components in cylindrical coordinates, (N)
h	: Heat transfer coefficient, (W/m^2 K)
J	: Electrical current density, (A/m^2)
k	: Thermal conductivity of the fluid, (W/m K)
L	: Length, (m)
L_h	: Hydraulic entrance length, (m)
L_t	: Thermal entrance length, (m)
$\mathcal{L}$	: Square root of flow field cross sectional area, (m)
$\mathcal{L}_p$	: Square root of pipe flow field cross sectional area, (m)
$\mathcal{L}_d$	: Square root of duct flow field cross sectional area, (m)
M	: Molecular mass (kg/kmol).
P	: Pressure, (Pa)
R^2	: Correlation coefficient
q	: Charge density (C/m^3)
r	: Radius, (m)

t	: Time (s)
T	: Temperature, (K)
T_w	: Wall temperature, (K)
T_i	: İnlet temperature, (K)
T_o	: Ambient temperature, (K)
U	: Velocity, (m/s)
u, v, w	: Velocity component in Cartesian coordinates, (m/s)
u_r, u_φ, u_z	: Velocity components in cylindrical coordinates, (m/s)
∇	: $i\,\partial/\partial x + j\,\partial/\partial y + k\,\partial/\partial z$; Del operator in Cartesian coordinates.
Δ, ∇^2	: $\partial^2/\partial x^2 + \partial^2/\partial y^2 + \partial^2/\partial z^2$; Laplace operator in Cartesian coordinates
x , y , z	: Unit vectors in Cartesian coordinates.
∇	: $e_r\,\partial/\partial r + e_\theta\,1/r\,\partial/\partial\varphi + e_z\,\partial/\partial z$; Del operator in cylindrical coordinates.
Δ, ∇^2	: $\partial^2/\partial r^2 + 1/r\,\partial/\partial r + 1/r^2\,\partial^2/\partial\varphi^2 + \partial^2/\partial z^2$; Laplace operator in cylindrical coordinates.
e_r, e_φ, e_z	: Unit vectors in cylindrical coordinates.

<u>In Greek Alphabets:</u>

σ	: Electrical permeability, (S/m)
ρ	: Density (kg/m^3)
ρ_e	: Resistivity (Ωm)
μ_e	: Magnetic permeability (H/m)
μ	: Dynamic viscosity, (kg/m s)
ϕ	: Viscous dissipation function

ABBREVIATIONS

CPU	: Central processing unit
Ha	: Hartmann number
MHD	: Magnetohydrodynamics
Nu	: Nusselt number
OQ	: Orthogonal quality
Pr	: Prandtl number
Re	: Reynolds number
UDF	: User defined function
UDM	: User defined material

PART 1

INTRODUCTION

Magnetohydrodynamics (MHD) which is the branch of fluid dynamics investigates the dynamic characteristics of electrically conductive fluids. First well known research was performed by Michael Faraday to observe the magnetic effects. He tried to measure the flow rate of the river Thames by a large scale open channel magmeter in 1832. Two large sheet metal electrodes were lowered from the Waterloo Bridge into the river. The source of natural magnetic field was provided by the earth. The study was unsuccessfully completed because of low sensitive instrumentation technology. The μV level signals could not be measured. Magnetohydrodynamics term is firstly taken place in the literature by Hannes Alfven in 1942. He explained MHD waves. Magnetohydrodynamic theoretical base practical devices have been in use since early of 20^{th} century. Pumping of liquid metals by the elimination of rotating parts is the first practical application. Stirring, levitating and controlling the flow of conducting fluids especially liquid metals in metallurgical processes are important application fields. Especially, MHD pumps and MHD turbines are practical to the radioactive systems as cooling cycle pumps of fusion reactors with their unattended service life. Gas phase MHD power generation with enhanced electric conversion efficiency, increased reliability by without moving parts, long service life and reduced gas emission are the profits of the MHD base power generation applications. Cyclic MHD liquid metal heating and cooling systems with single or double phase flow is another important practical applications. Control of turbulent flow lines to reduce drag is another practical advantage. Newly determined practical application areas of the magnetohydrodynamic keep relatively young this discipline which is about three centuries in the scientific area. In the recent years magnetic resonance imaging technologies in medicine, ships without propellers, breaking systems, trains without wheels, MHD flow technologies for controlling mineral scaling or descaling by MHD base instruments, cooling/heating, filling control of metal flow lines in metallurgical processes are new applications and research interest of academicians and engineers in the related fields. Magnetohydrodynamic commonly tried to be explained by analytical and experimental studies. Currently, due to the development in computer technologies, numerical base computational analysing methods become popular in the scientific area. Computational MHD analysing theory bases on the combination of the momentum, Ohm Law, continuity and energy equations of fluid dynamics to define the dynamic and thermal fluid behaviours. Vectorial expressions of momentum (Navier Stokes), Ohm Law, continuity and energy equation are given below as in eq.(1.1), eq.(1.2), eq.(1.3), and eq.(1.4), respectively in ref. [1, 2].

$$\rho\left[\left(\vec{U}\nabla\right)\vec{U}\right] = -\nabla P + \mu\Delta\vec{U} + \vec{J}x\vec{B} \tag{1.1}$$

$$\vec{J} = \sigma\left(\vec{E} + \vec{U}x\vec{B}\right) \tag{1.2}$$

$$div\vec{U} = 0 \tag{1.3}$$

$$\rho c_p\left[\left(\vec{U}\nabla\right)T\right] = k\Delta T + \phi \tag{1.4}$$

Given vectorial expressions of momentum (Navier Stokes), continuity and energy equations are given in Cartesian coordinates as seen in eq. (1.5a-1.5c), eq. (1.6), and eq. (1.7).

Momentum (Navier Stokes) equation is in eq. (1.5a-1.5c);

$$\rho\left[\frac{\partial u}{\partial t} + u\frac{\partial u}{\partial x} + v\frac{\partial u}{\partial y} + w\frac{\partial u}{\partial z}\right] = -\frac{\partial p}{\partial x} + \mu\left[\frac{\partial^2 u}{\partial x^2} + \frac{\partial^2 u}{\partial y^2} + \frac{\partial^2 u}{\partial z^2}\right] + F_x \tag{1.5a}$$

$$\rho\left[\frac{\partial v}{\partial t} + u\frac{\partial v}{\partial x} + v\frac{\partial v}{\partial y} + w\frac{\partial v}{\partial z}\right] = -\frac{\partial p}{\partial y} + \mu\left[\frac{\partial^2 v}{\partial x^2} + \frac{\partial^2 v}{\partial y^2} + \frac{\partial^2 v}{\partial z^2}\right] + F_y \tag{1.5b}$$

$$\rho\left[\frac{\partial w}{\partial t} + u\frac{\partial w}{\partial x} + v\frac{\partial w}{\partial y} + w\frac{\partial w}{\partial z}\right] = -\frac{\partial p}{\partial z} + \mu\left[\frac{\partial^2 w}{\partial x^2} + \frac{\partial^2 w}{\partial y^2} + \frac{\partial^2 w}{\partial z^2}\right] + F_z \tag{1.5c}$$

Mass conservation (Continuity) equation is in eq. (1.6);

$$\frac{\partial u}{\partial x}+\frac{\partial v}{\partial y}+\frac{\partial w}{\partial z}=0 \tag{1.6}$$

Energy equation is in eq. (1.7);

$$\rho c_p\left(\frac{\partial T}{\partial t}+u\frac{\partial T}{\partial x}+v\frac{\partial T}{\partial y}+w\frac{\partial T}{\partial z}\right)=k\left(\frac{\partial^2 T}{\partial x^2}+\frac{\partial^2 T}{\partial y^2}+\frac{\partial^2 T}{\partial z^2}\right)+\phi \tag{1.7}$$

In here "ϕ" could be given in open form as in eq. (1.8);

$$\phi=2\left[\left(\frac{\partial u}{\partial x}\right)^2+\left(\frac{\partial v}{\partial y}\right)^2+\left(\frac{\partial w}{\partial z}\right)^2\right]+\left[\frac{\partial u}{\partial y}+\frac{\partial v}{\partial x}\right]^2+$$
$$\left[\frac{\partial v}{\partial z}+\frac{\partial w}{\partial y}\right]^2+\left[\frac{\partial u}{\partial z}+\frac{\partial w}{\partial x}\right]^2-\frac{2}{3}\left[\left[\frac{\partial u}{\partial x}+\frac{\partial v}{\partial y}+\frac{\partial w}{\partial z}\right]\right] \tag{1.8}$$

Cylindrical coordinates form of momentum (Navier Stokes), continuity and energy equations are given as in eq.(1.9a-1.9c), eq.(1.10), and eq.(1.11).

Momentum (Navier Stokes) equation in eq. (1.9a-1.9c);

$$\rho\left[\frac{\partial u_r}{\partial t}+u_r\frac{\partial u_r}{\partial r}+\frac{u_\varphi}{r}\frac{\partial u_r}{\partial \varphi}+u_z\frac{\partial u_r}{\partial z}-\frac{u^2{}_\varphi}{r}\right]=$$
$$-\frac{\partial p}{\partial r}+\mu\left[\frac{\partial^2 u_r}{\partial r^2}+\frac{1}{r}\frac{\partial u_r}{\partial r}-\frac{u_r}{r^2}+\frac{1}{r^2}\frac{\partial^2 u_r}{\partial \varphi^2}+\frac{\partial^2 u_r}{\partial z^2}-\frac{2}{r^2}\frac{\partial u_\varphi}{\partial \varphi}\right]+F_r \tag{1.9a}$$

$$\rho\left[\frac{\partial u_\varphi}{\partial t}+u_r\frac{\partial u_\varphi}{\partial r}+\frac{u_r u_\varphi}{r}+\frac{u_\varphi}{r}\frac{\partial u_\varphi}{\partial \varphi}+u_z\frac{\partial u_\varphi}{\partial z}\right]=$$
$$-\frac{1}{r}\frac{\partial p}{\partial \varphi}+\mu\left[\frac{\partial^2 u_\varphi}{\partial r^2}+\frac{1}{r}\frac{\partial u_\varphi}{\partial r}-\frac{u_\varphi}{r^2}+\frac{1}{r^2}\frac{\partial^2 u_\varphi}{\partial \varphi^2}+\frac{\partial^2 u_\varphi}{\partial z^2}+\frac{2}{r^2}\frac{\partial u_r}{\partial \varphi}\right]+F_\varphi \tag{1.9b}$$

$$\rho\left[\frac{\partial u_z}{\partial t}+u_r\frac{\partial u_z}{\partial r}+\frac{u_\varphi}{r}\frac{\partial u_z}{\partial \varphi}+u_z\frac{\partial u_z}{\partial z}\right]=$$
$$-\frac{\partial p}{\partial z}+\mu\left[\frac{\partial^2 u_z}{\partial r^2}+\frac{1}{r}\frac{\partial u_z}{\partial r}+\frac{1}{r^2}\frac{\partial^2 u_z}{\partial \varphi^2}+\frac{\partial^2 u_z}{\partial z^2}\right]+F_z \tag{1.9c}$$

Mass conservation (Continuity) equation is in eq. (1.10);

$$\frac{\partial u_r}{\partial r} + \frac{u_r}{r} + \frac{1}{r}\frac{\partial u_\varphi}{\partial \varphi} + \frac{\partial u_z}{\partial z} = 0 \tag{1.10}$$

Energy equation is in eq. (1.11);

$$\rho c_p \left(\frac{\partial T}{\partial t} + u_r \frac{\partial T}{\partial r} + \frac{u_\varphi}{r}\frac{\partial T}{\partial \varphi} + u_z \frac{\partial T}{\partial z}\right) = k\left[\frac{1}{r}\frac{\partial}{\partial r}\left(r\frac{\partial T}{\partial r}\right) + \frac{1}{r^2}\frac{\partial^2 T}{\partial \varphi^2} + \frac{\partial^2 T}{\partial z^2}\right] + \phi \tag{1.11}$$

In here “ϕ” could be given in open form as in eq. (1.12);

$$\phi = 2\left[\left(\frac{\partial u_r}{\partial r}\right)^2 + \left(\frac{1}{r}\frac{\partial u_\varphi}{\partial \varphi} + \frac{u_r}{r}\right)^2 + \left(\frac{\partial u_z}{\partial z}\right)^2\right] +$$
$$\left[\frac{\partial u_\varphi}{\partial z} + \frac{1}{r}\frac{\partial u_z}{\partial \varphi}\right]^2 + \left[\frac{\partial u_z}{\partial r} + \frac{\partial u_r}{\partial z}\right]^2 + \left[\frac{1}{r}\frac{\partial u_r}{\partial \varphi} + r\frac{\partial}{\partial r}\left(\frac{u_\varphi}{r}\right)\right]^2 \tag{1.12}$$

This study aims to clarify the effect of applied magnetic field and combined effect of magnetic and electric field on hydrodynamic, thermophysical parameters and also heat transfer mechanism of internal steady state laminar and turbulent liquid lithium flow in a circular and rectangular cross sectional conduits.

PART 2

LITERATURE STUDIES

In this part of the dissertation, studies which are in scientific field were reviewed and related studies about the scope of this dissertation are presented in chronological order.

Mabood et al. (2015) studied numerically the MHD laminar boundary layer flow with heat and mass transfer of an electrically conducting water based nanofluid over a nonlinear stretching sheet with viscous dissipation effect. It is discussed that the skin friction coefficient increases with magnetic parameter [3].

Selimli et al. (2015) investigated computationally steady state incompressible magnetohydrodynamic liquid metal turbulent flow thermophysical parameters. According to the concluded results, temperature and heat flux decrease by the increase of applied magnetic field [4].

Mahmoudi et al. (2015) examined the natural convection in an open cavity with non-uniform thermal boundary condition. It is argued that the heat transfer rate decreases with the rise of the Hartmann number [5].

Recebli et al. (2015) studied incompressible magnetohydrodynamic steady state turbulent flow hydrodynamic flow characteristics. Results showed that turbulent intensity, turbulence kinetic energy, velocity and eddy viscosity decrease, but also density and dynamic viscosity increase with the increase in magnetic parameter [6].

Fakour et al. (2015) investigated laminar fluid flow and heat transfer in channel with permeable walls in the presence of a transverse magnetic field. It is concluded that by applied magnetic field, velocity in the channel reduces and the maximum amount of temperature increases [7].

Heidary et al. (2015) studied numerically heat transfer and nanofluid flow analysis in a straight channel, while flow field is under magnetic field. It is concluded that heat transfer in channels can be enhanced up to about 75% due to the presence of magnetic field [8].

Selimli et al. (2015) studied the magnetic effects on steady state laminar liquid lithium duct flow at hydrodynamically developing flow region. It is discussed that externally application and increase of magnetic field induction increased the local pressure [9].

Dada and Disu (2015) investigated the two dimensional heat transfer of a free convective MHD flow with radiation and temperature dependent heat source of a viscous incompressible fluid in a porous medium between two vertical wavy walls. The velocity decreases with an increasing magnetic field, but also temperature, fluid pressure and skin friction coefficient increase with increasing magnetic field [10].

Selimli et al. (2015) studied computationally combined effect of externally applied magnetics and electrical field on the hydrodynamic and thermophysical properties of incompressible steady state magnetoviscous flow of liquid lithium in an enclosure within the scope of this dissertation. It is concluded that increase of positive directional electrical and magnetic field decreases the flow velocity. However, shear stress, temperature, surface heat flux and Nusselt number are boosted by the increase of positive directional electrical and magnetic field. Negative directional electrical field reduce the impact of magnetic field [11].

Abd-Alla and Dahab (2015) studied the peristaltic flow of a Jeffrey fluid in an asymmetric rotating channel. It is observed that the pressure gradient and shear stress increase with increasing of Hartmann number [12].

Recebli et al. (2015) investigated analytically the effect of normally applied magnetic field on immiscible fluid flow hydrodynamic flow characteristics. As a result, overall velocity of the flow domain was reduced more by the magnetic forces in the event of low conductive fluid inner core and high conductive fluid outer regional flow case [13].

Sheikholeslami and Ganji (2015) investigated analytically the problem of nanofluid hydrothermal behaviour in the presence of variable magnetic field using Differential Transformation Method. Results show that skin friction coefficient and Nusselt number increase with increase of Hartmann number [14].

Selimli et al. (2015) studied numerically hydrodynamic characteristic of liquid metal magnetohydrodynamics (MHD) turbulent internal flow under the magnetoviscous forces. Due to the obtained results flow velocity, dynamic viscosity, turbulence kinetic energy, turbulent intensity decrease by the increase of applied magnetic field and also positive directional electrical field. Parameters which are eddy viscosity and density increase by the increase of magnetic and positive directional electrical field. But also, increase in negative directional electrical field intensity increases flow velocity, dynamic viscosity, turbulence kinetic energy, turbulent intensity, and decreases eddy viscosity and density [15].

Haq et al. (2015) presented model which is devoted for the stagnation point flow of nanofluid with magneto-hydrodynamics and thermal radiation effects passed over a stretching sheet. It is found that rising in Hartmann number gives the resistive type flow within the boundary layer; subsequently velocity profile shows the decreasing behaviour with an increase of magnetic parameter [16].

Recebli et al. (2015) cared with the thermophysical investigation of magnetohydrodynamics (MHD) liquid metal incompressible steady state turbulent closed conduit flow under the imposed transversely magnetic and electrical field. According to the results, temperature and heat flux decrease by the applied magnetics and positive directional electrical field. Also applied negative directional electrical field increases two of them [17].

Yamamoto and Kunugi (2015) investigated the high-Prandtl number passive scalar transport of the turbulent channel flow imposed a wall-normal magnetic field. As a result, with increasing Hartman number, the wall-normal turbulent heat flux decreases [18].

Recebli et al. (2015) studied steady state magnetohydrodynamic laminar three dimensional flow of an electrically conducting fluid in a circular pipe under the both magnetic and electrical field. The magnetic field leads to decrease the velocity of flow, whereas the electrical field applied with magnetic field acted to increase and decrease the velocity of flow depending on the direction of applied external electrical field [19].

Aurang and Shafie (2014) concerned with the effects of thermal diffusion on an unsteady MHD free convection boundary layer flow with heat and mass transfer of an electrically conducting fluid over a stretching sheet in the presence of strong magnetic field with Hall current, thermal stratification, chemical reaction, heat generation, thermal radiation, Joule heating and viscous dissipation. It is found that the shear stress increases with an increasing of current density [20].

Abbasbandy et al. (2014) examined the Falkne–Skan flow of magnetohydrodynamic Maxwell fluid. Both analytic and numerical solutions are established for the governing problem. It is concluded that skin friction coefficient increases when magnetic field increases [21].

Alam et al. (2014) investigated the effect of the transverse magnetic field on the thin film flow of pseudo-plastic fluid for lifting and drainage on a vertical (wall) surface. Physical quantities such as the velocity profile, volume flux, average velocity, shear stress, vorticity and the force exerted by fluid on the belt surface respectively for lift and drainage are calculated. It is discussed that the applied magnetic field generally reduces the flow velocity, the magnetic field and the velocity field have a direct relation [22].

Sirivinas et al. (2014) investigated the effect of heat transfer on MHD laminar viscous flow in a pipe with expanding or contracting permeable wall. It is clarified that wall shear stress increases as magnetic parameter increases [23].

Theuri and Makinde (2014) investigated the first and second law analyses of thermodynamic temperature dependent viscosity hydromagnetic generalized unsteady Couette flow with permeable walls. Nusselt number increases with Hartman number at the upper moving plate while at the lower fixed plate [24].

Jiang et al. (2014) numerically investigated the thermomagnetic convection of air in a two-dimensional porous square enclosure under a magnetic quadrupole field. The convection of the air is mainly determined by the magnetic buoyancy force, the heat transfer rate in the porous enclosure increases with the increase of the magnetic force number [25].

Cao et al. (2014) studied the flow field modulation concept was proposed and is called modulated heat transfer tube. The numerical simulation was performed in laminar flow regime at constant heat flux boundary condition with water as the working fluid. Results showed that the near wall region has larger velocity and velocity gradient, accounting for the heat transfer enhancement mechanism [26].

Chutia and Deka (2014) studied the steady laminar magnetohydrodynamic flow and heat transfer of an electrically conducting fluid in a rectangular duct in the presence of oblique transverse magnetic field. They observed that temperature distribution increases in both axes by the increase of Hartman number [27].

Selimli and Recebli (2014) cared with the effect of perpendicularly applied magnetic field up to about Ha = 375 on the steady state turbulent galinstan flow in a rectangular duct. It is concluded that temperature of fluid was firstly increased by the increase of Ha up to about 125 and then partially decreased for the further increase of Hartman number up to about 375 through the duct length [28].

Khan et al. (2014) studied two-dimensional steady flow of an electrically conducting, viscous incompressible nano fluid past a continuously moving surface is considered in the presence of uniform transverse magnetic field with chemical reaction. The results revealed that velocity and concentration decreases, whereas the temperature increases with increase in the magnetic field intensity parameter [29].

Sahin et al. (2014) carried out a numerical study about unsteady heat and mass transfer by free convection flow of a viscous, incompressible, electrically conducting Newtonian fluid along a vertical permeable plate under the action of transverse magnetic field taking into account thermal radiation as well as homogeneous chemical reaction of first order. It is found that velocity is reduced considerably with a rise in the magnetic body parameter, whereas the temperature and concentration are found to be markedly boosted with an increase in the magnetic body parameter [30].

Sarma et al. (2014) numerically studied steady MHD flow of liquid metal through a square duct under the action of strong transverse magnetic field. Results showed that by the increase of magnetic field strength the pressure dropped due to increase of JxB force [31].

Raju et al. (2014) dealt with a steady MHD forced convective flow of a viscous fluid of finite depth in a saturated porous medium over a fixed horizontal channel with thermally insulated and impermeable bottom wall in the presence of viscous dissipation and joule heating. It is presented that velocity and mean velocity distributions are observed to decrease with the increase in magnetic parameter, but also temperature distribution and mean temperature distributions increase with the increasing values of magnetic parameter [32].

Selimli et al. (2014) argued about the combine effect of externally applied magnetics and electrical field on the thermo-physical characteristics of magnetohydrodynamic steady state laminar flow of liquid lithium. Results showed that, the local temperature and Nusselt number were increased by the increase of the electrical field intensity (+) for each constant value of magnetic field induction the local temperature and Nusselt number values of liquid lithium were increased. Otherwise, by the change of the direction and increase of electrical field intensity (−), the local temperature and Nusselt number was decreased. Increase of Nusselt number is the designation of the enhancement of convectional heat transfer [33].

Mabood et al. (2014) developed an analytical solution for MHD boundary layer flow of a viscous incompressible fluid over an exponentially stretching sheet. It is mentioned that due to stronger magnetic field the dimensionless velocity decreases and temperature, skin friction coefficient increases [34].

Malvandi and Ganji (2014) studied theoretically magnetohydrodynamic flow and mixed convective heat transfer of Al_2O_3–water nano fluid inside a vertical microtube. It is concluded that increasing the Hartmann number, leads to an increase in the peak of the velocity profile near the walls; however, the peak of the velocity profile at the core region has a decreasing trend. Also, the heat transfer rate is enhanced in the presence of the magnetic field [35].

Gebre et al. (2014) studied numerically the combined effect of magnetic field, buoyancy force, thermal radiation, viscous and Ohmic heating on turbulent hydromagnetic flow of an incompressible electrically conducting fluid over a moving vertical plate in a rotating system. It is concluded that mean velocity and momentum boundary layer decreases with magnetic parameter. The skin friction coefficient decreases with magnetic parameter. The Nusselt number decreases with magnetic parameter [36].

Rashad (2014) studied unsteady magnetohydrodynamics boundary layer flow and heat transfer of a viscous laminar incompressible electrically conducting rotating fluid due to a stretching surface embedded in a saturated porous medium with a temperature dependent viscosity in the presence of a magnetic field and thermal radiation effects. It has been found that the surface skin friction coefficient and the Nusselt number increase with the increase in magnetic field [37].

Recebli et al. (2014) studied MHD steady state laminar lithium duct flow heat transfer characteristic by ANSYS Fluent 15.0 MHD module. Consequently, for each constant value of magnetic field induction, by the increase of E^+ field intensity the local temperature and Nu of liquid lithium were increased. Temperature and Nu was diminished by the application and rise of the E^- in the opposite direction. This means, the heat transfer could be enhanced or declined by the application of magnetic field or together with electrical field [38].

Mosayebidorcheh et al. (2014) studied turbulent nanofluid flow and heat transfer in the presence of a magnetic field by considering the Hall effect. Results show that velocity and temperature increase with increasing nanoparticle volume fraction whereas they decrease with increasing Hartmann number [39].

Olajuwon et al. (2014) studied analytically the MHD heat and mass transfer flow of an incompressible, electrically conducting viscoelastic micropolar fluid over an infinite vertical plate through porous medium. It is concluded that in the presence of a uniform magnetic field, increase in the strength of the applied magnetic field decelerated the fluid motion [40].

Selimli et al. (2014) studied magnetic effects on steady state laminar liquid lithium duct flow at hydrodynamically developing flow region. It is concluded that increase of magnetic field increased local pressure but also decreased local velocity, density and dynamic viscosity [41].

Alimohamadi et al. (2014) introduced the governing equations on a laminar steady and Newtonian flow in a rectangular duct under the magnetic force with different kinds of magnetic field. Where the magnetic field is located shear stress increases sharply by MHD. Another significant effect of applying magnetic force is increasing the amount of heat transfer. If one and seven dipoles locate below the duct, the value of Nusselt number increases 9.5% and 30% due to the magnetization force only. In MHD analysis Nusselt number is 2.5 times higher than simple case without magnetic force [42].

Recebli et al. (2014) presented the theoretical investigation of magnetic field effect on immiscible fluid steady state internal flow. As a result, electrically conductive fluid is decelerated by created magnetic forces and also nonconductive fluid affected indirectly and slows down because of shearing force between the two fluids [43].

Akram et al. (2014) discussed the influence of heat and mass transfer on the peristaltic flow of a Bingham fluid in an inclined magnetic field and channel with different wave forms. It is observed that the pressure rise increases with an increase in magnetic parameter [44].

Recebli and Selimli (2014) discussed about the effect of normally applied magnetic field on steady state laminar flow of liquid lithium in a horizontal circular pipe model. Results of the examination showed that, increase of magnetic field induction, decreased the local flow velocity, but also increased the Nusselt number through the pipe length. The fluid temperature was increased by the increase of magnetic field induction through the pipe length. Increase of magnetic field induction enhanced the convective heat transfer [45].

Adhikari and Sanyal (2013) studied steady three dimensional magnetohydrodynamic boundary layer viscous flow and heat transfer due to a permeable stretching sheet with prescribed surface heat flux in presence of a uniform applied magnetic field transverse to the flow. Observations showed that the effect of Hartman number on velocity and temperature profile, the velocity profiles decreases with the increase of Hartmann number and the temperature profiles increase with the increase of Hartmann number [46].

Ashraf and Batool (2013) numerically studied the axisymmetric steady laminar incompressible flow of an electrically conducting micropolar fluid over a stretchable disk when the fluid is subjected to an external transverse magnetic field. It is determined that magnetic field enhances the shear stresses and heat transfer rate [47].

Jat and Chand (2013) studied the steady two-dimensional laminar flow of a viscous incompressible electrically conducting fluid over an exponentially stretching sheet in the presence of a uniform transverse magnetic field with viscous dissipation and radiative heat flux. Results showed that heat transfer rate increases as magnetic parameter increases [48].

Mansour et al. (2013) studied numerically the effect of magnetic force, acting vertically downward on natural convection within a nanofluid filled tilted trapezoidal enclosure saturated with an electrically conducting fluid. As a result, magnetic force increases the temperature gradients, hence heat transfer rate increases [49].

Nyabuto et al. (2013) studied the steady MHD stokes free convection flow of an incompressible, electrically conducting fluid between two parallel infinite plates subjected to constant heat flux and pressure gradient. The results showed that, increase in Hartmann number causes a decrease in velocity profiles and an increase in temperature distribution [50].

Ozturk (2013) analytically investigated the steady fully developed laminar flow and heat transfer of an electrically conducting viscous fluid between two parallel plates heated with a constant heat flux in the presence of a transverse magnetic field. Study presented that the Nusselt number takes higher values with an increase of the Hartmann number [51].

Recebli et al. (2013) studied the effect of perpendicularly applied magnetic field on steady state laminar liquid lithium flow in a horizontal circular pipe with 3D computer base software. During the heating of liquid lithium Nusselt number was increased by the increase of magnetic field induction. So, heat convection rate was positively affected [52].

Uddin et al. (2013) studied the two-dimensional steady forced convective flow of a Newtonian fluid past a convectively heated permeable vertically moving plate in the presence of a variable magnetic field and radiation effect. The rate of heat transfer elevates with magnetic field parameters [53].

Vidyasagar et al. (2013) studied convective heat and mass transfer in a porous medium of an incompressible viscous conducting fluid over a permeable stretching surface with suction and internal heat generation/absorption. It can be seen that the velocity decreases with the increase of magnetic parameter. It is noticed that the temperature and concentration increases with the increase of magnetic parameter [54].

Zhang et al. (2013) explained the development of an efficient numerical algorithm for the solution of magneto hydrodynamics flow problems with either fully insulating walls or partially insulating and partially conducting walls. Toward this, they extend the influence domain of the shape function for the element free Galerkin method to have arbitrary shape [55].

Ahmed et al. (2013) studied numerically laminar magnetohydrodynamic mixed convection in an inclined lid-driven square cavity with opposing temperature gradients. The vertical sidewalls are assumed to have non-uniform temperature variation while the top and bottom walls are kept insulated with the top surface moving at a constant speed. It is concluded that increasing the Hartmann number leads to increase the heat transfer rate [56].

Sezgin et al. (2013) investigated numerically the biomagnetic fluid laminar flow between parallel plates imposed to a magnetic source placed below the lower plate. It is discussed that temperature increase with an increase in the intensity of the magnetic field [57].

Prasad et al. (2013) obtained numerical solutions for the hydro-magnetic mixed convection boundary layer flow of an electrically conducting fluid over a non-isothermal wedge in the presence of variable thermal conductivity. It is discussed that increasing the magnetic parameter also increases the local skin friction coefficient and the local Nusselt number [58].

Nadeem et al. (2013) investigated the magnetohydrodynamic Casson fluid flow in two lateral directions past a porous linear stretching sheet. It is seen that the magnitude of the skin friction coefficient increases with an increase in Hartmann number respectively [59].

Ibrahim and Shankar (2013) investigated the boundary layer flow and heat transfer over a permeable stretching sheet due to a nanofluid with the effects of magnetic field. It is found that velocity profiles decrease with an increase in magnetic parameter [60].

Hayat et al. (2013) investigated the heat transfer effects in magnetohydrodynamic axisymmetric flow of third-grade fluid between the stretching sheets. It is concluded that the temperature field is increasing function of Hartman number. It is also noted that shear stress at the surface of sheet increases by increasing the strength of applied magnetic field [61].

Ellahi (2013) examined the magnetohydrodynamic (MHD) flow of non-Newtonian nano fluid in a pipe. It is revealed that velocity and temperature profiles for both Reynolds and Vogel's models decrease by increasing the value of magnetic field [62].

Gururaj and Pavithra (2013) analysed the nonlinear hydromagnetic two dimensional steady, laminar, boundary layer flows of a viscous, incompressible, electrically conducting and radiating liquid metal, with nonlinear radiation past a porous plate stretching with power-law velocity in the presence of a variable magnetic field. It is found that the effect of magnetic field is to decelerate the velocity and increases in magnitude the skin friction coefficient. This result qualitatively agrees with the expectation since the Lorentz force which opposes the flow increases as magnetic parameter increases and leads to enhanced deceleration of the flow [63].

Sahoo (2013) presented unsteady flow of an electrically conducting and incompressible viscoelastic liquid of the Walter B model with simultaneous heat and mass transfer near an oscillating porous plate in slip flow regime under the influence of a transverse magnetic field of uniform strength. It is interesting to note that the skin friction increases with the increase in magnetic parameter [64].

Salehi et al. (2013) investigated MHD mixed convection laminar flow in a two parallel-plates vertical channel. The results showed that increase in the value of magnetic parameter have tendency to slow the movement of the fluid in the centerline of channel and as a result of this, velocity increases near the walls associated with constant flow rate of each section of channel. It is also observed that, while the overall value of pressure gradient increases steadily with magnetic parameter [65].

Jafar et al. (2013) presented that steady magnetohydrodynamic (MHD) laminar boundary layer flow of an incompressible electrically conducting fluid. It is determined that increasing the ratio of magnetic to dynamic pressure will be reduced [66].

Alammar et al. (2012) simulated the fully-developed average turbulent MHD pipe flow with wall heating. Effect of Reynolds, Hartmann, and Prandtl numbers on heat transfer characteristics was investigated. Increasing the Reynolds number decreased the effect of the Hartmann number [67].

Ashraf and Rashid (2012) numerically analysed MHD two-dimensional boundary layer stagnation point flow with radiation and heat generation characteristics towards a heated shrinking sheet immersed in an electrically conducting incompressible micropolar fluid in the presence of a transverse magnetic field. Results showed that the heat transfer rate from the sheet to the fluid boundary layer thickness increases by increasing the increases for strong applied magnetic field [68].

Attia and Abdeen (2012) studied unsteady magnetohydrodynamic flow of an electrically conducting; viscous, incompressible fluid bounded by two parallel non-conducting porous plates with heat transfer. It is observed that increasing the magnetic field increases the temperature [69].

Gedik et al. (2012) presented a two-dimensional computational fluid dynamics simulation for the steady, laminar flow of an incompressible magneto-rheological fluid between two fixed parallel plates in the presence of a uniform magnetic field. The purpose of this study is to develop a numerical tool that is able to simulate MR fluids flow in valve mode and determine B0, applied magnetic field effect on flow velocities and pressure distributions. A uniform transverse external magnetic field is applied perpendicular to the flow direction. The numerical solutions for velocity and pressure distributions were obtained for different magnetic fields. It was observed that increase in magnetic parameter leads to decrease flow velocity [70].

Lakshmi et al. (2012) analysed the MHD effects on the steady free convective boundary layer flow of a viscous incompressible fluid over a linearly moving porous vertical semi-infinite plate with suction and viscous dissipation. It is observed that as the magnetic parameter increases, the temperature increases [71].

Li et al. (2012) referred to as exponential higher-order compact,, finite difference scheme has been formulated for solving the two-dimensional coupled equations representing the steady incompressible, viscous MHD flow though a straight channel of rectangular section. The computational results show that when compared with other numerical methods developed in the literature, the present method has the advantage of better scale resolution with smaller number of grid nodes [72].

Makinde (2012) explained the combined effects of Navier slip and Newtonian heating on an unsteady hydro magnetic boundary layer stagnation point flow towards a flat plate in the presence of a magnetic field. It is revealed that the thermal boundary layer thickens with a rise in the flow unsteadiness and as Newtonian heating intensifies, while the local skin friction and the rate of heat transfer at the plate surface change significantly due to the slip parameter [73].

Rushikumar and Gangadhar (2012) analysed the influence of the heat and mass transfer characteristics of a two dimensional steady laminar free convective flow of a viscous incompressible fluid between two parallel porous walls. The temperature component increases with an increase of magnetic field parameter [74].

Ibrahim and Shanker (2012) dealt with the numerical study of unsteady laminar magnetohydrodynamics boundary layer flow and heat transfer of incompressible, viscous and electrically conducting fluid. It is determined that increase in magnetic parameter increases the skin friction coefficient [75].

Abbassi (2012) investigated laminar flow of a viscous incompressible electrically conducting fluid in a plane channel with a built in square cylinder under the usual magnetohydrodynamic hypothesis. It is found through the calculation of reattachment length that an external magnetic field acts to decrease the size of recirculation zone when Hartman number exceeds a critical value. It is shown that the flow is damped by magnetic force, whereas flow near the walls channel is accelerated. Heat transfer is significantly enhanced by the magnetic field [76].

Dey and Zikanov (2012) conducted the turbulent flow and passive scalar transport in a channel for the situation when the fluid is electrically conducting (for example, a liquid metal) and the flow is affected by an imposed magnetic field. It is found that the magnetic fields, especially those in the wall-normal and spanwise directions, significantly reduce the turbulent scalar transport and modify the properties of the scalar distribution. Decrease of Nusselt number is rather accurately approximated by linear functions of the magnetic interaction parameter [77].

Miyazaki et al. (2012) studied experimentally the MHD effects on heat transfer of flowing lithium with an emphasis on temperature fluctuations. The result showed that temperature decreases monotonically with magnetic parameter [78].

Aminossadati et al. (2011) examined the laminar forced convection of a water–Al2O3 nanofluid flowing through a horizontal micro channel. The middle section of the micro channel is heated with a constant and uniform heat flux. The middle section is also influenced by a transverse magnetic field with a uniform strength. Temperature fields and the heat transfer performance of the micro channel were examined against numerical predictions. The results show that the micro channel performs better heat transfers at higher values of the Reynolds and Hartmann numbers [79].

Aydın and Kaya (2011) studied numerically the steady laminar magneto-hydrodynamic (MHD) mixed convection heat transfer about a vertical slender cylinder. A uniform magnetic field is applied perpendicular to the cylinder. The resulting governing equations are transformed into the non-similar boundary layer equations and solved using the Keller box method. Generally, it is determined that the local skin friction coefficient and the local heat transfer coefficient increase [80].

Chamka and Ahmed (2011) focused on the study of the problem of MHD heat and mass transfer by mixed convection flow in the forward stagnation region of a rotating sphere in the presence of heat generation and chemical reaction effects. Increasing the value of the magnetic field parameter resulted in increases in both of the local coefficients of surface shear stresses, temperature and solute concentration in the fluid whereas the velocity components decreased with the increasing values of the magnetic parameter [81].

Hayat et al. (2011) dealt with the effects of mass transfer on the two-dimensional stagnation point flow of an upper-convected Maxwell fluid over a stretching surface. The similarity transformations convert the governing nonlinear partial differential equation into nonlinear ordinary differential equation. Computations for the out coming systems are presented by a homotopy analysis method [82].

Ishak et al. (2011) investigated the steady two-dimensional stagnation point flow of an incompressible viscous and electrically conducting fluid, subject to a transverse uniform magnetic field, towards a stretching sheet. It is found that the heat transfer rate at the surface increases with the magnetic parameter when the free stream velocity exceeds the stretching velocity. It is found that the magnitude of the skin friction coefficient increases with magnetic field [83].

Yacob and Ishak (2011) studied numerically the problem of a steady mixed convection stagnation point flow towards a permeable vertical plate with prescribed surface heat flux immersed in an incompressible micropolar fluid. It is found that the skin friction coefficient and the local Nusselt number increase in the presence of magnetic field [84].

Kaya (2011) studied numerically steady state laminar magnetohydrodynamic flow mixed convection heat transfer about a vertical slender hollow cylinder, under the effect of wall conduction. A uniform magnetic field is applied perpendicular to the cylinder. Results determined that the local skin friction and the local heat transfer coefficients increase with the increase of magnetic parameter and buoyancy parameter and decrease with conjugate heat transfer parameter [85].

Makinde and Chinyoka (2011) studied the unsteady hydromagnetic flow and heat transfer characteristics of a reactive variable viscosity incompressible electrically conducting third grade fluid in a channel with asymmetric convective cooling at the walls in the presence of uniform transverse magnetic field. It is observed that there is an increase in both fluid velocity and temperature with an increase in the reaction strength, viscous heating and fluid viscosity parameter. The velocity decreases with the increased magnetic field whereas the temperature is noticed to increase under these conditions. A decrease in both fluid velocity and temperature is observed with an increase in the non-Newtonian character at low values of the non-Newtonian parameter, higher values of this parameter lead to blow up of solutions [86].

Makinde and Onyejekwe (2011) investigated the steady flow and heat transfer of an electrically conducting fluid with variable viscosity and electrical conductivity between two parallel plates in the presence of a transverse magnetic field. Results revealed that the combined effect of magnetic field, viscosity, exponents of variable properties, various fluid and heat transfer dimensionless quantities and the electrical conductivity variation, have significant impact on the hydro magnetic and electrical properties of the fluid [87].

Rao and Sankar (2011) numerically studied lithium flow under the applied magnetic field ranging from 0 to 1 T. The Hartmann and Stuart number of the study ranges from 0 to 700 and 0 to 50 respectively. The Reynolds number of the study is 104. It was shown that the convective heat transfer and hence the Nusselt number decreases near the walls perpendicular to the magnetic field due to reduction in turbulent fluctuations with increase of magnetic field [88].

Yazdi et al. (2011) presented an analysis of the energy exchange resulting from a two dimensional steady magnetohydrodynamics flow past a permeable surface with partial slip in the presence of the viscous dissipation effect under convective heating boundary conditions. The results indicate that the heat transfer rate increases with the increase of magnetic parameter [89].

Hussam et al. (2011) studied numerically the fluid flow and heat transfer of a liquid metal past a circular cylinder in a rectangular duct under a strong transverse magnetic field using a quasi-two-dimensional model. The heat transfer rate is strongly dependent on the Hartmann number and blockage ratio. For small Hartmann number, it increases significantly as blockage ratio is increased. However, there is a gradual increase in the Nusselt number for high Hartmann number as blockage ratio is increased [90].

Malekzadeh et al. (2011) studied experimentally the influence of a transverse magnetic field on the local heat transfer of an electrically-conducting laminar fluid flow with high Prandtl number through a pipe. It is also observed that the value of Hartman number decreases the temperature of fluid layers inside the boundary layer [91].

Yamamoto and Kunugi (2011) performed direct numerical simulation of MHD turbulent channel flow for Prandtl number up to Pr=25. It is determined that the friction drag coefficient and Nusselt number as a function of magnetic parameter and monotonically decreased with increase of magnetic parameter [92].

Yamamoto and Kunugi (2011) mentioned the execution of large scale direct numerical simulations of a magnetohydrodynamics turbulent heat transfer on massively parallel processing supercomputer systems. Results showed that degradation of heat transfer as a function interaction parameter [93].

Malekzadeh et al. (2011) studied experimentally the influence of a magnetic field on the skin friction factor of steady fully-developed laminar flow through a pipe. It is discussed that skin friction factor increases with an increase in the magnetic field [94].

Murakami and Okuno (2011) described a magnetohydrodynamic electrical power generator equipped with a convexly divergent channel, through shock-tunnel-based experiments and quasi three dimensional numerical calculations based on large eddy simulation. It is concluded that the slight enhancement in a MHD channel divergence upstream provides boundary layer relief in a MHD flow decelerated by a retarding Lorentz force; an excessive increase in static pressure [95].

Ahmed and Batin (2010) studied the influence of thermal radiation and magnetic Prandtl number on the steady MHD heat and mass transfer by mixed convection flow of a viscous, incompressible, electrically-conducting, Newtonian fluid taking into account the induced magnetic field. It is found that, velocity is reduced considerably with a rise in conduction-radiation parameter or Hartmann number whereas the rate of heat transfer is found to be markedly boosted with an increase in Hartmann number [96].

Ellahi et al. (2010) aimed to determine analytic solutions for a nonlinear problem governing the magnetohydrodynamic flow of a third grade fluid in the annulus of rotating concentric cylinders. For no magnetic field, an increase in magnetic parameter leads to a decrease in the velocity profile and increase in the boundary layer thickness [97].

Gavili et al. (2010) clarified the two-dimensional, incompressible and laminar time dependant combined natural and magnetic convective heat transfer flow through a magnetic fluid. The cavity is under the influence of an imposed two dimensional magnetic field which is created by Helmholtz coils. It is concluded that the average Nusselt number increases under the magnetic field effect [98].

Hayat et al. (2010) concerned with the magnetohydrodynamic flow of a Jeffery fluid in a porous channel. Series solution to the nonlinear problem is constructed by a powerful analytic approach namely the homotopy analysis method. Suction parameter decreases the boundary layer thickness [99].

Hayat et al. (2010) argued about homotopy analysis method to study the influence of radiation on the MHD mixed convection stagnation-point flow in a porous medium. The values of the skin friction coefficient and the local Nusselt number are found to decrease by opposing the flow with magnetic forces [100].

Huang and Li (2010) employed due to the magnetohydrodynamic effect, which degrades heat transfer coefficients by pulsation suppression of the external magnetic field, on the electrically conducting flow, the wall with nonuniform electrical conductivity in a MHD flow system for heat transfer enhancement. Results show that heat transfer augmentation increases monotonically with increasing Hartmann numbers [101].

Loganathan et al. (2010) studied numerically the effects of thermal conductivity on unsteady MHD free convective flow over an isothermal semi-infinite vertical plate. The temperature increases with increasing of thermal conductivity and magnetic parameters [102].

Makinde (2010) studied the hydromagnetic boundary layer flow with heat and mass transfer over a vertical plate in the presence of magnetic field and a convective heat exchange at the surface with the surrounding. It was found that the local skin-friction coefficient, local heat and mass transfer rate at the plate surface increases with an increase in intensity of magnetic field, buoyancy forces and convective heat exchange parameter [103].

Mohebujjaman et al. (2010) considered the steady two-dimensional MHD heat transfer mixed convection flow of a viscous incompressible fluid near a stretching permeable sheet in presence of a uniform magnetic field with heat generation when the buoyancy force assists or opposes the flow. Study clearly showed that velocity decreases but the temperature increases as we increase the magnetic field parameter [104].

Motozawa et al. (2010) explained experimentally that effect of magnetic field on heat transfer in rectangular duct laminar flow of a magnetic fluid. Experiment was performed with changing magnetic field intensity and this magnetic field can be varied from 0 mT to 500 mT. Magnetic fluid in the rectangular duct is heated with uniform heat flux. As a result of this experiment, heat transfer coefficient increases locally in the region where magnetic field exists and becomes larger with increasing magnetic field intensity. About 20 % of maximum increasing rate of heat transfer was obtained in the laminar flow of the magnetic fluid with applying magnetic field [105].

Kumari et al. (2010) studied the transient boundary layer flow and heat transfer of a viscous incompressible electrically conducting non-Newtonian power law fluid in a stagnation region of a two dimensional body in the presence of an applied magnetic field. It is obvious that the skin friction coefficient and the Nusselt number increase with the magnetic parameter due to the enhanced Lorentz force. The surface shear stress and heat transfer increase with the magnetic parameter [106].

Muzychka (2010) examined the solutions to the classical Graetz, slug flow problem in noncircular ducts. They considered two choices for the selection of the characteristics length is the traditional hydraulic diameter and the square root of the cross sectional area. They argued that Nusselt number is a constant when based on the wall to bulk temperature difference; it depends strongly on geometry if hydraulic diameter is used as a length scale. It is a weak function of channel shape when square root of cross sectional flow area is used as a length scale [107].

Zueco et al. (2010) studied the variations with velocity of suction, Hall effect, Reynolds and Hartmann number, particle concentration and Eckert number on the unsteady MHD Couette flow and heat transfer of a dusty and electrically conducting fluid between parallel plates in the presence of an external uniform magnetic field. Presented that when Ha records higher values, velocity and temperature increases [108].

Zijovin et al. (2010) investigated the magnetohydrodynamic flow of two immiscible and electrically conducting fluids between isothermal, insulated moving plates in the presence of an applied electric and inclined magnetic field. It is determined that with the increase of the Hartmann number temperature in the middle of the channel decreases, velocity profiles become flatter, and velocity gradient near the plates become steeper [109].

Chaudhary et al. (2010) described the effects of a magnetic field on the turbulent flow in a square duct at a nominal Reynolds number of 5500. The strong magnetic field was found to annihilate turbulence followed by flattening of the velocity profile. Magnetic field in suppressing turbulence is clearly visible by approximately 40% and suppression of turbulence reduces the frictional losses [110].

Mahmoud and Waheed (2010) performed a theoretical study the flow and heat transfer characteristics of magnetohydrodynamic mixed convection flow of a micropolar fluid past a stretching surface with slip velocity at the surface and heat generation absorption. It is concluded local Nusselt number decreases as the magnetic parameter increases [111].

Abbasbandy and Hayat (2009) studied the mathematical analysis for boundary layer flow is subjected to a transverse magnetic field. Results showed that magnetic field increases the skin friction coefficient [112].

Abelman et al. (2009) studied the numerical solutions of steady state rotating and magneto hydrodynamic flow of a third grade fluid past a rigid plate with slip. The velocity profile velocity profile decreases with increasing magnetic parameter far away from the plate [113].

Atik and Recebli (2009) discussed about the flow velocities of fluids change due to the effects of magnetic fields, thus affecting heat convection. According to results of the numerical solution, it is observed that velocities and temperatures change depending on the flow and direction of the electric field when effects of perpendicularly located electric and magnetic fields are increased. It is determined that while velocity, temperature and Nusselt number increase for a fluid that is cooled in a positive electric field and, velocity, temperature and Nusselt number decrease for a negative electric field [114].

Dehghan and Mirzaei (2009) argued about the meshless local boundary integral equation method to obtain the numerical solution of the coupled equations in velocity and magnetic field for unsteady magnetohydrodynamic flow through a pipe of rectangular and circular sections with non-conducting walls. Computations have been carried out for different Hartmann numbers and at various time levels. Numerical results are presented to show the behaviour of velocity and induced magnetic field [115].

Grigoriadis et al. (2009) investigated MHD simulations of liquid metals. It can be concluded that the proposed extension of the immersed boundary method can provide a valuable numerical tool for efficient and accurate three dimensional simulations of wall-bounded MHD flows with arbitrarily shaped nonconducting surfaces [116].

Samad and Mohebujjaman (2009) studied the steady state magnetohydrodynamic two dimensional heat and mass transfer of a viscous incompressible fluid flow near an isothermal linearly stretching sheet in the presence of a uniform magnetic field with heat generation. It is observed that the temperature field increases with the increase of magnetic field [117].

Srinivas et al. (2009) studied the effects of both wall slip conditions and heat transfer on peristaltic flow of MHD Newtonian fluid in a porous channel with elastic wall properties under the assumptions of long-wavelength and low-Reynolds number. The results for velocity, temperature, stream function and heat transfer coefficient obtained in the analysis evaluated numerically and discussed briefly. The numerical result shows that more trapped bolus appears with increasing Knudsen number [118].

Khedr et al. (2009) considered steady, laminar, MHD flow of a micropolar fluid past a stretched semi-infinite, vertical and permeable surface in the presence of temperature dependent heat generation or absorption, magnetic field and thermal radiation effects. The presence of a magnetic field has the tendency to produce a drag-like force called the Lorentz force which acts in the opposite direction of the fluids motion. This causes the fluid velocity and microrotation to decrease and the fluid temperature to increase as the Hartmann number increases [119].

Hayat et al. (2008) looked at the mass transfer of the steady two-dimensional magnetohydrodynamic boundary layer flow of an upper-convected Maxwell fluid past a porous shrinking sheet in the presence of chemical reaction. It is noted that the magnitude of the velocity decreases for large values of magnetic parameter. However, this change in the velocity near the surface is maximum and far away from the surface, this change is small and finally approaches to zero [120].

Hayat et al. (2008) clarified the flow and heat transfer problem of a second grade fluid film over an unsteady stretching sheet. The fluid is incompressible and electrically conducting in the presence of a uniform applied magnetic field. The series solutions of the governing boundary value problems are obtained by employing homotopy analysis method. The dependence of velocity and temperature profiles on various parameters is shown and discussed through graphs. The values of skin-friction coefficient, Nusselt number and free surface temperature are given in tabular form for various emerging parameters [121].

Misra et al. (2008) studied steady incompressible viscoelastic and electrically conducting fluid flow and heat transfer in a parallel plate channel with stretching walls in the presence of a magnetic field applied externally. The study shows that with the increase in the strength of the magnetic field, the fluid velocity decreases but the temperature increases [122].

Rahman et al. (2008) analysed the MHD natural convection flow of an electrically conducting fluid along a vertical flat plate with temperature dependent thermal conductivity and conduction effects. The temperature within the boundary layer increases for the increasing magnetic parameter [123].

Recebli et al. (2008) presented the effect of magnetic field on heat convection. Momentum, continuity and energy equations including electromagnetic force affecting the fluid were used in the solution. Temperatures at axial and radial directions and Nusselt numbers were calculated depending on magnetic field intensity and other physical properties of fluid by solving the equation system written in cylindrical coordinates system by means of one of the numerical methods which is finite difference method. According to results, velocity and temperature of the cooled fluid decreased following an increase in the intensity of magnetic field placed vertically to flow direction. As determined in the previous one, this study also indicated that increasing the effect of magnetic field increases Nusselt number [124].

Ishak et al. (2008) presented the numerical solution of MHD flow and heat transfer outside a stretching cylinder. The effect of transverse magnetic field is to suppress the velocity field, which in turn causes the enhancement of the temperature field. The magnitude of the skin friction coefficient increases with magnetic parameter, too [125].

Khan et al. (2008) developed exact analytical solutions for magnetohydrodynamic flow of an incompressible second grade fluid in a porous medium. Results showed that the increase of magnetic parameter decreases the shear stress in the channel [126].

Yamamoto et al. (2008) investigated the magnetohydrodynamic pressure loss and heat transfer characteristics of the low-magnetic Reynolds number and higher Prandtl number fluid, by means of direct numerical simulation and the evaluation of MHD turbulence models was also carried out in higher Reynolds number condition. Results evaluated as the suppression of Reynolds shear stress is bigger with increase of Hartmann number [127].

Takeuchi et al. (2008) reported experimental results on turbulent pipe flow of an aqueous potassium hydroxide solution under magnetic field using particle image velocimetry technique. It is observed that Hartmann numbers, and the modification of the mean flow velocity as well as turbulence reduction [128].

Abbasi and Nassrallah (2007) discussed about the laminar flow of a viscous incompressible electrically conducting fluid under the usual magnetohydrodynamic hypothesis. Numerical simulations are performed for Reynolds numbers less then Re = 380 in the range of $0 \leq N \leq 0.2$, where N is the Stuart number or interaction parameter which is the ratio of electromagnetic force to inertia force. Heat transfer is investigated for Prandtl number ranging from Pr = 0.02 corresponding to liquid metal, to Pr = 7 corresponding to water. Heat transfer is significantly enhanced by the magnetic field in the case of fluids of high Prandtl numbers [129].

Sajid et al. (2007) investigated the magnetohydrodynamic flow and heat transfer characteristics in the presence of a uniform applied magnetic field. The skin friction coefficient decreases as the magnetic parameter or the third grade parameter increases [130].

Boeck et al. (2007) studied mean flow properties of turbulent magnetohydrodynamic channel flow with electrically insulating channel walls. It is pointed that turbulent stresses typically decay more rapidly away from the walls than predicted by mixing-length models by imposed magnetic field [131].

Satake et al. (2006) simulated numerically MHD flow structure behind a square rod inserted in a parallel channel to enhance the heat transfer to clarify the interaction between the flow structure and the magnetic field by using a low-Reynolds number k–ε turbulent model and including MHD effects. The turbulent flow analysis confirms that turbulent kinetic energy decreases with increasing Hartmann number [132].

Yokomine et al. (2007) studied MHD effects on Flibe simulant fluid (aqueous potassium hydroxide solution) flows. They determined that the decrease in Nusselt number as a function of interaction parameter [133].

Huang and Fang (2007) discussed the MHD heat transfer using passive scalar transport method and the induced-magnetic-field equation by scalar transport equation with a penalty factor method for liquid metal flow around a cylinder located in an open channel. It is determined that the magnetic field could suppress the turbulent intensity and turbulent viscosity, degrade surface heat transfer coefficient and delay the fluid separation [134].

Jalil and Al-Tae'y (2007) studied numerically by k-epsilon method the turbulent natural convection of molten sodium (Pr = 0.01085) in a square enclosure heated from one vertical wall and cooled from an opposing vertical wall. Results presented that the magnetic field in any direction decreases the Nusselt number [135].

Nakaharai et al. (2007) studied experimentally the influence of a transverse magnetic field on the local and average heat transfer of an electrically conducting, turbulent fluid flow with high Prandtl number. It is mentioned the magnetic field suppresses the turbulent velocity fluctuation, and then the turbulent heat flux is decreased. Because the production term in the transport equation of turbulent heat flux includes the Reynolds stress, finally the production of the temperature fluctuation is decreased [136].

Jordan (2006) analysed the effects of thermal radiation and viscous dissipation on magnetohydrodynamic unsteady free convection flow over a semi-infinite vertical porous plate. It is discussed that magnetic field in an electrically conducting fluid tends to produce a body force against the flow. This type of resistive force tends to slow down the motion of the fluid in the boundary layer which, in turn, reduces the rate of heat convection in the flow. Also, local skin friction coefficient decreases as the magnetic field parameter increases [137].

Guo-yan et al. (2007) analysed two phase flow model to simulate the variation of static pressure in MHD channel, and several factors related to the flow. Results showed that the electromagnetic force produced is greater, and the static pressure is higher [138].

Jalil et al. (2006) studied numerically three dimensional turbulent natural convection of molten sodium (low Prandtl number fluid) in a cubic cavity heated from one vertical wall and cooled from an opposing vertical wall, with the other walls thermally insulated. It is discussed that the average Nusselt number values decrease with increase in Hartmann number values [139].

Nishihara (2006) studied the low temperature supersonic flow experiments using magneto-hydrodynamic interaction. Static pressure measurements in the MHD section showed that a retarding Lorentz force applied to the flow produced a static pressure increase of up to 17-20% [140].

Kobayashi (2006) investigated turbulent channel flows with a uniform magnetic field perpendicular to insulated walls, the performance of the coherent structure Smagorinsky model in comparison to the Smagorinsky model and the dynamic Smagorinsky model. Results showed that the turbulence suppression by the magnetic field decreases the Reynolds shear stress near the wall, so that the skin friction coefficient decreases [141].

Recebli et al. (2005) studied the fluids inside an electromagnetic field are affected from this field. According to the result of numerical solutions, it is seen that the increase on the magnetic field intensity which is located perpendicular to flow way, causes a decrease flow speed and flow rate, and also seen that heat convection and heat dispersion for a fluid that is cooled were lessened. It is determined that while magnetic field increases, the Nusselt number increases. The theoretical results obtained from the study are covered with the results obtained by analytically and finite element difference method [142].

Zniber et al. (2005) argued that MHD laminar flow through a two dimensional channel subjected to a uniform magnetic field and heated at the walls of the conduit over the whole length with a sinusoidal heat flux of vanishing mean value or not. General expressions of the temperature distribution and of the local and mean Nusselt numbers are obtained by using the technique of linear operators in the case of negligible Joule and viscous dissipation and by taking into account the axial conduction effect. The principal results show that an increase of the local Nusselt number with Hartmann number is observed, and, far from the inlet section, the average heat transfer between the fluid and the walls shows a significant improvement [143].

Attia and Ahmed (2005) investigated the unsteady flow of a dusty viscous incompressible electrically conducting Bingham fluid through a circular pipe under the effect of the magnetic field parameter. It is found that all the flow parameters are velocity, volumetric flow rates, and skin friction coefficient decrease as the magnetic field increases [144].

Andreev et al. (2005) served as a physical model for the industrial process where structure and intensity of flow are controlled by magnetic field. It is concluded that the growing Reynolds number a relative value of the intensity of velocity fluctuations decreases and tends to a constant value 3.5% at Re > 5000 and also dynamic pressure is dependent parameter to flow velocity. Decrease in flow velocity by magnetic field means the decrease in dynamic pressure [145].

Pang and Choi (2004) investigated experimentally an electromagnetic technique to reduce skin-friction drag of turbulent boundary layers with an electro conductive solution in water, with potential applications to ships and underwater vehicles. It is observed that more than 40% of turbulent skin-friction reductions when the electromagnetic force is oscillated across the flow [146].

Ganesan and Palani (2004) presented numerical solution of the transient free convection MHD flow of an incompressible viscous fluid past a semi-infinite inclined plate with variable surface heat and mass flux. Concluded that magnetic field parameter has a retarding effect on the velocity. Temperature increases with the increasing value of the magnetic parameter [147].

Postelnicu (2004) studied the heat and mass transfer characteristics of natural convection about a vertical surface embedded in a saturated porous medium subjected to a magnetic field. The governing partial differential equations are transformed into a set of coupled differential equations, which are solved numerically using a finite difference method. Increasing the value of magnetic field increases the local Nusselt number and local Sherwood number [148].

Chamka et al. (2003) focused on the steady state, hydromagnetic forced convective boundary-layer flow of an incompressible Newtonian, electrically conducting and heat generating/absorbing fluid over a non-isothermal wedge in the presence of thermal radiation effects. The local skin friction coefficient and the local Nusselt number increased with increases in the strength of magnetic field as long as the wall mass transfer parameter is greater than or equal to zero [149].

Lahjomri et al. (2003) presented thermal developing laminar Hartmann flow through a parallel plate channel, with prescribed transversal uniform magnetic field, including both viscous dissipation, Joule heating and axial heat conduction with uniform heat flux is studied analytically by using a functional analysis method. The analytical expressions for the developing temperature and local Nusselt number in the entrance region are obtained in the general case. Results show that as long as magnetic parameter increases, the heat transfer increases until certain saturation is reached, for which the effect of magnetic field on Nusselt number vanishes completely [150].

Ke et al. (2003) studied on numerical simulation of magnetohydrodynamic flow by using the commercial code package PHOENICS, in which the momentum source term of Lorentz force is added by applying FORTAN subroutine. Results showed that the high velocity of closing wall side improved the heat transfer between liquid metal and the walls of duct, due to high Hartmann number [151].

Uda et al. (2002) discussed about a large lithium circulation loop. The heat transfer characteristics were measured with applying magnetic field. The Nu number was found to enhance in some magnetic field region, depending on the flow velocity and size of test channels. The enhancement in Nu was predicted over two different electrically conducting ducts in magnetic field. However, to assess a general applicability of the present conclusion, it is required to be examined with more annular and other shape of channels [152].

Smolentsev et al. (2002) presented that K–epsilon model equations for turbulent flows and the free surface boundary condition are adjusted with taking into account MHD effects. It is concluded that in magnetohydrodynamic flows turbulence reduction occurs due to the Joule dissipation. It results in heat transfer degradation [153].

Lahjomri et al. (2002) studied analytically thermally developing laminar Hartmann flow through a parallel plate channel, including both viscous dissipation, Joule heating and axial heat conduction with a step change in wall temperatures. Results show that Nusselt number decreases near the entrance section with increasing magnetic field intensity and the trend is opposite in the thermally developed region where Nu number is sensitive to magnetic field [154].

Lee and Choi (2001) investigated the effect of the Lorentz force on turbulence structures by using the direct numerical simulation technique with assumption of no induced magnetic field at low magnetic Reynolds number. It is clarified that the Lorentz force induced from magnetic field suppresses the dynamically significant coherent structures near the wall and decreases skin friction by increasing magnetic field. It is also reducing velocity fluctuations and Reynolds shear stress decreases [155].

Umeda and Takashi (2000) investigated numerically the heat transfer characteristic of a lithium flow in a conducting rectangular channel in the presence of a transverse magnetic field. Special attention was paid to the effect of convective heat transport by jets generated in side layers on heat transfer enhancement. The Nusselt number increased by 42–50% at the Hartmann number of 1900 compared with hydrodynamic flow [156].

Yih (1999) analysed the effects of viscous dissipation and stress work on the MHD forced convection adjacent to a non-isothermal wedge. It has been found that, the local friction coefficient and the local Nusselt number increase with increasing the pressure gradient parameter and the magnetic parameter [157].

Takahashi et al. (1998) investigated experimentally lithium cooling for magnetic-confinement fusion reactors, the characteristics of the pressure drop and heat transfer for a lithium single phase flow in horizontal conducting rectangular channels under a horizontal transverse magnetic field up to 1.4 T. The bottom of the channel was electrically heated uniformly. When the Hartmann number was increased further beyond 200-300, the Nusselt number increased remarkably, which corresponded to the typical MHD heat transfer enhancement. This heat transfer result is expected to be the basis for future studies on the MHD heat transfer enhancement [158].

Muzychka and Yovanovich (1998) examined solutions to thermally developing flow in circular and non-circular ducts. They argued that the appropriate characteristic length should minimize the difference between solutions for different geometries when the results are non-dimensionalized. Three obvious choices for a characteristic length are the perimeter, the hydraulic parameter and square root of the flow area was studied. Results showed that the square root of the cross sectional area was more effective than the hydraulic diameter [159].

Zikanov and Thess (1998) investigated turbulent flow of electrically conducting incompressible viscous fluid under the influence of an imposed homogeneous magnetic field by using direct numerical simulation. It is found that the pathway transversed by the flow transformation depends decisively on the magnetic interaction parameter. In the case of a strong magnetic field a rapid transformation to a purely two dimensional steady state is obtained in agreement with earlier analytical and numerical results for decaying MHD turbulence [160].

Cuevas et al. (1997) analysed the heat transfer in fully-developed liquid metal flow in a square duct with a uniform, transverse magnetic field. Velocity profiles obtained for laminar and turbulent regimes are employed to solve the heat transfer equation through finite differences, in a duct with one side wall (parallel to the magnetic field) uniformly heated and three adiabatic walls. Numerical calculations for liquid lithium show that for thin conducting wall duct cases, the laminar MHD heat transfer mechanism, characterized by high velocity side wall jets, appears to be more efficient than turbulent mixing in the boundary layer for a given Peclet number. With respect to the laminar case, turbulent profiles present a dramatic decrease of the side layer velocity and a thickening of the boundary layer. [161].

Ji and Gardner (1997) explored the damping of turbulence by a constant transverse magnetic field using standard k-epsilon turbulence model modified to account for the direct interaction of the applied field with turbulent fluctuations. It is mentioned at a fixed value of Reynolds number, increasing the Hartmann number results in a decrease in the Nusselt number [162].

Hua and Walker (1995) examined the three dimensional liquid metal MHD flow in rectangular ducts with thin conducting walls and with an inclined non-uniform transverse magnetic field. It is mentioned that magnetic field cause the velocity to increase near the side and decrease elsewhere, leaving a slowly moving region in the center. The increase in flow velocity near the side enhances the heat transfer [163].

Kirillov et al. (1995) presented an experimental work on magnetohydrodynamic and heat transfer characteristics of liquid metal flows in fusion relevant conditions. It is discussed that transverse magnetic field changes the velocity distribution in channels and suppresses turbulent pulsations. This leads in general to a decrease of heat transfer characteristics Nusselt number with increasing magnetic field [164].

Branover et al. (1995) studied the influence of the transverse magnetic field on turbulence in mercury flow with various turbulizers. It is discussed that the temperature fluctuation intensity decreases in field [165].

Branover and Unger (1994) discussed MHD generation of turbulent flow disturbances using electrically conductive inserts placed on the bottom of an experimental ring shaped channel. Results presented that decrease in mean flow velocity fluctuations decreased the temperature [166].

Takase and Hasan (1993) analysed numerically the convective heat transfer in MHD laminar flow through a square duct in the plasma facing components of fusion reactors to investigate the effects of a transverse magnetic field and the nonuniformity of surface heat flux. It is concluded for uniform heat flux, a transverse magnetic field increases Nusselt number at the plasma facing side, but the increase is small at the corners. [167].

Lee et al. (1991) investigated that the effects of body shape and orientation on laminar natural convection heat transfer from isothermal, two dimensional and axisymmetric bodies. The square root of the total surface area is obtained from the analysis as the characteristic body length. They argued that square root of the surface area is superior to the other length scales [168].

Kumari et al. (1990) discussed about the flow and heat transfer over a stretching sheet with a magnetic field in an electrically conducting ambient fluid. The effects of the induced magnetic field and sources or sinks have been included in the analysis. Both non-isothermal wall and constant heat flux conditions have been considered. The governing equations have been solved numerically using a shooting method. It is observed that for the prescribed wall temperature the skin friction, induced magnetic field at the wall and heat transfer are enhanced due to the magnetic field [169].

Sukoriansky et al. (1989) showed that the effect of a uniform magnetic field on the heat transfer of liquid metal forced flows in straight rectangular channels subjected to a uniform heat flux on one of the walls parallel to the field. The experiments covered the domain $3.8 > U > 18$ cm/s; $0 > B > 0.9$ T; $0 > m > 300$ and $4 \times 103 > Re > 2 \times 104$. It is found that the application of the magnetic field improves the heat transfer in channels made of both non-conducting walls and of conducting walls [170].

Soundalgekar et al. (1977) discussed about the boundary layer solutions for the velocity and temperature profiles are found for flow of an electrically conducting fluid over a semi-infinite flat plate in the presence of a transverse magnetic field and on taking into account the heat due to viscous dissipation and stress-work. It is observed that for air the skin-friction and the rate of heat transfer increase with increasing the magnetic field parameter [171].

Gardner and Lykoudis (1971) presented that a transverse magnetic field on the turbulent heat transfer was to inhibit the convective mechanism of heat transfer through its damping of the turbulent velocity fluctuations, resulting in up to 70% reductions in Nusselt number [172].

Hwang et al. (1967) studied two dimensional steady state laminar compressible flow of an electrically conducting fluid inside a flat duct with a transversely applied magnetic field. The results showed that skin friction and heat transfer are increased with the increase of magnetic field strength [173].

In the light of the studies in literature, we realized that most of the studies about the magnetic effects care about the only magnetic field effect on internal flow regimes in different geometrical shaped models. Practically magnetic field production is restricted because of the limited magnetization capacity of ferrous metals. Externally applied magnetic field on ferromagnetic materials increases their magnetization up to the saturation point; further increase in magnetic field cannot increase the magnetization of materials. Experimentally creation of magnetic field induction is possibly up to about 2 T. Enhancement of applicable Lorentz force on electrically conductive fluid flow is seeing only possible by the combined application of magnetic field induction and electrical field intensity that are included in Lorentz force equation as ($F = q(\boldsymbol{E} + \boldsymbol{U}x\, \boldsymbol{B})$). We inspired by this theory and investigated the effect of magnetic field and also combined effect of magnetic and electrical field on hydrodynamic, thermophysical properties and heat transfer mechanisms of incompressible liquid metal flow in circular pipe and rectangular duct under steady state laminar and turbulent flow regimes.

PART 3

MATERIAL and METHOD

Effect of externally applied magnetic field and combined effect of applied magnetics and electrical field on the hydrodynamic and thermophysical behaviours of steady state internal liquid lithium flow in a circular pipe and rectangular duct was studied by computer base ANSYS Fluent 15.0 software MHD module.

3.1. MODELLING

Studied models were constructed by using Gambit software. The theoretical similarities of constructed models are important to the evaluation of the similarity in results. According to the literature [159, 168, 107], the most appropriate similarity parameter which is the square root of the flow areas for different flow geometries was referred the equality of the models. In this respect, the appropriate similarities of the models were provided by the equality of the square root of the circular pipe and rectangular duct flow cross sectional areas. The chosen characteristic length square root of the flow cross sectional area is designated by $\mathcal{L}$ as in eq. (3.1).

$$\mathcal{L} = \sqrt{A_c} \tag{3.1}$$

Characteristic length for circular pipe model, $\mathcal{L}_p$ in eq. (3.2);

$$\mathcal{L}_p = \sqrt{A_{cp}} = \sqrt{\pi r^2} \tag{3.2}$$

Characteristic length for duct model, $\mathcal{L}_d$ in eq. (3.3);

$$\mathcal{L}_d = \sqrt{A_{cd}} = \sqrt{axb} \tag{3.3}$$

Circular pipe and rectangular duct model sizes were chosen as below;

Circular pipe model is illustrated in Figure 3.1; R=0.005m, L=0.15m

$$\mathcal{L}_p = \sqrt{A_{cp}} = \sqrt{\pi r^2} = \sqrt{\pi 0.005^2} = 8.86x10^{-3}m$$

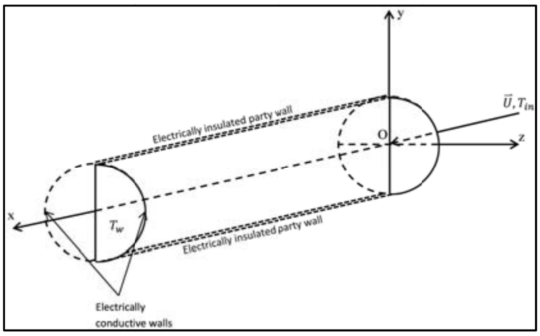

Figure 3.1. Circular pipe model.

Duct Model is shown in Figure 3.2; a=0.0157, b=0.005, L=0.15m

$$\mathcal{L}_d = \sqrt{A_{cd}} = \sqrt{axb} = \sqrt{15.7x10^{-3}x5x10^{-3}} = 8.86x10^{-3}m$$

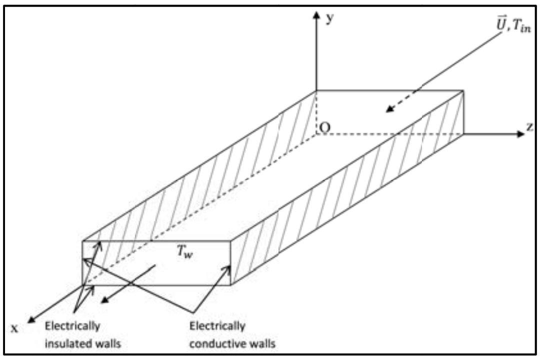

Figure 3.2. Rectangular duct model.

Characteristic lengths of models which are constructed by Gambit software are equal to each other ($\mathcal{L}_p = \mathcal{L}_d$).

3.2 MESH STUDY

Three critical points should be taken into consideration to decide the optimum mesh size. These are computational efficiency, accuracy and processor time. Computational fluid dynamics and heat transfer analyses require the high quality meshing to obtain accurate results. Samir and Longest (2008) argued in their studies that flow domains, structured hexahedral meshes are often associated with high quality solutions [174]. Biswas and Strawn (1998) suggested that hexahedral meshes yield more accurate solutions than their tetrahedral counterparts for the same number of edges [175]. Studied models were meshed with hexahedral mesh type. The mesh size is important to obtain accurate results. The optimum mesh size was specified by software base parameters (skewness, aspect ratio, orthogonal quality and number of cell) and the comparison of the analyse results converge rates to each other's for different mesh size models. Mesh sizes which were given below was assumed to decide the optimum high quality meshing by mesh study. Mesh sizes which were used to the mesh study are 0.0002m, 0.00025m, 0.0005m, 0.00075m, 0.001m, 0.0015m.

The pipe and duct model were meshed by Gambit software. Different mesh sized models a) isometric and b) cross sectional views are given in Figure 3. 3.

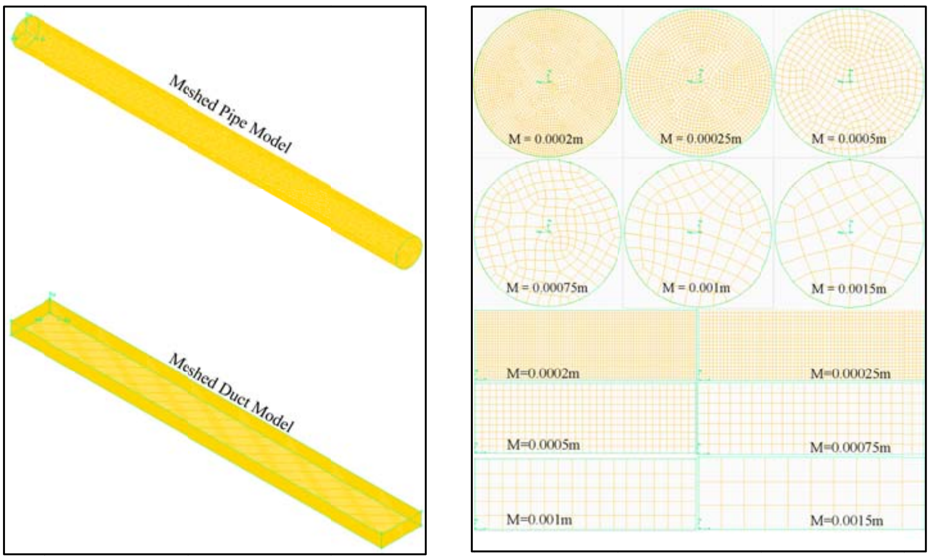

a) Isometric views (b) Cross sectional views

Figure 3.3. Meshed models isometric and cross sectional views.

3.2.1. Parametric Base Mesh Study

Parametric base mesh quality parameters were taken from Gambit and ANSYS Fluent 15.0 software. Taken mesh quality assessment parameters and quality scale values were given in Table 3.1.

Table 3.1. Software base mesh quality parameters and mesh cell information.

Model	Meshing Size (m)	Aspect Ratio >1	Skewness <0.85	0< Orthogonal Quality <1 (OQ≈1 excellent)	Number of cell	Number of nodes
Pipe	0.0002	4.12	0.52	0.98	1,671,618	1,734,235
	0.00025	4.1	0.54	0.97	836,178	876,159
	0.0005	3.13	0.67	0.87	116,280	126,791
	0.00075	3.02	0.75	0.83	33,567	38,178
	0.001	2.63	0.83	0.81	13,617	16,324
	0.0015	2.59	0.92	0.59	5,250	6,572
Duct	0.0002	1.74	0.23	1	1,462,500	1,542,554
	0.00025	1.71	0.24	1	756,000	807,744
	0.0005	1.7	0.31	1	93,000	105,952
	0.00075	1.68	0.47	1	29,400	35,376
	0.001	1.65	0.53	1	12,000	15,402
	0.0015	1.53	0.65	1	3,000	4,444

Parametric base mesh study parameters are seen in Table 3.1. Smaller mesh sized pipe and duct model meshing quality parameters converges to the optimum ranges and satisfies the quality requirements for 0.0002 m and 0.00025 m mesh sized models. Parametric base mesh study showed that minimum mesh sized pipe and duct models which are the best for the analyses. Lower mesh size means the longer CPU time, too. Optimization of the mesh quality and size is important to obtain accurate results and CPU time for this study.

Accuracy of the results and the CPU time could have been evaluated by analysing the problem and comparison of the results. In this respect, analyses base mesh studies were done on different mesh sized models without magnetic effects. Owing to the results, the local flow velocity profiles were compared to decide the optimum analysing mesh size. Analyses base mesh study requires the determination of liquid metal physical properties and the boundary conditions of the flow models.

Liquid lithium was chosen as the studied liquid metal, because of its high electrical conductivity and suitable viscosity to flow continuously during the analysis. Physical properties of liquid lithium which were given as below in the form of temperature dependent empirical relations which were taken from ref. [176, 177] and written as user defined function (UDF) and also defined as the user defined material (UDM) to the Fluent 15.0 software.

Physical properties of liquid lithium is in the range are $453.7 \leq T \leq 1700\ K$;

Thermal conductivity (k) is in eq. (3.4);

$$k = 21.42 + 0.0523T - 1.371x10^{-5}T^2 \quad W/mK \tag{3.4}$$

Density (ρ) is in eq. (3.5);

$$\rho = 558.4 - 0.101T \quad kg/m^3K \tag{3.5}$$

Dynamic viscosity (μ) is in eq. (3.6);

$$\mu = 0.1157x10^{-3} - 1.418x10^{-7}T + 4.229x10^{-11}T^2 + \frac{243.7x10^{-3}}{T} \quad Pa.s \tag{3.6}$$

User defined material data definition to the ANSYS Fluent 15.0 software requires the polynomial equation input which is given in eq. (3.7), the equation curve fitting was occurred by Microsoft Excel and the obtained equation was used as input.

$$\mu = 0.0015 - 3x10^{-6}T + 2x10^{-9}T^2\ Pa.s \qquad for\ R^2 = 1 \tag{3.7}$$

Specific heat (c_p) is in eq. (3.8a);

$$c_p = \frac{1.044x10^5}{T^2} - \frac{135.1}{T} + 4.18 \quad kJ/kgK \tag{3.8a}$$

The equation curve fitting was occurred to the eq. (3.8a) by Microsoft Excel and the obtained equation is given eq. (3.8b).

$$c_p = 5714.5 - 4.417T + 0.0033T^2 \quad kJ/kgK \qquad for\ R^2 = 1 \tag{3.8b}$$

Molecular mass (M) is in eq. (3.9);

$$M = 6.94\ kg/kmol \tag{3.9}$$

Electrical conductivity ($1/\rho_e$) is in eq.(3.10);

$$\frac{1}{\rho_e} = 4x10^6\ S/m \tag{3.10}$$

ρ_e = Resistivity (Ωm)

Magnetic permeability (μ_e) is in eq.(3.11) ;

$$\mu_e = 1.2x10^{-6}\ H/m \tag{3.11}$$

3.2.2. Laminar Flow Computational Base Mesh Study

Boundary conditions of liquid lithium flow which are specified for laminar steady state internal flow conditions.

Reynolds number of laminar internal flow has to be $Re < 2300$ for circular pipe and rectangular duct flow to obtain laminar flow regime.

In this respect, Reynolds number which is given in eq. (3.12) was chosen as 2200 to obtain laminar flow condition. Inlet velocity which is seen in eq. (3.13) was calculated as below to satisfy the laminar flow;

$$Re = \frac{\rho x D x U}{\mu} = \frac{516x0.01xU}{6.4x10^{-4}} = 2200 \tag{3.12}$$

$$U = 0.275\ m/s \tag{3.13}$$

Calculated inlet velocity that is 0.275 m/s to the laminar flow condition was chosen as inlet velocity for both circular pipe and rectangular duct model analyses.

The hydrodynamic similarity is obtained by the equality of flow internal flow velocity. Flow regime characteristic in the rectangular duct model for U = 0.275 m/s was checked as below,

Hydraulic diameter is determined in eq. (3.14);

$$D_h = \frac{2xaxb}{a+b} = \frac{2x0.0157x0.005}{0.0157+0.005} = 7.56x10^{-3}m \tag{3.14}$$

$$Re = \frac{\rho x D_h x U}{\mu} = \frac{516x7.56x10^{-3}xU}{6.4x10^{-4}} \cong 1676 \text{ flow is laminar} \tag{3.15}$$

Thermal and hydrodynamic boundary conditions of the circular pipe and rectangular duct models was chosen for the laminar flow condition as given in Table 3.2 by taking into consideration to the liquid lithium melting temperature and calculated hydrodynamic limits.

Table 3.2. Laminar flow regime boundary conditions.

Laminar Flow Model Boundary Conditions	
T_w (K)	573.15
T_i (K)	473.15
T_o (K)	293.15
U(m/s)	0.275

Hydrodynamic and thermal developments were qualified before the study to determine accurate data taking regions.

For circular pipe laminar flow hydrodynamic and thermal entry lengths which are defined as in eq. (3.16) and eq. (3.17), respectively;

$$L_h = 0.05xRexD = 0.05x2200x0.01 = 1.1\ m \tag{3.16}$$

$$L_t = 0.05xRexDxPr = 0.05x2200x0.01x0.065 = 0.07\ m \tag{3.17}$$

Prandtl number in eq. (3.18);

$$Pr = \frac{c_p\mu}{k} = \frac{4363x6.4x10^{-4}}{43} = 0.065 \tag{3.18}$$

Flow is hydraulic fully developed at 1.1 m of the model length. The longer model length than 0.15 m means more number of cells, higher computing capacity and longer time. So, restricted computer capacity and time push the study on hydraulically undeveloped laminar flow investigation. Thermal development is completed at 0.07 m, and so a heat transfer analysis was occurred in thermal developed MHD flow region.

For rectangular duct laminar hydrodynamic and thermal entry lengths which were defined as in eq. (3.19) and eq. (3.20), respectively;

$$L_h = 0.05xRexD_h = 0.05x1676x7.56x10^{-3} = 0.63\ m \tag{3.19}$$

$$L_t = 0.05xRexD_hxPr = 0.05x1676x7.56x10^{-3}x0.065 = 0.04\ m \tag{3.20}$$

Prandtl number (Pr) is in eq.(3.21);

$$Pr = \frac{c_p\mu}{k} = \frac{4363x6.4x10^{-4}}{43} = 0.065 \tag{3.21}$$

Hydraulic development of the flow is completed at 0.63 m of the model length. The length of the model is 0.15 m and it is inadequate to the complete hydraulic development of the flow. Creating longer model than 0.63 m requires higher computing capacity and time. Because of this, the analysing model which is inadequate to the hydrodynamic development. The thermal development completes at 0.04 m and model length could be accepted sufficient to the thermal analyses.

Determined boundary conditions and liquid lithium physical properties were estimated as input data for ANSYS Fluent 15.0 software. Analyses were occurred on meshed models and the local velocity values were compared. The comparisons of local velocities at 0.12 m of the models were done for laminar flow case according to the visualizations in Figure 3.4. Figure 3.4 presents the flow velocities for a) circular pipe model and b) rectangular duct model.

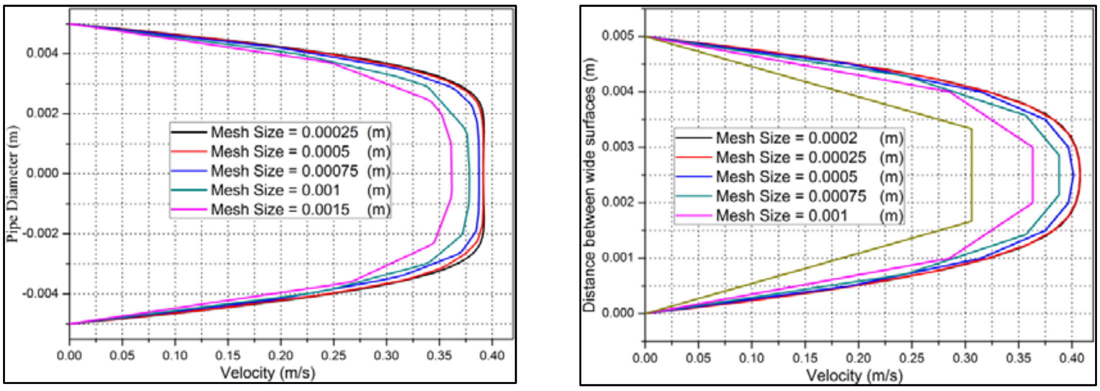

a) Pipe flow b) Duct flow

Figure 3.4. Laminar flow local velocities for mesh study.

Figure 3.4 shows that the local flow velocity values converge to each other for 0.00025 m and 0.0005 m mesh sizes for a) pipe flow. For that reason, it does not require the illustration of smaller mesh sized model which is 0.0002 m in the Figure 3.4.

Figure 3.4 presents that the local velocity values converge to each other for 0.0002 m and 0.00025 m sized mesh b) duct model. Equal accuracy would be possible by choosing the same mesh sized models. So, the examination mesh size was chosen as 0.00025 m for circular pipe and rectangular duct models.

3.2.3. Turbulent Flow Computational Base Mesh Study

Boundary conditions were specified for turbulent steady state internal liquid lithium flow conditions. Reynolds number has to be $Re > 2300$ for circular pipe and rectangular duct flow to obtain turbulent flow regime;

Reynolds number (Re) that is given in eq. (3.22) was chosen as 6050 to obtain turbulent flow condition. Inlet velocity that is in eq. (3.23) was calculated as below to satisfy the turbulent flow;

$$Re = \frac{\rho x D x U}{\mu} = \frac{516x0.01xU}{6.4x10^{-4}} = 6050 \qquad (3.22)$$

$$U \cong 0.75\ m/s \qquad (3.23)$$

The hydrodynamic similarity requires the equality of flow characteristics. Flow regime characteristic was checked for U = 0.75 m/s rectangular duct flow as below,

Hydraulic diameter is in eq. (3.24)

$$D_h = \frac{2xaxb}{a+b} = \frac{2x0.0157x0.005}{0.0157+0.005} = 7.56x10^{-3}m \qquad (3.24)$$

$$Re = \frac{\rho x D_h x U}{\mu} = \frac{516x7.56x10^{-3}xU}{6.4x10^{-4}} \cong 4570 \text{ flow is turbulent} \qquad (3.25)$$

Chosen thermal and calculated hydrodynamic boundary conditions were given in Table 3.3 for turbulent flow condition.

Table 3.3. Turbulent flow regime boundary conditions.

Turbulence Model Boundary Conditions	
T_w (K)	573.15
T_i (K)	473.15
T_o (K)	293.15
U(m/s)	0.75

Hydrodynamic and thermal development was qualified before the study to determine accurate data taking regions.

For circular pipe turbulent flow hydrodynamic and thermal entry lengths which are defined as in eq. (3.26), respectively;

$$L_h = L_t = 10D \tag{3.26}$$

$$L_h = L_t = 10x0.01 = 0.1\, m$$

The pipe model length is 0.15 m. Flow is hydrodynamic and thermal fully developed at 0.1 m of the model length and so the length of the pipe model is adequate to the hydrodynamic and thermal development.

Hydrodynamic and thermal entry lengths which are defined as in eq. (3.27) for rectangular duct model turbulent flow, respectively;

$$L_h = L_t = 10D \tag{3.27}$$

$$L_h = L_t = 10x7.56x10^{-3} = 0.0756\, m$$

Hydrodynamic and thermal developments of turbulent duct flow are completed at 0.0756 m. The pipe length is adequate to examine the thermal and hydrodynamic developed turbulent flow condition.

Estimated boundary conditions of the studied models which are given above were used as input data for the turbulent flow model mesh study. Mesh study was occurred by the comparison of local flow velocity values of different mesh sized models. The comparison of local flow velocities at 0.12 m of the models was done due to the flow velocity profiles are presented in Figure 3.5 for turbulent flow case. Figure 3.5 designates the local flow velocities for circular pipe model and rectangular duct model.

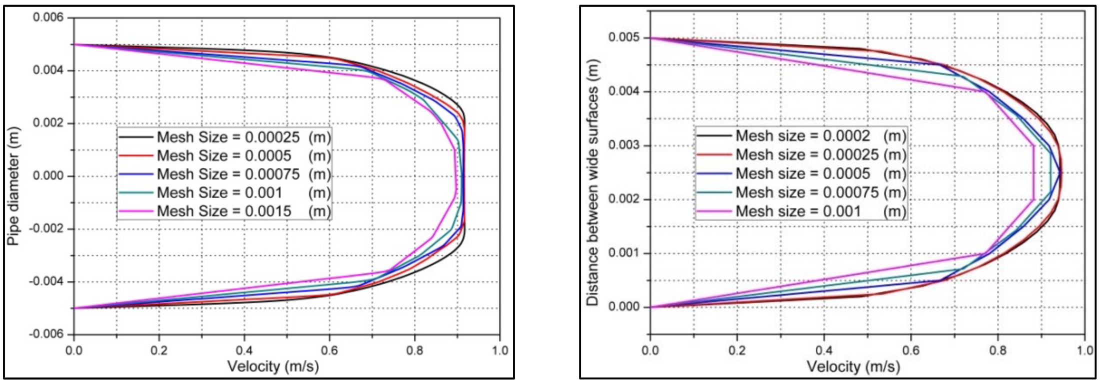

a) Pipe flow b) Duct flow

Figure 3.5. Turbulent flow local velocities for mesh study.

Figure 3.5 shows that the local flow velocity values converge to each other for 0.00025 m and 0.0005 m mesh sizes for pipe model. For that reason, it does not require the illustration of smaller mesh sized model which is 0.0002 m in the Figure 3.5.

Figure 3.5 presents that the local velocity values converge to each other for 0.0002 m and 0.00025 m mesh sized duct model. Equal accuracy would be possible by choosing the same mesh sized models. So, the optimum mesh size was chosen as 0.00025 m for circular pipe and rectangular duct models to the analyses.

PART 4

RESULTS AND DISCUSSION

Variation of the hydrodynamic, thermophysical parameters and heat transfer of liquid lithium internal flow case was investigated in two main titles. The first main title aimed to clarify the variation of hydrodynamic, thermophysical properties and heat transfer of liquid lithium for laminar internal flow condition and the second main title aimed to explain the properties for turbulent flow regime under the imposed magnetic forces which are externally applied magnetic field and combined application of magnetic field together with electrical field.

4.1. LAMINAR FLOW

In this section of the dissertation, laminar steady state incompressible magnetoviscous internal flow of liquid lithium in constant wall temperature models which are circular pipe and rectangular duct was investigated. Circular pipe and rectangular duct models were used to realise the effect of magnetic and electrical field on different geometrical conduit flows. Also, magnetic field and combined with electrical field effects were studied separately. Due to the Lorentz force expression which is F = q(E+UxB), magnitude of created magnetic force on conductive fluid body directly depends on the magnetic field induction and electrical field intensity. Direction of the electrical field directly influences the magnitude of the created Lorentz force on flow body. "+" positive directional electrical field enforces the magnetic field induction and enlarges the value of created reverse directional magnetic force on the flow domain. Also, "-" negative directional electrical field weakens the impact of magnetic field and causes the creation of lower magnetic force against to the flow domain. In this respect, this section of the study is presented in four subgroups. In first subgroup of this section, effects of externally applied magnetic field that are B = 0 T, B = 0.05 T, B = 0.1 T and B = 0.15 T on hydrodynamic, thermophysical properties and heat transfer of liquid lithium pipe flow were investigated. In the second one, effects of externally applied magnetic field that are B = 0 T, B = 0.05 T, B = 0.1 T and B = 0.15 T on hydrodynamic, thermophysical parameters and heat transfer of liquid lithium rectangular duct flow were studied. In the third one, combined effect of externally applied magnetics and electrical field on hydrodynamic, thermophysical parameters and heat transfer of liquid lithium pipe flow were investigated during magnetic field that was constantly imposing and electrical field applied with values which are taken as $E^{\pm}$ = 3e-6 V/m, $E^{\pm}$ = 6e-6 V/m, $E^{\pm}$ = 9e-6 V/m. In the fourth one, combined effect of externally applied magnetics and electrical field on hydrodynamic, thermophysical parameters and heat transfer of liquid lithium duct flow were studied during magnetic field which was constantly imposing and electrical field applied with values that are taken as $E^{\pm}$ = 3e-6 V/m, $E^{\pm}$ = 6e-6 V/m, $E^{\pm}$ = 9e-6 V/m.

4.1.1. Pipe Flow under the Imposed Magnetic Field

Laminar, steady state, incompressible magnetoviscous flow of liquid lithium in constant wall temperature circular pipe model was studied. Magnetic field was directed normally on to the flow lines and boundary conditions of the model are seen in Figure 4.1.

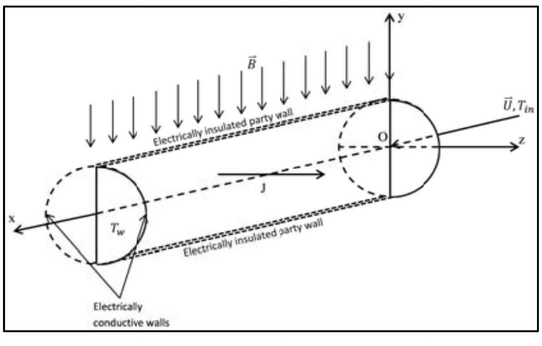

Figure 4.1. Circular pipe model.

The model wall temperature that is T_w = 573.15 K is constant, inlet liquid velocity that is U = 0.75 m/s and inlet flow temperature that is T_i = 473.15 K were estimated. Liquid lithium heating flow condition was studied in a constant wall temperature conduit.

Normally applied external magnetic field shows the adverse effect on flow velocity because of created reverse directional Lorentz force on the flow regime. Figure 4.2 illustrates the argued treatment for constantly applied magnetic field values.

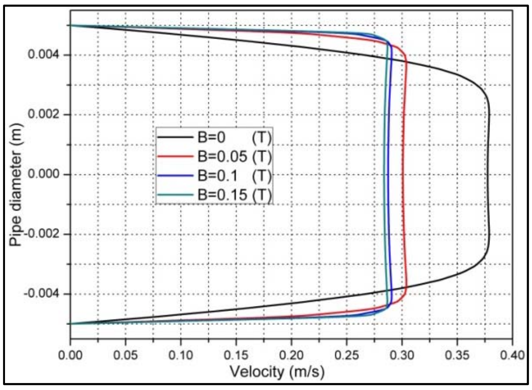

Figure 4.2. Local flow velocity under the magnetic field.

Local flow velocity profiles were compared at 0.12 m of the pipe length under the effect of magnetic field induction values which are B = 0 T, B = 0.05 T, B = 0.1 T and B = 0.15 T. Figure 4.2 shows that increase in magnetic field induction damps the local flow velocity. The flow velocity decreases at the centre of the model and slightly increases at the adjacent region of the model wall. The hydrodynamic boundary layer thickness and average flow velocity are decreased by the increase of magnetic field induction. B=0 T was accepted as a reference state and achieved a statistical analysis to identify the decrease rates of average flow velocity. Decrease rates of local flow velocity were specified as approximately about 10.42% for B= 0.05 T, 13.07% for B = 0.1 T, and 13.88% for B = 0.15 T. The similar case was also determined in ref. [7] as applied magnetic field on the laminar fluid flow reduced the velocity. In ref. [10] expressed that the velocity decreases with an increasing magnetic field.

Externally applied normal magnetic field on electrically conductive fluid flow creates an opposite force against to the flow direction. The opposite force means the back pressure load on the flow domain. Variation of static pressure through the central axis of the pipe model was presented in Figure 4.3 by the appliance of magnetic field induction with the values which are B = 0 T, B = 0.05 T, B = 0.1 T, B = 0.15 T.

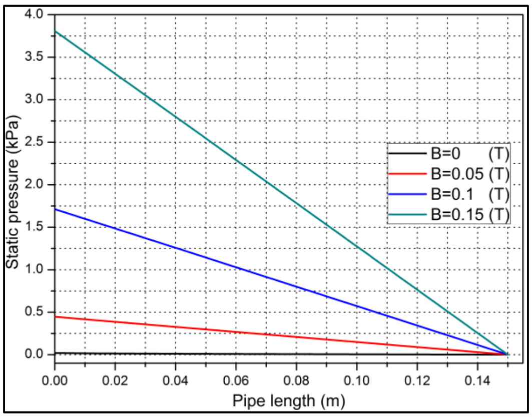

Figure 4.3. Central static pressure under the magnetic field.

Figure 4.3 displayed that central static pressure is increased by the increase of magnetic field induction. The increase rate of static pressure was determined due to the application of magnetic field with the values which are B = 0.05 T, B = 0.1 T, B = 0.15 T, and increase rates that are in the order as 3,012%, 11,861% and 26,525%. Increase of pressure by the imposed magnetic field was discussed in ref. [12] as the pressure gradient increases with increasing of magnetic parameter.

The dynamic pressure of flow domain was observed at 0.12 m of the pipe length, and dynamic pressure is seen in Figure 4.4.

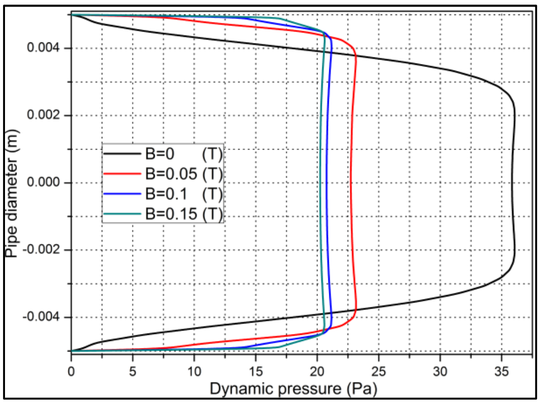

Figure 4.4. Local dynamic pressure under the magnetic field.

Figure 4.4 designates that increase in magnetic field caused the decrease of dynamic pressure due to the dynamic pressure is the hydrodynamic parameter which is dependent to flow velocity. Decrease in flow velocity means the decrease of local dynamic pressure, too. The decrease rate of dynamic pressure is determined as

23.74%, 27.85%, 28.83% by the increase of magnetic field induction from B = 0 T to B = 0.15 T. In ref. [31], it is discussed that increase in magnetic field strength, decreases the pressure because of increase in JxB force.

Skin friction coefficient was observed under the effect of magnetic field at the adjacent region of the pipe wall (R = 0.0049 m) through the pipe length while magnetic field was being applied perpendicularly on the flow and the obtained data which is seen in Figure 4.5.

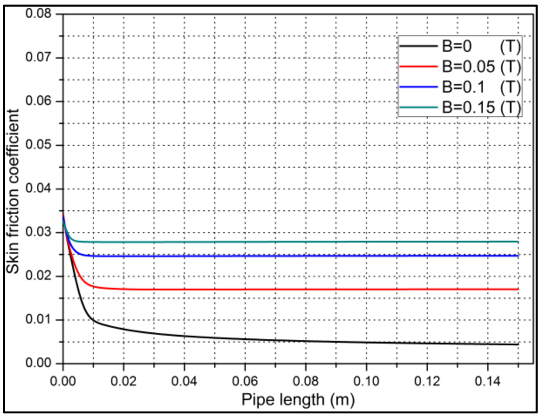

Figure 4.5. Skin friction coefficient under the magnetic field.

Figure 4.5 designates that skin friction coefficient increases by the increase of magnetic field induction. B = 0 T taken as a reference state and a statistical analyses is achieved to determine the increase rate of skin friction coefficient by the increase of magnetic field induction. Skin friction coefficient increases with the rates that are 168% for B = 0.05 T, 281% for B = 0.1 T, and 330% for B = 0.15 T by the increase of constantly applied magnetic field. In ref. [3], it is discussed that skin friction coefficient increases with magnetic parameter. Similarly, it is shown that skin friction coefficient increases with increase of Hartmann number in ref. [14].

Magnetic field effects the skin friction coefficient and so shear stress between the flow lines, too. Shear stress between stream lines of liquid lithium was investigated under the effect of magnetic field by taking data from the adjacent region of the model wall through the pipe length and taken data which are visualised in Figure 4.6.

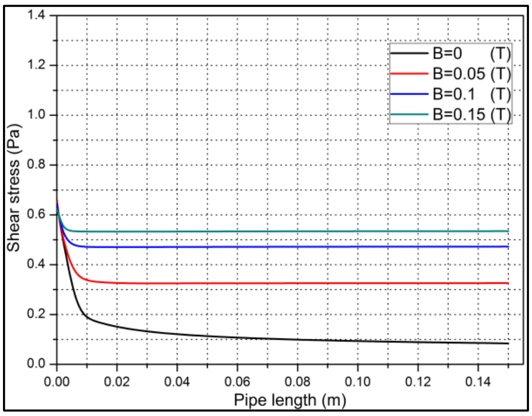

Figure 4.6. Shear stress under the magnetic field.

As seen in Figure 4.6, shear stress between the flow lines increases by the increase of magnetic field strength and the increase rates of shear stress were determined statistically for further increase of magnetic field induction from B = 0.05 T to B = 0.15 T. The average value of shear stress increases with the rates that are 168% for B = 0.05 T, 281% for B = 0.1 T and 330% for B = 0.15 T. This case is supported in ref. [23] as wall shear stress increases as magnetic parameter increases. It is mentioned that where the magnetic field is located shear stress increases sharply in ref. [42].

Variation of liquid lithium temperature was studied by the effect of externally applied magnetic field induction for the induction values which are B = 0 T, B = 0.05 T, B = 0.1 T, B = 0.15 T, and taken data were evaluated. Temperature values that are at the central region through pipe length under the influence of externally applied magnetic field are seen in Figure 4.7.

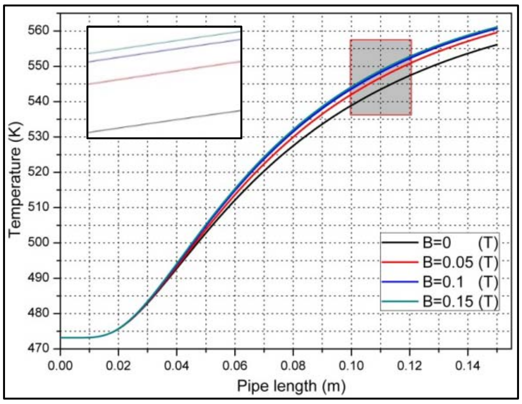

Figure 4.7. Central temperature under the magnetic field.

Liquid lithium temperature increases by the increase of magnetic field through the pipe length as seen in Figure 4.7. The percentage of temperature increase rates were evaluated for the magnetic induction values which are B = 0.05 T, B = 0.1 T, B = 0.15 T and by taking the B = 0 T as a reference state and increase rates, are presented in the same order as 0.37%, 0.56%, 0.64%. Similar opinions were given in ref. [11] as temperature is boosted with applied magnetic field. Also, ref. [27], it is observed that temperature distribution increases by the increase of Hartman number.

Magnetic effects on local temperature of flowing liquid lithium were studied and local temperature data that are taken from 0.12 m thermally fully developed region of the model was presented in Figure 4.8.

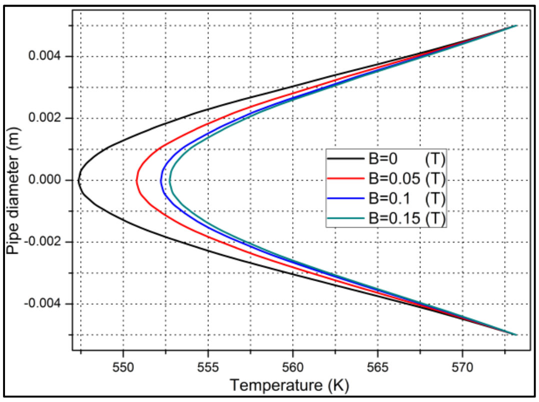

Figure 4.8. Local temperature under the magnetic field.

Illustrated profiles in Figure 4.8 could be interpreted that local liquid lithium temperature increases by the increase of magnetic field induction from B = 0.05 T to B= 0.15 T. Increase rates were determined for further increase of magnetic field induction by statistical analyses. B = 0 T is determined as a reference state and so the increase rates were evaluated as 0.32%, 0.48%, 0.53% in the range of applied magnetic field induction. It is revealed that temperature increases with increase in the magnetic field parameter in ref. [29]. Also, in ref. [30], it is found that the temperature is to be markedly boosted with an increase in the magnetic parameter.

Nusselt number was examined at the adjacent region of the pipe wall through the pipe length under the effect of perpendicularly applied magnetic field. Variation of

Nusselt number is demonstrated in Figure 4.9 by the appliance of magnetic field induction values that are as B = 0 T, B = 0.05 T, B = 0.1 T, B = 0.15 T in regard to the heating of flowing liquid lithium by a constant wall temperature enclosure.

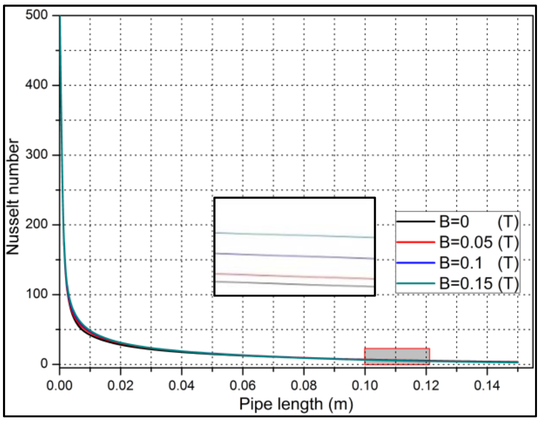

Figure 4.9. Nusselt number under the magnetic field.

Figure 4.9 designates that by the increase of magnetic field induction, Nusselt number increases. By taking of B = 0 T as a reference, it was achieved a statistical analysis to determine the increase rates of average Nusselt number by the increase of magnetic field induction. Under the effect of imposed magnetic field the increase rates were evaluated as 0.032% for B = 0.05 T, 0.039% for B = 0.1 T, and 0.041% for B = 0.15 T. Variation of Nusselt number by imposed magnetic field for laminar flow regime is discussed in ref. [37] as the Nusselt number increases with the increase in magnetic field. Likewise in ref. [14], it is concluded that Nusselt number increases with increase of Hartmann number. Increase in Nusselt number means the increase of heat transfer. Reason of this case which is concluded in ref. [35, 76] as increasing the magnetic parameter, leads to an increase in the peak of the velocity profile near the walls; however, the peak of the velocity profile at the core region has a decreasing trend. Also, the heat transfer rate is enhanced in the presence of the magnetic field.

4.1.2. Duct Flow under the Imposed Magnetic Field

Rectangular duct laminar, steady state, incompressible magnetoviscous flow condition was studied and the effect of magnetic field on hydrodynamic, thermophysical properties and heat transfer of liquid lithium flow were searched. The normally applied magnetic field on the flow streamlines and boundaries of the studied rectangular duct model are presented in Figure 4.10.

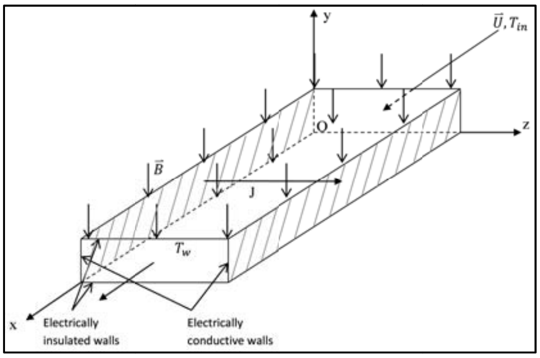

Figure 4.10. Duct model.

Wall temperature that is T_w = 573.15 K of the model which is constant, inlet liquid velocity that is U = 0.75 m/s and inlet flow temperature that is T_i = 473.15 K were estimated. Liquid lithium heating flow condition in a constant wall temperature conduit was studied.

Local flow velocity of the liquid lithium within the effect of constantly applied magnetic field was observed by taking data from the 0.12 m of the model through the distance of narrow model surfaces and is visualized in Figure 4.11.

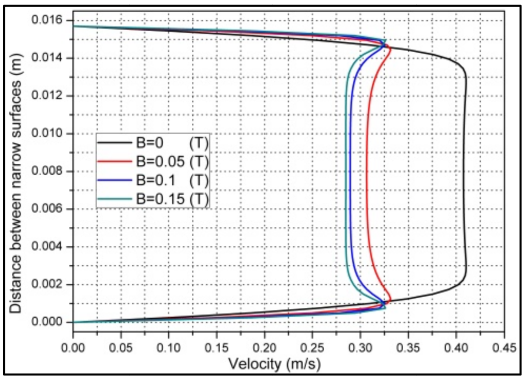

Figure 4.11. Local flow velocity under the magnetic field.

Figure 4.11 clarifies that the local flow velocity decreases by the effect of applied magnetic field. The local flow velocity behaves as a similar characteristic with pipe flow. The local flow velocity slightly increases at the adjacent region of the model wall but also the velocity decreases at the central region of the model by the magnetic force. Average local flow velocity is decreased by the increase of magnetic field induction that are from B = 0 T to B = 0.15 T. Decrease rates are about 19.59%, 23.24%, and 24.32% for B = 0. 05 T, B = 0.1 T and B = 0.15 T. This case is concluded in ref. [16] as velocity profile shows the decreasing behaviour with an increase of magnetic parameter. Also in ref. [22], it is discussed that the applied magnetic field reduces the flow velocity, the magnetic field and the velocity field have a direct relation.

Magnetic field effect on static pressure was investigated through the model central axis and taken data that are from the model central axis is presented in Figure 4.12.

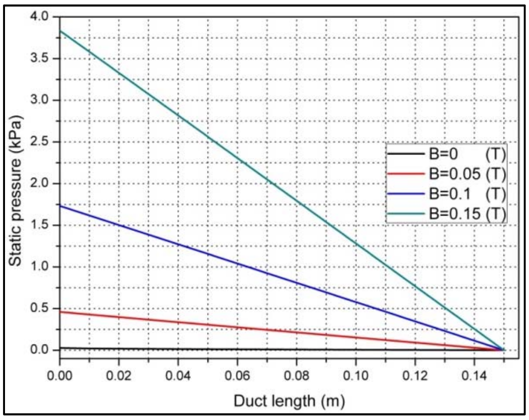

Figure 4.12. Central static pressure under the magnetic field.

Linear lines as seen in Figure 4.12 shows that the central static pressure of the model increases by the increase of magnetic field induction. Increase rates of static pressure were evaluated as 2,214%, 8,640%, and 19,257% for each step of increase of applied magnetic field induction from B = 0.05 T to B = 0.15 T. Similar results discussed in ref. [44] as the pressure rise increases with an increase in magnetic parameter and also in ref. [10], it is mentioned that fluid pressure increases with increasing magnetic field.

The local dynamic pressure was observed to determine the effect of magnetic field and is presented in Figure 4.13.

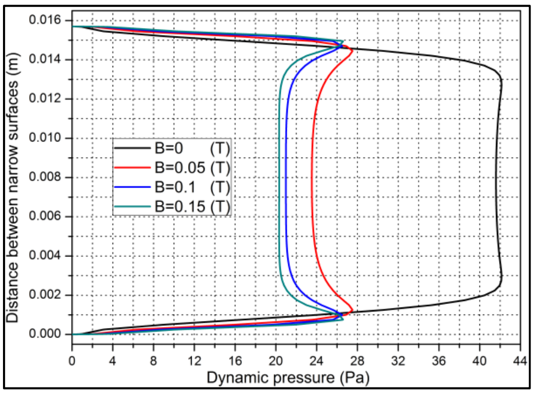

Figure 4.13. Local dynamic pressure under the magnetic field.

Figure 4.13 shows that increase in magnetic field induction decreases the local dynamic pressure indirectly, because the dynamic pressure is the dependent hydrodynamic parameter to the flow velocity. The local dynamic pressure decrease rates were determined as 36.76%, 42.53%, 44.18% by the increase of magnetic field that are from B = 0 T to B = 0.15 T. This case is discussed in ref. [127] as increase in magnetic parameter enhances the pressure loss.

Effect of magnetic field on skin friction coefficient was evaluated and visualized in Figure 4.14.

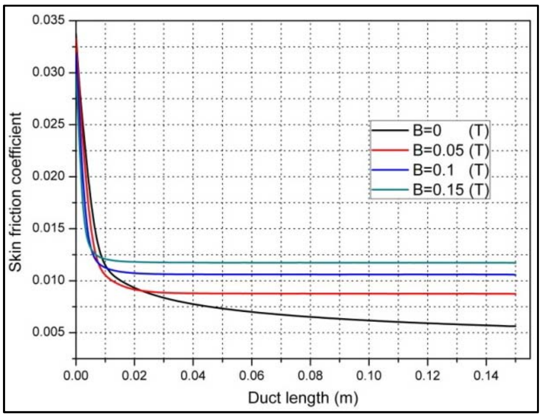

Figure 4.14. Skin friction coefficient under the magnetic field.

Figure 4.14 illustrates that increase in applied magnetic field induction increases the skin friction coefficient. Average value of skin friction coefficient is affected by the magnetic field with variable rates. Increase rates of skin friction coefficient were estimated as 21.16%, 41.05%, and 53.64% for each applied magnetic field induction values which are B = 0.05 T, B = 0.1 T, and B = 0.15 T. This case similarly assessed in ref. [21] as skin friction coefficient increases when magnetic field increases and another study is ref. [58] discussed that increase in magnetic parameter also increases the local skin friction coefficient.

Variation of shear stress which is between the flow stream lines under the influence of magnetic field was evaluated and given in Figure 4.15.

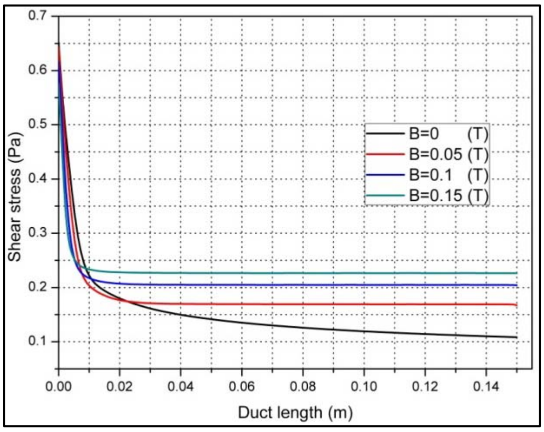

Figure 4.15. Shear stress under the magnetic field.

Figure 4.15 illustrates that shear stress increases in same rates with the skin friction coefficient by the increase of applied magnetic field induction because of the linear relation between them. Increase rates of average value of shear stress were determined as 21.16%, 41.05%, and 53.64% for each constantly applied magnetic field induction values. Increase in shearing that is between the flow stream lines because of the magnetic forces is discussed in ref. [20] as the shear stress increases with an increasing of current density. In another one is ref. [47], it is mentioned that the magnetic field enhances the shear stresses.

Effect of magnetic field on central temperature of flowing liquid lithium was studied and temperature data that is taken from the central axis of the model through the model length is presented in Figure 4.16.

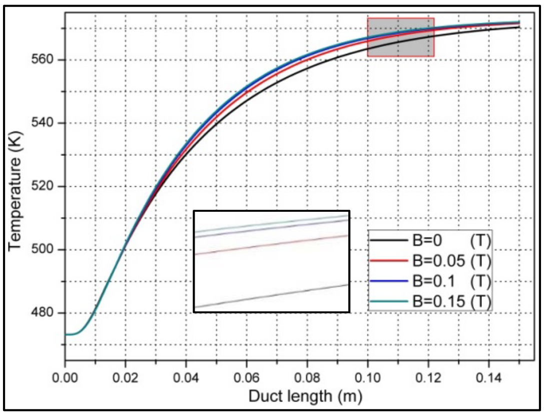

Figure 4.16. Central temperature under the magnetic field.

Central temperature of the liquid lithium was boosted by the effect of magnetic field as seen in Figure 4.16. Applied each magnetic field induction values which are B = 0.05 T, B = 0.1 T, B = 0.15 T increases the central temperature with rates that are 0.31%, 0.46%, and 0.51%. Temperature distribution increases with the increasing values of magnetic parameter in ref. [32]. It is clarified that due to stronger magnetic field temperature increases in ref. [34].

Local temperature of the flow was examined by taking local temperature data from the 0.12 m of thermal developed region of the model and is visualised in Figure 4.17.

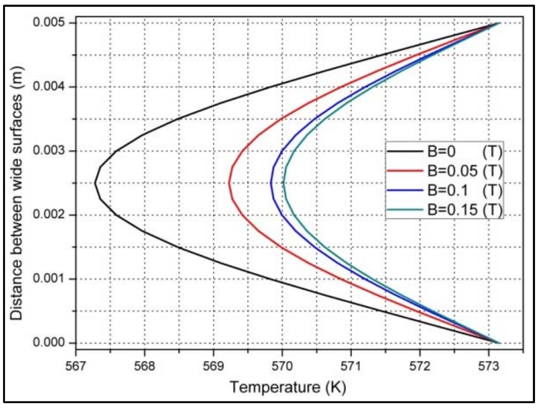

Figure 4.17. Local temperature under the magnetic field.

Figure 4.17 presents that application of magnetic field increases the local temperature of the flowing liquid lithium. Average value of local temperature was increased by the each step of increase of magnetic field induction with the values that are B = 0.05 T, B = 0.1 T and B = 0.15 T. The increase rates that are 0.20% for B =

0.05 T, 0.27% for B = 0.1 T and 0.29% for B = 0.15 T. Temperature profiles increase with the increase of Hartmann number in ref. [39]. It is mentioned that increase of magnetic parameter increases the temperature gradient in ref. [49].

Nusselt number data were taken from the adjacent region of the duct wall and variation of it was investigated through the duct length in Figure 4.18.

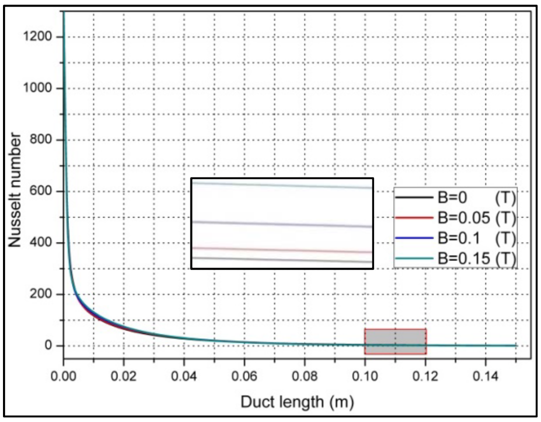

Figure 4.18. Nusselt number under the magnetic field.

Figure 4.18 designates that applied magnetic field enhances the Nusselt number. The increase rates of Nusselt number were determined as 0.97% for B = 0.05 T, 1.63% for B = 0.1 T, and 2% for B = 0.15 T. It could be concluded that the heat transfer rate which is from the wall to the central axis of the model increased by the increase of magnetic field induction. Nusselt number increases with Hartmann number in ref. [24]. Applied magnetics force increases the amount of heat transfer in ref. [42]. In MHD analysis Nusselt number is 2.5 times higher than simple case that is without magnetic force.

4.1.3. Pipe Flow under the Imposed Magnetic and Electrical Field

As seen in Figure 4.19, the pipe model was constructed with two part walls which are used as two different (+) and (-) poles and part wall disconnected from each other with electrically nonconductive party wall. The positive and negative electrical potentials were applied on these two conductive walls to create an external electrical field. Change of the poles changes the created electrical field direction from E^+ to E^-.

Magnetic field applied on to the pipe model through the - y direction. Fluid flow determined in the + x direction.

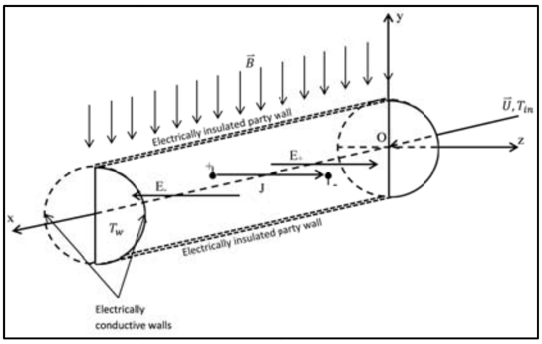

Figure 4.19. Pipe model.

The local flow velocity of liquid lithium was examined at 0.12 m of the model under the magnetic field that are B = 0.05 T, effect of electrical field. Data were taken from the distance between narrow model walls and is visualised in Figure 4.20.

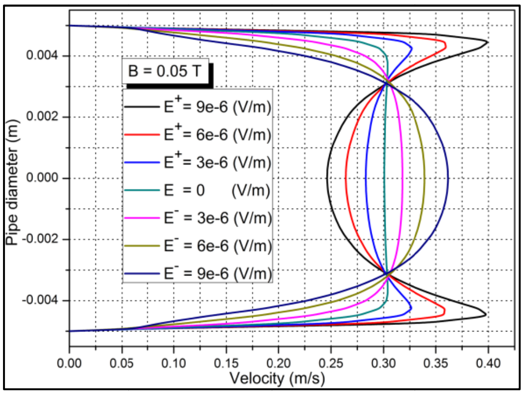

a) B = 0.05 T

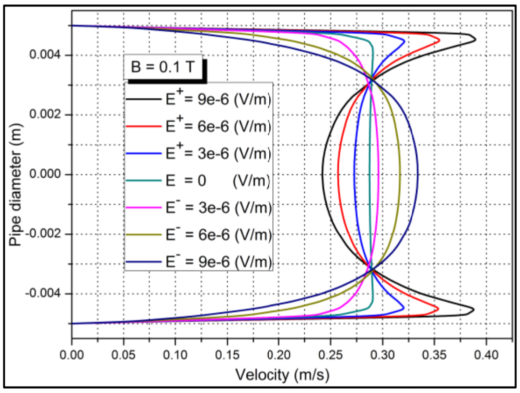

b) B = 0.1 T

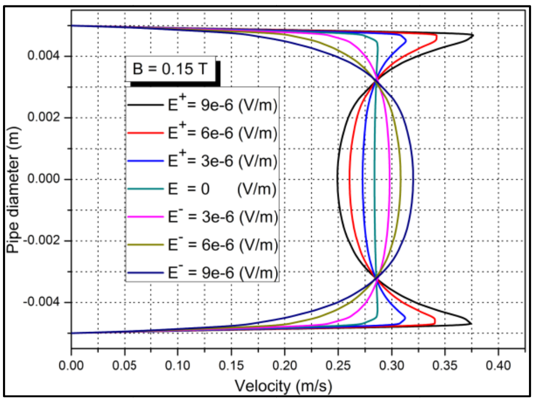

c) B = 0.15 T

Figure 4.20. Flow velocity under the magnetic and electrical field.

It is apparent that from the profiles is seen in Figure 4.20, the effect of magnetic field on liquid lithium flow streamlines were boosted by the increase of applied positive directional electrical field (E^+). Increase of the electrical field (E^+) causes the increase of flow velocity at the close region of the pipe wall. However, flow velocity shows the decreasing behaviour in the central region of model. Changing the direction of electrical field (E^-) to opposite, the effect of magnetic field was lessened and the flow velocity increased in central region and decreased at close region of the model wall by the increase of electrical field. In ref. [76] mentioned that the flow is damped by magnetic induced force, whereas flow near the walls channel is accelerated. For each constantly applied magnetic field value, the increase or decrease rates of local flow velocity were estimated by the variation of electrical field. The decrease rates of flow velocity are about 0.16%, 0.33%, 0.36% when B = 0.05 T and electrical field was applied in the positive direction with values are E^+ = 3e-6 V/m, E^+ = 6e-6 V/m, E^+ = 9e-6 V/m. In other case for B = 0.05 T and electrical field was applied in the negative direction with values are E^- = 3e-6 V/m, E^- = 6e-6 V/m, E^- = 9e-6 V/m, the velocity is increased with a rates are 0.14%, 0.24%, 0.49%. For B = 0.1 T, the velocity decrease rates are 0.12%, 0.30%, 0.32% and increase rates are 0.12%, 0.21% and 0.45%. For B = 0.15 T, the velocity decrease rates are 0.08%, 0.25%, 0.29% and increase rates are 0.08%, 0.18% and 0.37%. In ref. [81], it is determined that the velocity decreased with the increase in magnetic parameter.

Change of central static pressure of the fluid was evaluated according to demonstrated linear lines as seen in Figure 4.21(a, b, c).

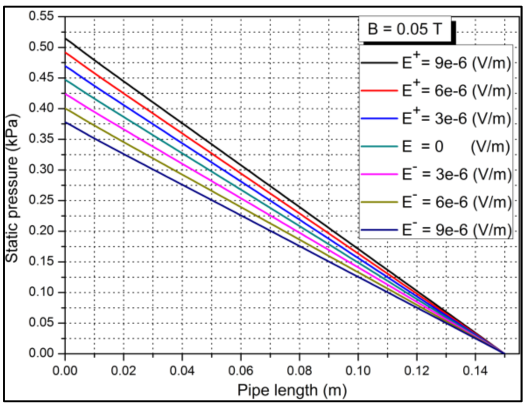

a) B = 0.05 T

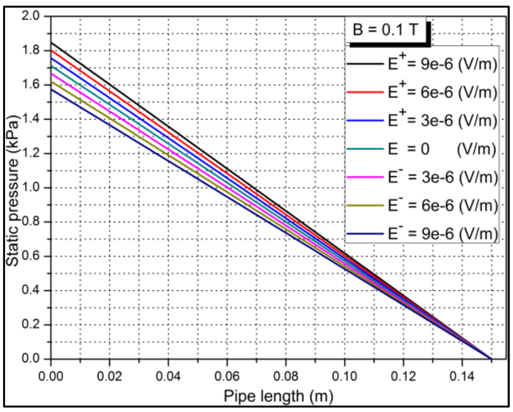

b) B = 0.1 T

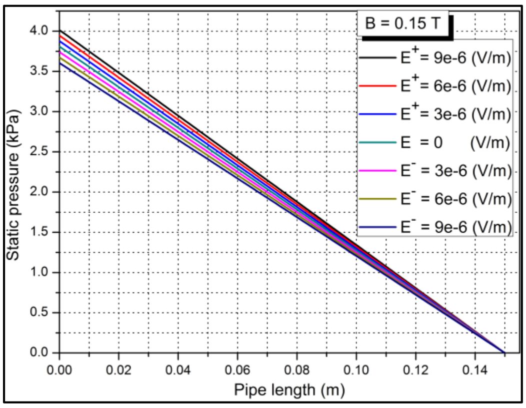

c) B = 0.15 T

Figure 4.21. Central static pressure under the magnetic and electrical field.

Figure 4.21 show that static pressure increases by the increase of electrical field (E^{+}) in positive direction. If the field direction change and increases, the static pressure decreases. This case would be clarified with conservation of energy principle, increase in velocity decreases the static pressure or vice versa. The increase and decrease rates were calculated statistically for each constant magnetic field induction values which are B = 0.05 T, B = 0.1 T and B = 0.15 T and variable electrical field intensity values which are $E^{\pm}$=3e-6 V/m, $E^{\pm}$=6e-6 V/m, $E^{\pm}$=9e-6 V/m). While magnetic field was being applied with a constant value of B = 0.05 T, electrical field was applied with values that are $E^{\pm}$=3e-6 V/m, $E^{\pm}$=6e-6 V/m, $E^{\pm}$=9e-6 V/m and the rate of increase in static pressure determined as 5%, 9.92%, 14.99% and by the change of direction of electrical field the decrease rates in static pressure were determined as 5.22%, 10.59%, 15.64%. In case of applied magnetic field with constant value is B = 0.1 T, electrical field was applied with values are $E^{\pm}$=3e-6 V/m, $E^{\pm}$=6e-6 V/m, $E^{\pm}$=9e-6 V/m, the positive directional application of electrical field increased the central static pressure with rates that are 2.62%, 5.28%, 7.92% and reverse directional application of electrical field decreased the central static pressure with rates that are 2.63%, 5.33%, 8.03%. Lastly for externally applied magnetic field is B = 0.15 T, positive directional application of electrical field enhanced the effect of magnetic field and so central static pressure was increased with rates are 1.78%, 3.57%, 5.36%. Applied electrical field in negative direction decreases the influence of magnetic field and the pressure decreased with the rates are 1.78%, 3.58%, 5.37%. Pressure gradient increases with magnetic parameter in ref. [65].

Given profiles in Figure 4.22 shows the variation of local dynamic pressure at 0.12 m of the pipe length under the imposed magnetic and electrical field.

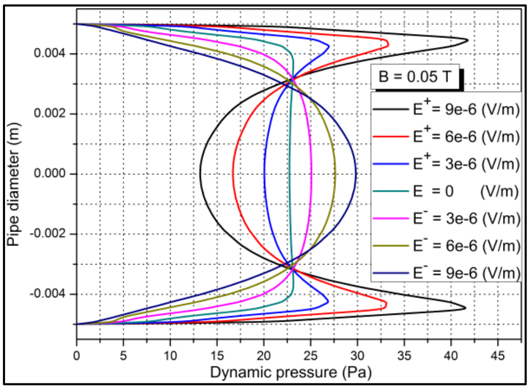

a) B = 0.05 T

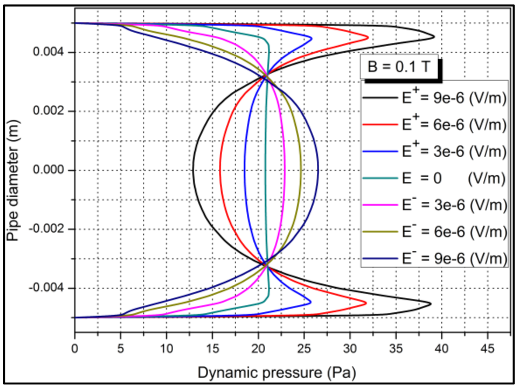

b) B = 0.1 T

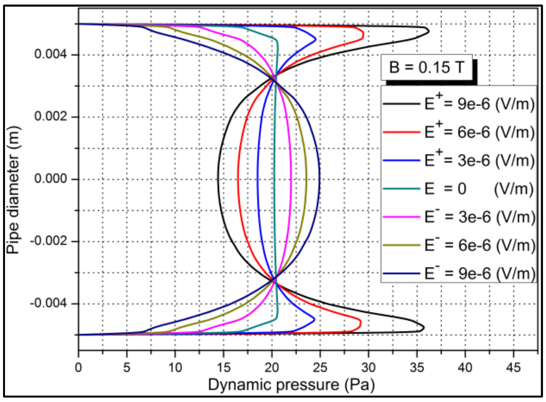

c) B = 0.15 T

Figure 4.22. Local dynamic pressure under the magnetic and electrical field.

Visualised local dynamic pressure data from occurred analyses were given in Figure 4.22. It is clearly seen that local dynamic pressure under the influence of externally applied magnetic field increases or decreases according to the direction of applied electrical field together with it. Increase in electrical field that is in positive direction increases the dynamic pressure at the close region of the wall and decreases at the central region of the model. Application of electrical field that is through the negative way reduced the local dynamic pressure at the adjacent region of the model wall, but also increased at the central region. Decrease and increase rates of local dynamic pressure were determined by the increase of electrical field in positive and negative directions for each constantly applied magnetic field induction values. For constantly applied magnetic field with the value that is B = 0.05 T, the dynamic pressure decrease rates that are 0.16%, 0.33%, 0.36% and increase rates that are 0.14%, 0.24% and 0.49%. For B = 0.1 T, the dynamic pressure decrease rates that are 0.12%, 0.30%, 0.32% and increase rates that are 0.12%, 0.21% and 0.45%. For B = 0.15 T, the dynamic pressure decrease rates that are 0.08%, 0.25%, 0.29% and increase rates that are 0.08%, 0.18% and 0.37% for each step of change of electrical field intensity from $E^{\pm}$ = 3e-6 to $E^{\pm}$ = 9e-6. In ref. [66], it is determined that dynamic pressure is reduced by increasing the ratio of magnetic.

Skin friction coefficient was presented in Figure 4.23 under the effect of magnetic and electrical field.

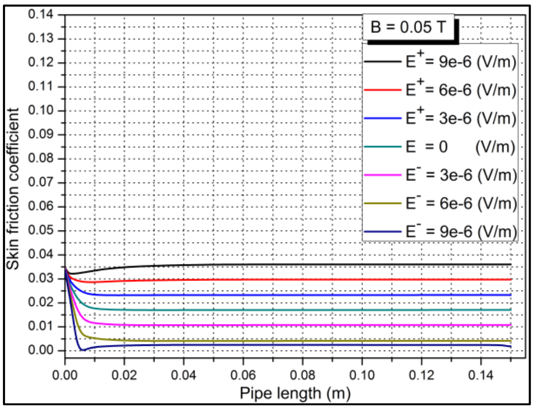

a) B = 0.05 T

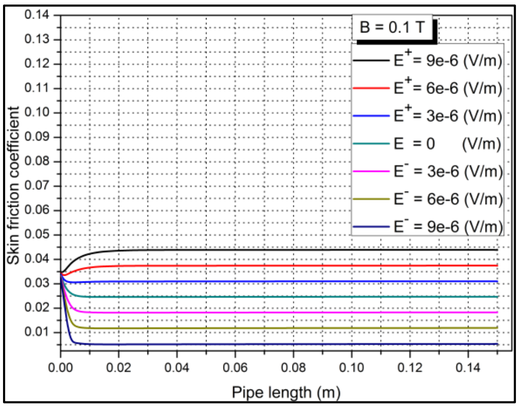

b) B = 0.1 T

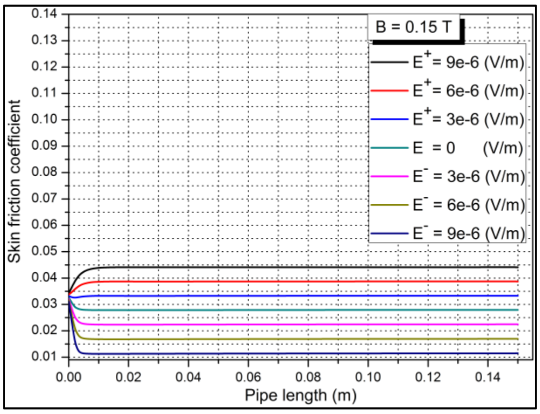

c) B = 0.15 T

Figure 4.23. Skin friction coefficient under the magnetic and electrical field.

Figure 4.23 shows that increase in positive directionally applied electrical field which is imposed together with externally applied magnetic field increases the skin friction coefficient. However, in case and increase in negative directional electrical field that is applied together with constantly applied external magnetic field decreases the skin friction coefficient. For B = 0.05 T, electrical field was applied with values are $E^{\pm}$=3e-6 V/m, $E^{\pm}$=6e-6 V/m, $E^{\pm}$=9e-6 V/m and increase rates of the friction coefficient are determined as 34.55%, 69.72, 103.89%. Decrease rates of the skin friction are determined as 35.14%, 72.09%, 83.51% in case of redirecting the electrical field through negative direction. For B = 0.1 T, the increase rates of the friction coefficient that are in the order as 25.04%, 50.22%, 75.40% and decrease rates that are 25.46%, 50.9%, 77.19% by the increase of $E^{\pm}$ = 3e-6 to $E^{\pm}$ = 9e-6. In case of application of B = 0.15 T, increase of E^{+} increases the skin friction coefficient with rates are 18.98%, 38.08%, 57.03%, and applied electrical field in negative direction causes the decrease with rates that are 19.35%, 38.90%, 58.43%. Friction coefficient increases by the increase of Hartmann number in ref. [59, 63].

The shear stress between streamlines of flow domain is visualised in Figure 4.24 to the case of imposed magnetic field together with electrical field.

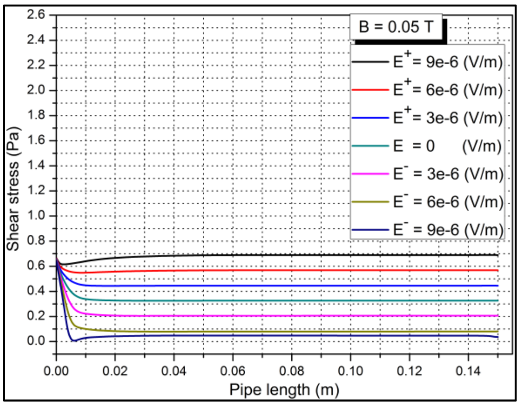

a) B = 0.05 T

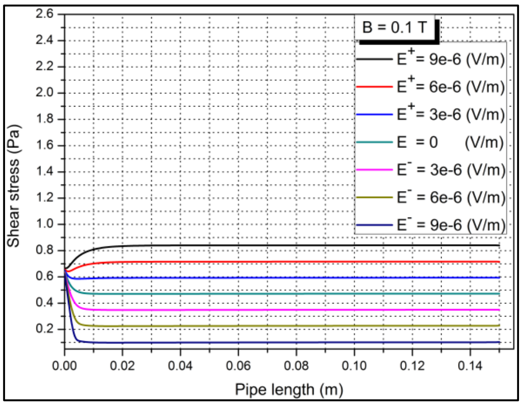

b) B = 0.1 T

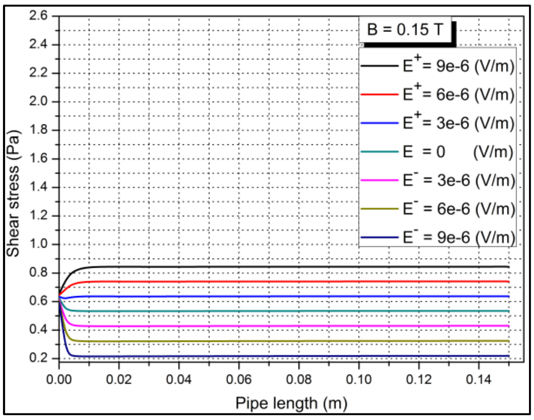

c) B = 0.15 T

Figure 4.24. Shear stress under the magnetic and electrical field.

Figure 4.24 could be interpreted to the constantly applied magnetic field, increase in externally imposed positive directional electrical field increases the shear stress and by the change of electrical field direction to the negative way shear stress decreases by the each step of increase of the electrical field. Increase rates that are 34.55%, 69.72%, 103.89% by the application of electrical field in positive direction and decrease rates that are 35.14%, 72.09%, 83.51% by the directing of electrical field in negative direction under the imposed constant magnetic field induction is B = 0.05 T. While applying B = 0.1 T, increase rates that are 25.04%, 50.23%, 75.4% for the application and increase of electrical field in positive direction and decrease rates that are 25.46%, 50.9%, 77.19% by the change of electrical field direction to negative way. Similar effect was determined for B = 0.15 T, the increase rates of the shear stress that are 18.98%, 38.08%, 57.03% and decrease rates that are 19.35%, 38.9%, 58.43% for negatively directed electrical field. The obtained result supported in ref [12] as the pressure gradient increases with increasing of Hartmann number. It is concluded that shear stress increases by increasing magnetic field in ref. [61].

Temperature distribution was examined for constantly applied magnetic field on flow model and electrical field was varied with the values that are $E^{\pm}$ = 3e-6 V/m, $E^{\pm}$ = 6e-6 V/m, $E^{\pm}$ = 9e-6 V/m. Central temperature distribution is shown under the influence of magnetic and electrical field in Figure 4.25 for the heating flow condition of liquid lithium in a constant wall temperature model.

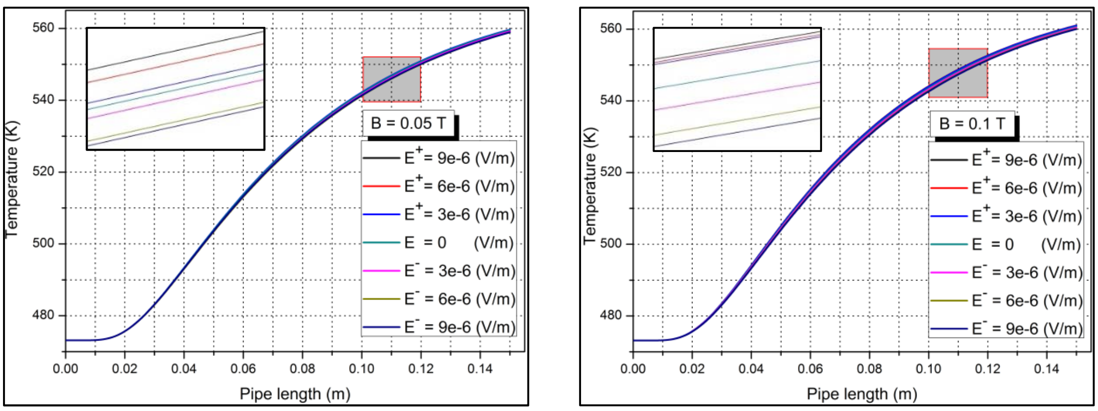

a) B = 0.05 T b) B = 0.1 T

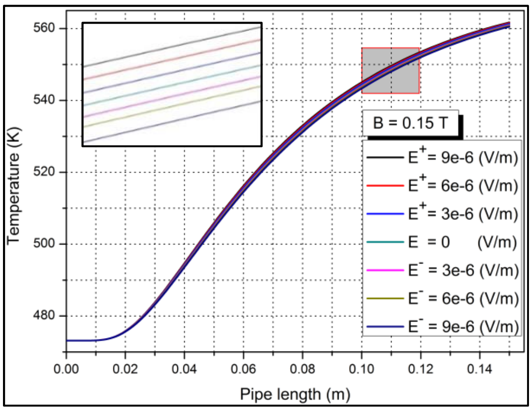

c) B = 0.15 T

Figure 4.25. Central temperature under the magnetic and electrical field.

As seen in Figure 4.25, the axial temperature values were increased by the increase of applied E^+ field while magnetic field is constantly being applied whereas the axial temperature values were decreased by the appliance of the E^- electrical field values. While constant magnetic field was applied with the value of B = 0.05 T, increase rates of temperature were evaluated in the order as 0.02%, 0.03%, 0.04% by the appliance of E^+ = 3e-6 V/m, E^+ = 6e-6 V/m, E^+ = 9e-6 V/m and the temperature values were decreased as 0.05%, 0.08%, 0.09% by the appliance of E^- = 3e-6 V/m, E^- = 6e-6 V/m, E^- = 9e-6 V/m. Similarly, for B = 0.1 T, the increase rates of temperature values were evaluated in the order as 0.04%, 0.05%, 0.06% by the appliance of E^+ = 3e-6 V/m, E^+ = 6e-6 V/m, E^+ = 9e-6 V/m and the temperature values were decreased as 0.06%, 0.10%, 0.12% by the appliance of E^- = 3e-6 V/m, E^- = 6e-6 V/m, E^- = 9e-6 V/m. For B = 0.15 T, the increase rates of temperature values were evaluated in the order as 0.06%, 0.08%, 0.12% by the appliance of E^+ = 3e-6 V/m, E^+ = 6e-6 V/m, E^+ = 9e-6 V/m and the temperature values were decreased as 0.08%, 0.13%, 0.14% by the appliance of E^- = 3e-6 V/m, E^- = 6e-6 V/m, E^- = 9e-6 V/m. It is concluded that the maximum amount of temperature increases by applied magnetic field in ref. [7]. Temperature distribution and mean temperature distributions increase with the increase in magnetic parameter in ref. [32].

Temperature profile of the liquid lithium was studied at thermal fully developed region where is 0.12 m of the pipe of the model and was illustrated in Figure 4.26 for the applied magnetic field induction together with electrical field intensity. For each applied constant magnetic field induction values that are B = 0 T, B = 0.05 T, B = 0.1 T, B = 0.15 T, the electrical field was being applied with the values that are $E^{\pm}$ = 3e-6 V/m, $E^{\pm}$ = 6e-6 V/m, $E^{\pm}$ = 9e-6 V/m on the flow domain.

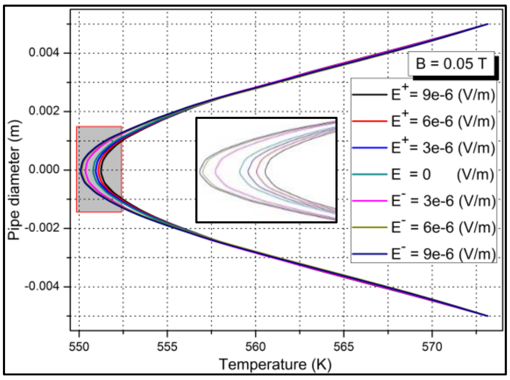

a) B = 0.05 T

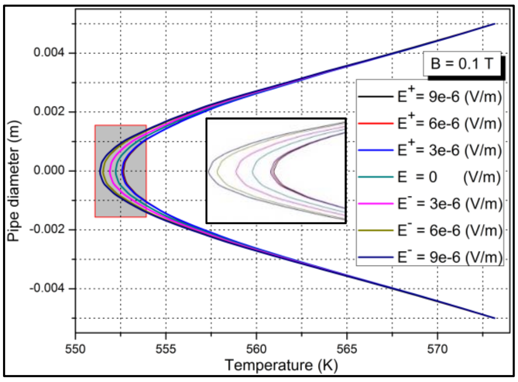

b) B = 0.1 T

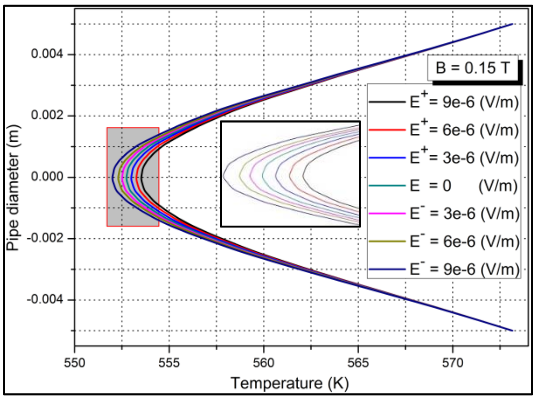

c) B = 0.15 T

Figure 4.26. Local temperature under the magnetic and electrical field.

Figure 4.26 represents the effect of applied electrical field on the local temperature of the flowing liquid lithium under the influence of applied constant magnetic field. Local temperature increases by the increase of electrical field intensity that is from E^{+} = 3e-6 V/m to E^{+} = 9e-6 V/m while flow body is under the imposed magnetic field. For B = 0.05 T, the increase rate of local temperature were determined as 0.005%, 0.01%, 0.015% by the increase of positive directional electrical field intensity. Within the appliance of electrical field with values that are E^{-} = 3e-6 V/m, E^{-} = 6e-6 V/m, E^{-} = 9e-6 V/m, the temperature were decreased with rates that are 0.036%, 0.037%, 0.039%. For applied B = 0.1 T, the increase rate of the temperature are in the order as 0.022%, 0.026%, 0.03% by the appliance of electrical field which are E^+ = 3e-6 V/m, E^+ = 6e-6 V/m, E^+ = 9e-6 V/m, and the temperature were decreased as 0.026%, 0.059%, 0.069% by the appliance of E^- = 3e-6 V/m, E^- = 6e-6 V/m, E^- = 9e-6 V/m. Lastly, for B = 0.15 T, the increase rate of temperature in the order were evaluated as 0.025%, 0.045%, 0.067% by the appliance of electrical field that are E^+ = 3e-6 V/m, E^+ = 6e-6 V/m, E^+ = 9e-6 V/m, and the temperature were decreased as 0.019%, 0.035%, 0.063% by the appliance of E^- = 3e-6 V/m, E^- = 6e-6 V/m, E^- = 9e-6 V/m. In literature the similar results are discussed in ref. [34, 46] as the temperature profiles increase with the increase of magnetic parameter for the viscous heat transfer condition.

The change of Nusselt number was observed at the adjacent region of the pipe wall through the pipe length under the effect of normally applied magnetic field inductions which are as B = 0.05 T, B = 0.1 T, B = 0.15 T and electrical field intensities that are as $E^{\pm}$ = 3e-6 V/m, $E^{\pm}$ = 6e-6 V/m, $E^{\pm}$ = 9e-6 V/m and presented in Figure 4.27.

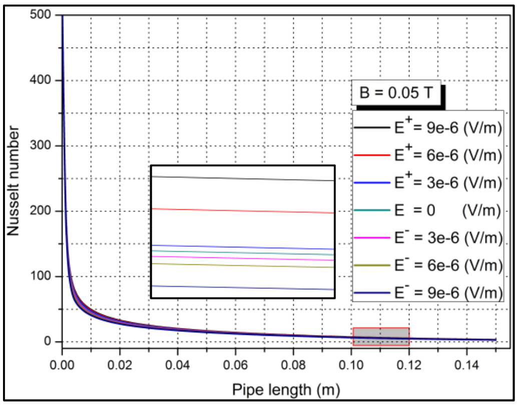

a) B = 0.05 T

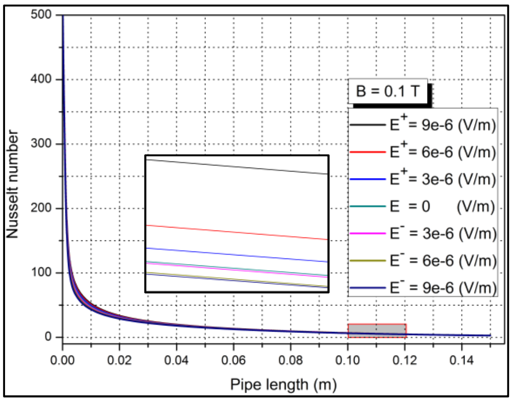

b) B = 0.1 T

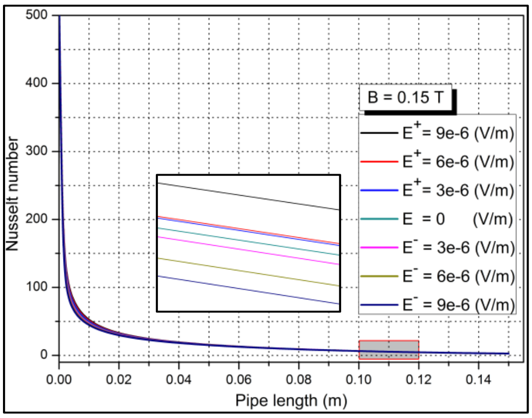

c) B = 0.15 T

Figure 4.27. Nusselt number under the magnetic and electrical field.

Figure 4.27 presents that, increase in positive directional electrical field, enhanced the effect of the applied magnetic field induction and so the Nusselt number was increased for each value of applied positive directional electrical field. However, by the change of electrical field direction to negative, the Nusselt number was decreased for each step of increase of negative directional electrical field. For applied B = 0.05 T, the Nusselt number was enhanced by the application of electrical field with the values that are E^+ = 3e-6 V/m, E^+ = 6e-6 V/m, E^+ = 9e-6 V/m and the rates of enhancement that are as 1.85%, 4.09%, 6.16% and the Nusselt number was decreased with the rates that are 1.72%, 3.84%, 6.37% by the appliance of E^- = 3e-6 V/m, E^- = 6e-6 V/m, E^- = 9e-6 V/m. For B = 0.1 T, the increase rates of Nusselt number were evaluated in the order as 1.58%, 3.44%, 5.35% by the appliance of E^+ = 3e-6 V/m, E^+ = 6e-6 V/m, E^+ = 9e-6 V/m and the Nusselt number was decreased as 1.67%, 3.28%, 5.21% by the appliance of E^- = 3e-6 V/m, E^- = 6e-6 V/m, E^- = 9e-6 V/m. For B = 0.15 T, the increase rates were evaluated in the order as 1.39%, 2.78%, 4.17% by the increase of applied E^+ = 3e-6 V/m, E^+ = 6e-6 V/m, E^+ = 9e-6 V/m and the decrease rates are determined as 1.46%, 2.94%, 4.32% by the appliance of E^- = 3e-6 V/m, E^- = 6e-6 V/m, E^- = 9e-6 V/m. Increase in Nusselt number was mentioned in ref. [51, 84] as Nusselt number increases in the presence of magnetic field.

4.1.4. Duct Flow under the Imposed Magnetic and Electrical Field

This part of the study cares about the effect of imposed electrical field together with constantly applied magnetic field induction on hydrodynamic, thermopysical properties and heat transfer of the electrical conductive liquid lithium flow while heating with a constant wall temperature model. Studied duct model was given in Figure 4.28. The positive (+) and negative (-) directional electrical potentials were applied while magnetic field induction was constantly being applied on the model conducting walls through the -y direction. Fluid flow estimated in the + x direction.

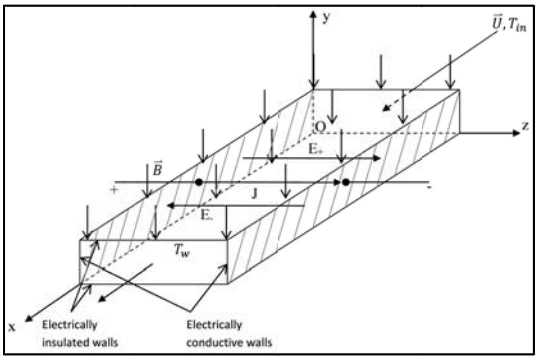

Figure 4.28. Duct model.

The evaluated first hydrodynamic parameter of the duct flow is the velocity and combined effect of magnetic and electrical field on the parameter is visualised in Figure 4.29.

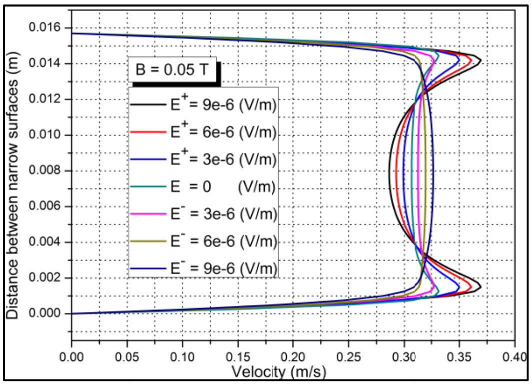

a) B = 0.05 T

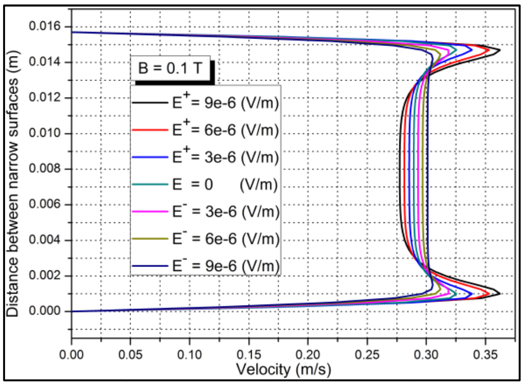

b) B = 0.1 T

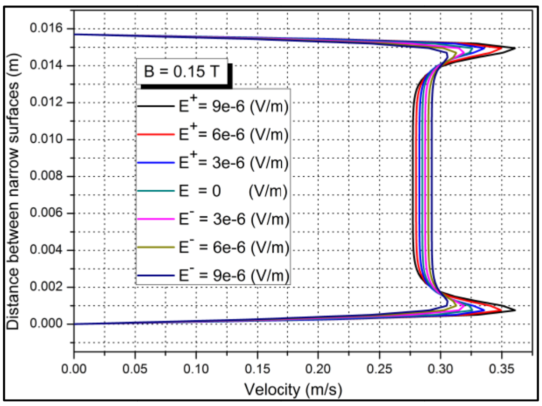

c) B = 0.15 T

Figure 4.29. Local flow velocity under the magnetic and electrical field.

Figure 4.29 illustrates that liquid lithium flow velocity decreases by the application and increase of magnetic field. Application of electrical field together with magnetic field boosts or lessens the magnetic effects on the flow velocity due to the direction of the electrical field. In case of the application of electrical field in negative direction, the created Lorentz force that is in same direction with the flow velocity shows the supporting effect to the flow. In reverse directional application of electrical field that creates the Lorentz force through the backward direction of flow stream causes a resistance against to flow. The decrease rates of flow velocity were determined as 0.13%, 0.18%, 0.23% while magnetic field was B = 0.05 T and electrical field was being applied with values are E^+ = 3e-6 V/m, E^+ = 6e-6 V/m, E^+ =9e-6 V/m. Application of electrical field in the opposite direction with values that are E^- = 3e-6 V/m, E^- = 6e-6 V/m, E^- = 9e-6 V/m enhance the flow velocity and the increase rates that are in the order as 0.12%, 0.22%, 0.42%. For B = 0.1 T, the decrease rates that are 0.11%, 0.16%, 0.21% by the increase of E^+ and increase rates that are 0.11%, 0.21%, 0.39% by the increase of E^-. For B = 0.15 T, the decrease rates that are 0.06%, 0.09%, 0.16% by the increase of E^+ and increase rates that are 0.06%, 0.17%, 0.31% by the increase of E^-. In ref. [96], it is determined that velocity is reduced considerably with a rise in Hartmann number. Also, the effect of magnetic field is clarified in ref. [70] as increase in magnetic parameter leads to decrease flow velocity.

The static pressure through the centreline of the model is investigated in Figure 4.30.

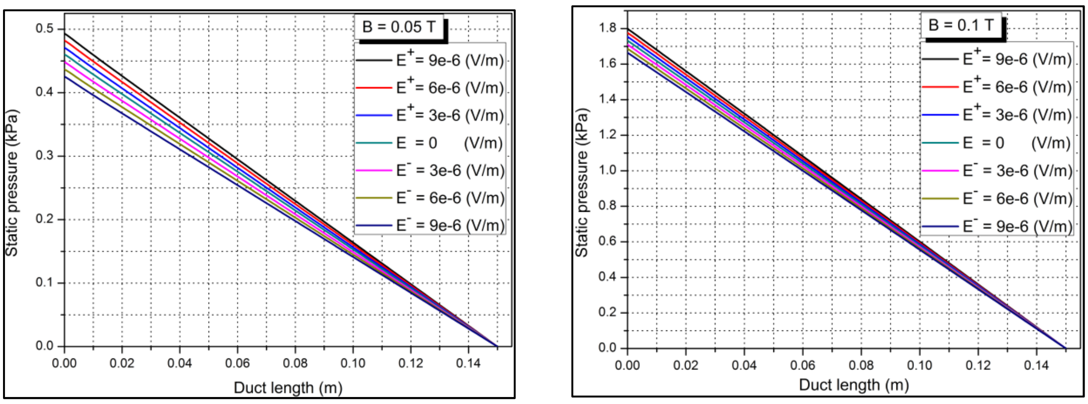

a) B = 0.05 T b) B = 0.1 T

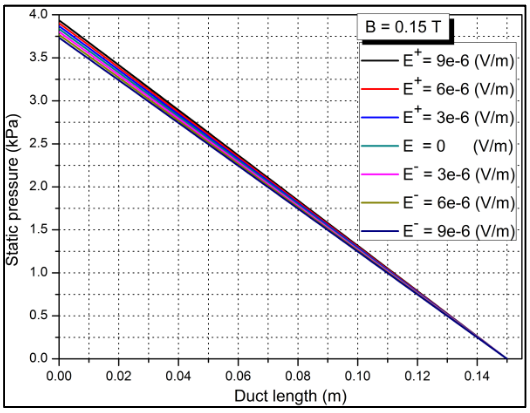

c) B = 0.15 T

Figure 4.30. Central static pressure under the magnetic and electrical field.

Figure 4.30 show that static pressure increases by the increase of electrical field in positive direction. If the field direction change and increases, the static pressure decreases. The increase and decrease rates were calculated statistically for each applied constant magnetic field induction values together with changing electrical field intensities. For B = 0.05 T, electrical field was applied with values are $E^{\pm}$=3e-6 V/m, $E^{\pm}$=6e-6 V/m, $E^{\pm}$=9e-6 V/m and the rates of increase in static pressure determined as 2.25%, 4.75%, 7.09% and the decrease rates in static pressure are determined as 2.71%, 5.21%, 7.69% by the change of direction of electrical field. In case of applied magnetic field with constant value is B = 0.1 T, electrical field was applied with values are $E^{\pm}$=3e-6 V/m, $E^{\pm}$=6e-6 V/m, $E^{\pm}$=9e-6 V/m, the positive directional application of electrical field increased the central static pressure with rates that are 1.31%, 2.65%, 3.97% and reverse directional application of electrical field decreased the central static pressure with rates that are 1.26%, 2.54%, 3.84%. Lastly for externally applied magnetic field is B = 0.15 T, positive directional application of electrical field enhanced the effect of magnetic field and so central static pressure is increased with the rates that are 0.87%, 1.74%, 2.63%. Applied electrical field in negative direction decrease the influence of magnetic field and the pressure decreased with the rates that are 0.87%, 1.76%, 2.65%. In ref. [12], it is argued that pressure gradient increases with increase of Hartmann number.

Local dynamic pressure was taken into account in Figure 4.31.

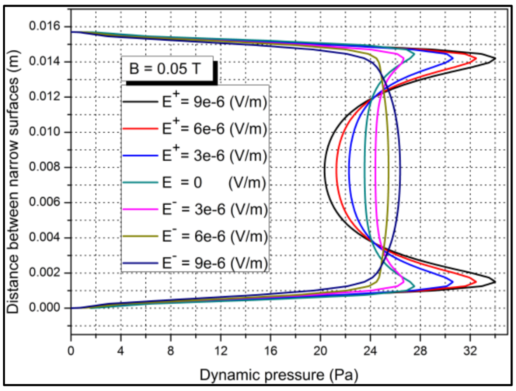

a) B = 0.05 T

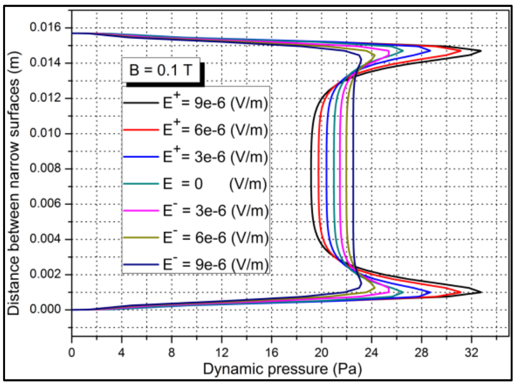

b) B = 0.1 T

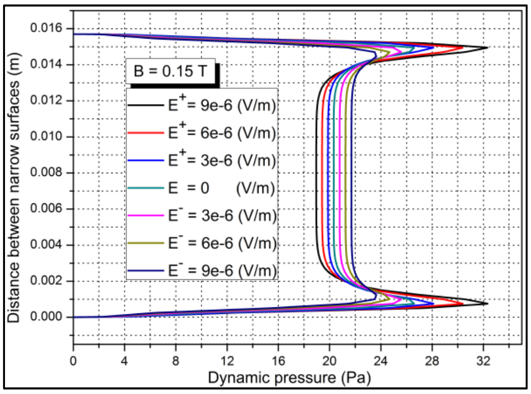

c) B = 0.15 T

Figure 4.31. Local dynamic pressure under the magnetic and electrical field.

Figure 4.31 shows that constantly applied magnetic field effect would be developed or weaken by the externally applied magnetic field. Positive directional electrical field that is from E^+ = 3e-6 to E^+ = 9e-6 enhances the effect of magnetic field. The rates of enhancement are 0.12%, 0.22%, 0.42% for constantly applied B = 0.05 T, 0.11%, 0.21%, 0.39% for B = 0.1 T and 0.006%, 0.013%, 0.02% for B = 0.15 T. Negative directionally applied electrical field dominates the effect of constantly applied magnetic field with different rates. The rates of reduction in local dynamic pressure are 0.13%, 0.18%, 0.23% for B = 0.05 T, 0.11%, 0.16%, 0.21% for B = 0.1 T and 0.005%, 0.009%, 0.011% for B = 0.15 T. In ref. [31], it is mentioned that increase in magnetic field strength increases the reverse directional Lorentz force on flow domain an so reactional force against the flow decreases the local dynamic pressure.

The given Figure 4.32 demonstrates the skin friction coefficient and the variation of it by imposed magnetic and electrical field.

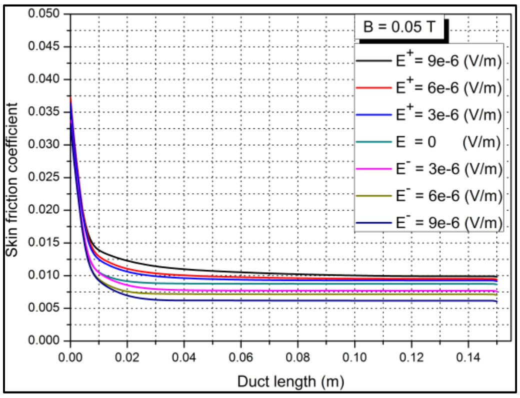

a) B = 0.05 T

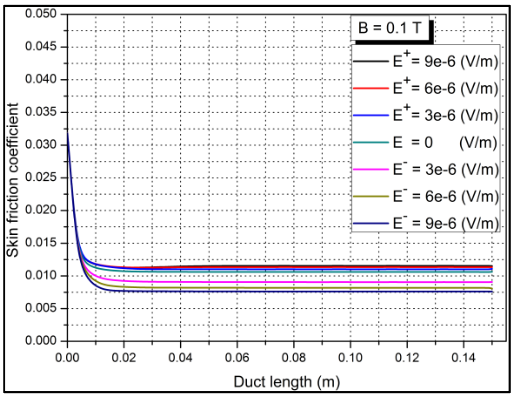

b) B = 0.1 T

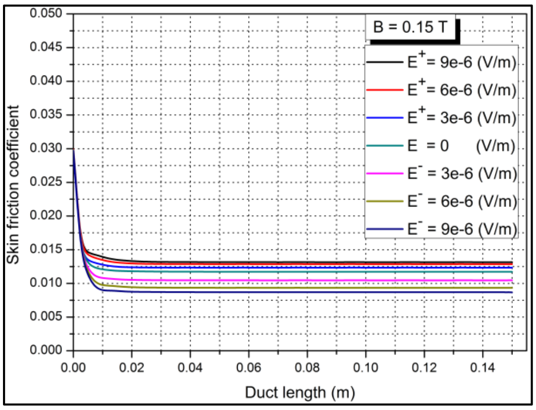

c) B = 0.15 T

Figure 4.32. Skin friction coefficient under the magnetic and electrical field.

Figure 4.32 presents that externally applied positive directional electrical field creates the increasing effect on the effect of constantly applied magnetic field and so friction coefficient increases more and more. Negative directionally applied external electrical field weaken the magnetic force which is created by magnetic field and skin friction coefficient decreases. Decrease rates are determined as 9.29%, 15.92%, 24.97% for the applied magnetic field B = 0.05 T together with electrical field that is from E^- = 3e-6 V/m to E^- = 9e-6 V/m. Decrease rates are 13.27%, 20.09, 25.92% for B = 0.1 T and electrical field are that are from E^- = 3e-6 V/m to E^- = 9e-6 V/m. Decrease rates are 10.23%, 19.07%, 24.38% for B = 0.15 T and electrical field are that are from E^- = 3e-6 V/m to E^- = 9e-6 V/m. Positive directionally applied electrical field with values are that are from E^+ = 3e-6 to E^+ = 9e-6, increased the skin friction with different rates that are 8.79%, 12.6%, 19.14% for B = 0.05 T, 3.74%, 6.18%, 7.47% for B = 0.1 T, and lastly 4.76%, 9.27%, 11.84% for B = 0.15 T. In ref. [75, 80], it is argued that increase in magnetic parameter increases the skin friction coefficient.

Shear stress between streamlines was evaluated in Figure 4.33.

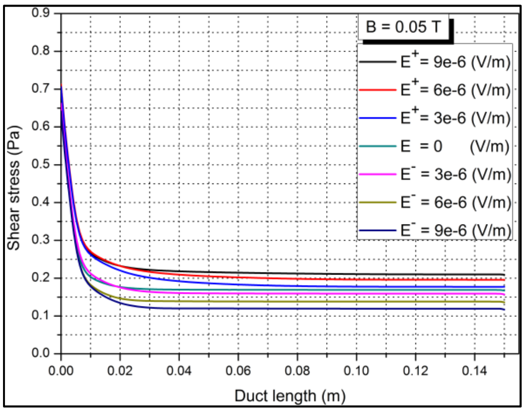

a) B = 0.05 T

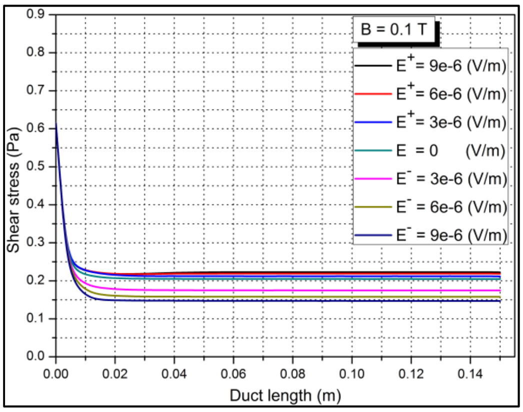

b) B = 0.1 T

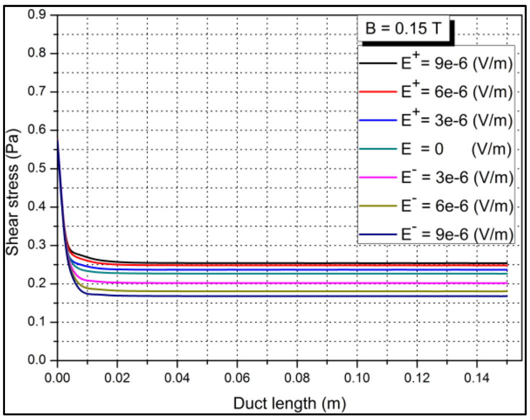

c) B = 0.15 T

Figure 4.33. Shear stress under the magnetic and electrical field.

Increase in positive directionally applied electrical field increases the shear stress as seen in Figure 4.33. Negative directionally applied electrical field decreases the shearing that is between flow lines as seen in Figure 4.33. The average of shear stress dedicated that increase in positive directional electrical field increases the shearing with rates that are 8.79%, 12.6%, 19.14% during the application of B = 0.05 T. Increases with rates that are 3.74%, 6.18%, 7.47% for B = 0.1 T and increases with rates that are 4.76%, 9.27%, 11.84% for B = 0.15 T. The decrease rates of shearing are 9.29%, 15.92%, 24.97% by negative directionally applied electrical field. Decrease rates are 13.27%, 20.09%, 25.92% for B = 0.1 T, lastly the decrease rates of shear stress are 10.23%, 19.07%, 24.38% for B = 0.15 T. Decrease in shear stress between flow lines evaluated in ref. [23, 106] as shear stress and heat transfer increase with the magnetic parameter.

Temperature distribution was examined through the centreline of the duct under the applied of magnetic and electric field. For each constant value of magnetic field inductions that are B = 0.05 T, B = 0.1 T, B = 0.15 T, the electrical field was applied with values that are $E^{\pm}$ = 3e-6 V/m, $E^{\pm}$ = 6e-6 V/m, $E^{\pm}$ = 9e-6 V/m. The temperature distribution is seen in Figure 4.34 for the heating flow condition of lithium with constant wall temperature.

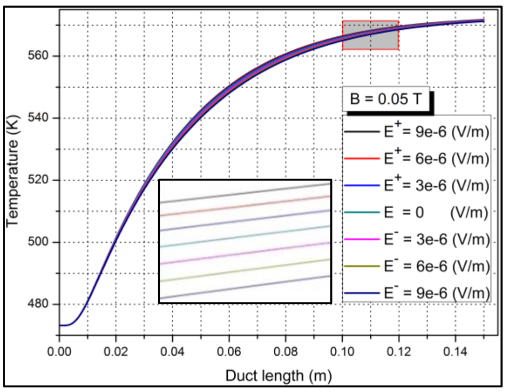

a) B = 0.05 T

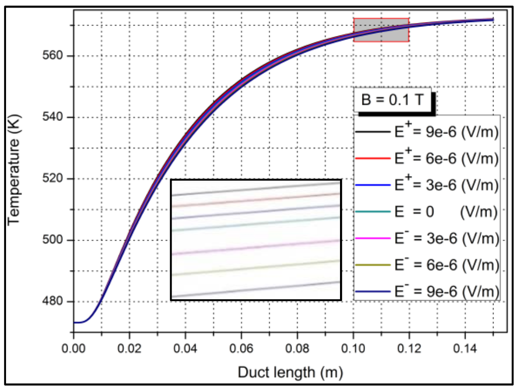

b) B = 0.1 T

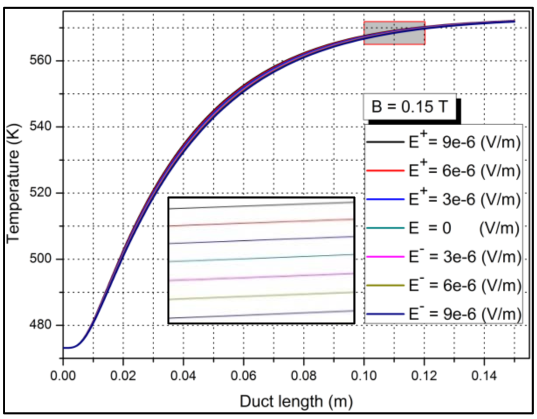

c) B = 0.15 T

Figure 4.34. Central temperature under the magnetic and electrical field.

Figure 4.34 presents that, the temperature values were increased by the increase of applied E^+ field whereas the axial temperature values were decreased by the appliance of the E^- for each constant magnetic field induction. While applying B = 0.05 T, increase rates of temperature were determined in the order as 0.02%, 0.05%, 0.07% by the appliance of E^+ = 3e-6 V/m, E^+ = 6e-6 V/m, E^+ = 9e-6 V/m and the temperature values decreased with the rates that are 0.06%, 0.12%, 0.17% by the appliance of E^- = 3e-6 V/m, E^- = 6e-6 V/m, E^- = 9e-6 V/m. Similarly, while B = 0.1 T was being applied, the increase rates were evaluated in the order as 0.04%, 0.06%, 0.13% for E^+ = 3e-6 V/m, E^+ = 6e-6 V/m, E^+ = 9e-6 V/m, and the decrease rates were evaluated as 0.04%, 0.09%, 0.14% by the appliance of E^- = 3e-6 V/m, E^- = 6e-6 V/m, E^- = 9e-6 V/m. Lastly, under the effect of B = 0.15 T, the increase rates were specified in the order as 0.05%, 0.07%, 0.15% by the appliance of E^+ = 3e-6 V/m, E^+ = 6e-6 V/m, E^+ = 9e-6 V/m and the temperature values were decreased as 0.03%, 0.07%, 0.10% by the appliance of E^- = 3e-6 V/m, E^- = 6e-6 V/m, E^- = 9e-6 V/m. Similar case determined in ref. [10, 27] as temperature increases with increasing magnetic field.

Temperature profile was represented at thermal fully developed region in which the 0.12 m of the model length in Figure 4.35. For each magnetic field induction values are B = 0.05 T, B = 0.1 T, B = 0.15 T, the electrical field was applied with values that are $E^\pm$ = 3e-6 V/m, $E^\pm$ = 6e-6 V/m, $E^\pm$ = 9e-6 V/m in the positive and negative directions.

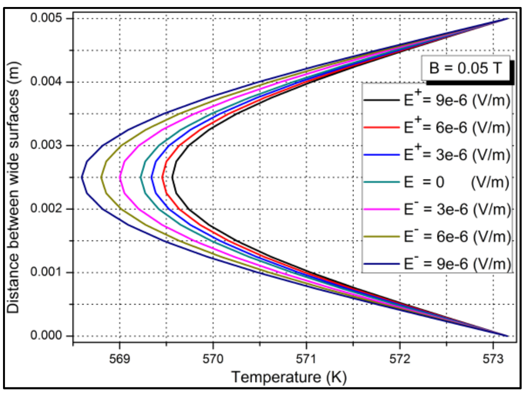

a) B = 0.05 T

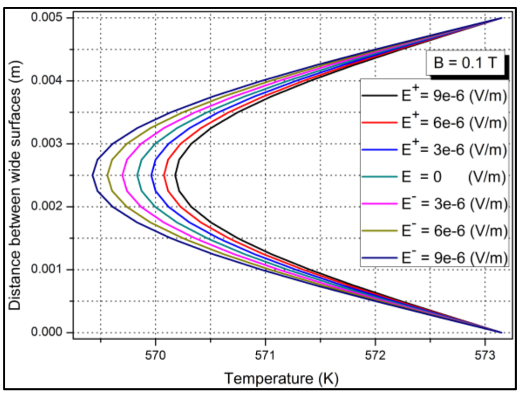

b) B = 0.1 T

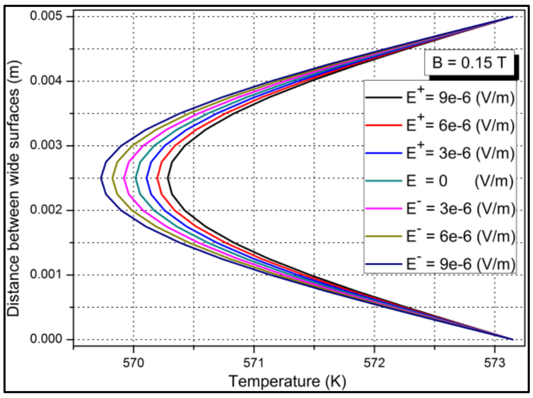

c) B = 0.15 T

Figure 4.35. Local temperature under the magnetic and electrical field.

Figure 4.35 clarifies that the impact of the applied electrical field on the local temperature distribution of flow domain under the influence of applied constant magnetic field induction. While magnetic field was applied as B = 0.05 T, the local temperature was increased by the increase of electrical field intensity as E^+ = 3e-6 V/m, E^+ = 6e-6 V/m, E^+ = 9e-6 V/m. In the same order, the increase rates were acquired as 0.01%, 0.02%, and 0.03%. The decrease rates of temperature were evaluated as 0.02%, 0.04%, 0.07% by the appliance of E^- = 3e-6 V/m, E^- = 6e-6 V/m, E^- = 9e-6 V/m. The increase rates were evaluated as 0.01%, 0.02%, 0.03% by the increase of electrical field intensity as E^+ = 3e-6 V/m, E^+ = 6e-6 V/m, E^+ = 9e-6 V/m, and the decrease rates of temperature are 0.01%, 0.03%, 0.04% for E^- = 3e-6 V/m, E^- = 6e-6 V/m, E^- = 9e-6 V/m for constantly applied B = 0.1 T. During the appliance of B = 0.15 T, the temperature increase rates were evaluated as 0.01%, 0.02%, 0.03% by the increase the electrical field as E^+ = 3e-6 V/m, E^+ = 6e-6 V/m, E^+ = 9e-6 V/m, and the temperature were decreased with rates that are 0.01%, 0.02%, 0.03% by the appliance of opposite directional electrical field as E^- = 3e-6 V/m, E^- = 6e-6 V/m, E^- = 9e-6 V/m. In ref. [108, 138], it is determined that temperature increases with the increase in magnetic field.

The variation of Nusselt number at the adjacent region of the duct wall through the duct length was expired under the effect of normally applied magnetic field induction values that are B = 0.05 T, B = 0.1 T, B = 0.15 T and electrical field intensity values that are as $E^{\pm}$ = 3e-6 V/m, $E^{\pm}$ = 6e-6 V/m, $E^{\pm}$ = 9e-6 V/m and visualised in Figure 4.36.

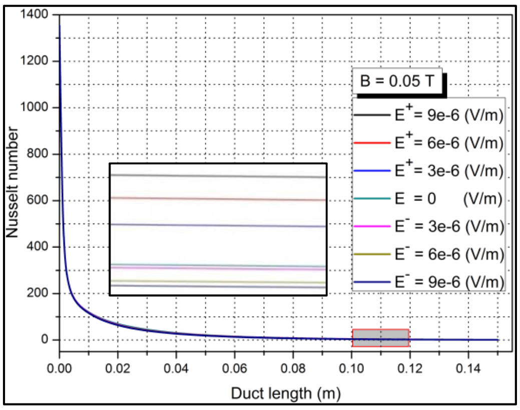

a) B = 0.05 T

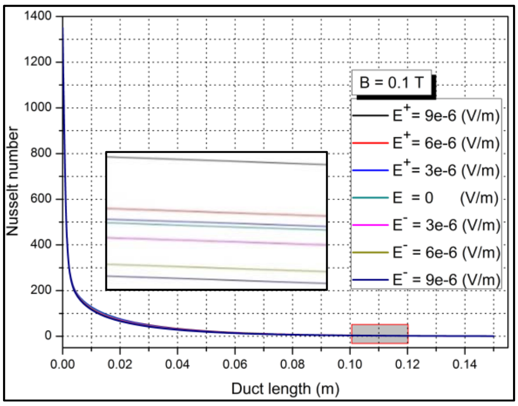

b) B = 0.1 T

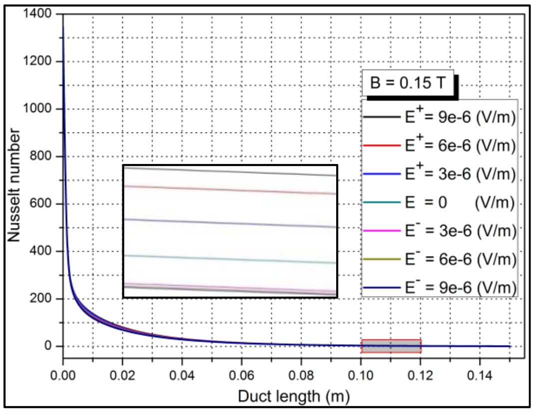

c) B = 0.15 T

Figure 4.36. Nusselt number under the magnetic and electrical field.

Figure 4.36 shows that increase in electrical field intensity in positive direction enhances the influence of the applied magnetic field and so the Nusselt number increases for each value of E^+. By the change of the direction of electrical field intensity through the negative direction, Nusselt number decreases for each E^- value. While applying the magnetic field induction with the value is B = 0.05 T, the increase rates of Nusselt number were determined as 0.03%, 0.16%, 0.20% for each value of E^+ = 3e-6 V/m, E^+ = 6e-6 V/m, E^+ = 9e-6 V/m and the decrease rates were determined as 1.69%, 2.85%, 3.98% by the appliance of electrical field in the opposite direction with the values that are E^- = 3e-6 V/m, E^- = 6e-6 V/m, E^- = 9e-6 V/m. In case of application of B = 0.1 T, increase in Nusselt number were evaluated as 1.20%, 1.87%, 2.42% by the appliance of E^+ = 3e-6 V/m, E^+ = 6e-6 V/m, E^+ = 9e-6 V/m and the Nusselt number was decreased with the rates are 1.65%, 3.03%, 4.29% by the appliance of E^- = 3e-6 V/m, E^- = 6e-6 V/m, E^-= 9e-6 V/m. Nusselt number were increased about 1.36%, 2.32%, 3.36% by the increase of applied E^+ =

3e-6 V/m, E^+ = 6e-6 V/m, E^+ = 9e-6 V/m, and Nusselt number was decreased with rates that are 1.38%, 2.67%, 3.80% in case of appliance of E^- = 3e-6 V/m, E^- = 6e-6 V/m, E^- = 9e-6 V/m for B = 0.15 T. In ref. [58, 84], it is mentioned that Nusselt number increases in the presence of magnetic field.

4.2. TURBULENT FLOW

In this section of this dissertation, turbulent steady state incompressible magnetoviscous internal flow of liquid lithium was investigated by ANSYS Fluent 15.0 software MHD module in constant wall temperature models which are circular pipe and rectangular duct. Turbulent flow case was solved by k-epsilon-realizable model with considering enhanced wall treatment. Spatial discretization type was used Least Squares Cell based second order solution. Circular pipe and rectangular duct models were used to realise the effect of magnetic and electrical field on different geometrical conduit flows. Also, magnetic field and combined with electrical field effect were studied separately. Due to the Lorentz force expression that is F = q(E+UxB), magnitude of created magnetic force on conductive fluid body is directly depend on the magnetic field induction and electrical field intensity. Direction of the electrical field directly influences the magnitude of the created Lorentz force. "+" positive directional electrical field enforces the magnetic field induction and enlarges the value of created reverse directional magnetic force that is on the flow domain. Also, "-" negative directional electrical field weaken the impact of magnetic field and causes the creation of lower magnetic force that is against the flow domain. In this respect, this section of the study was presented in four subgroups. In first subgroup of this section effects of externally applied magnetic field that are B = 0 T, B = 0.4 T, B = 0.5 T and B = 0.6 T on hydrodynamic, thermophysical flow parameters and heat transfer of liquid lithium was investigated for circular pipe turbulent flow. In the second subgroup, effects of externally applied magnetic field that are B = 0 T, B = 0.4 T, B = 0.5 T and B = 0.6 T on hydrodynamic, thermophysical flow parameters and heat transfer of liquid lithium was studied for rectangular duct turbulent flow. In the third subgroup, combined effect of externally applied magnetics and electrical field on hydrodynamic, thermophysical flow parameters and heat transfer was studied during magnetic field was being constantly imposed and electrical field applied with values that are $E^{\pm}$ = 3e-5 V/m, $E^{\pm}$ = 6e-5 V/m, $E^{\pm}$ = 9e-5 V/m for circular pipe turbulent flow case. In the fourth subgroup, combined effect of externally applied magnetics and electrical field on hydrodynamic, thermophysical flow parameters and heat transfer of liquid lithium rectangular duct flow was studied during the magnetic field was being constantly imposed and electrical field applied with values are $E^{\pm}$ = 3e-5 V/m, $E^{\pm}$ = 6e-5 V/m, $E^{\pm}$ = 9e-5 V/m.

4.2.1. Pipe Flow under the Imposed Magnetic Field

Turbulent steady state incompressible magnetoviscous liquid lithium flow in a circular pipe was studied in this section. Pipe model, boundary conditions and applied magnetic field induction are illustrated in Figure 4.37.

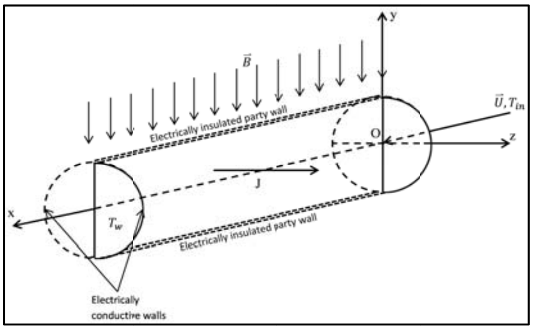

Figure 4.37. Circular pipe model.

Model constant wall temperature that is T_w = 573.15 K, inlet liquid velocity that is U = 0.75 m/s and inlet flow temperature that is T_i = 473.15 K. Liquid lithium turbulent flow was studied in a constant wall temperature boundary model under the transversely applied magnetic field.

Normally applied external magnetic field shows the adverse effect on the flow velocity because of created Lorentz force that is in the reverse direction to the flow regime. Figure 4.38 illustrates the argued treatment for constantly applied magnetic field value.

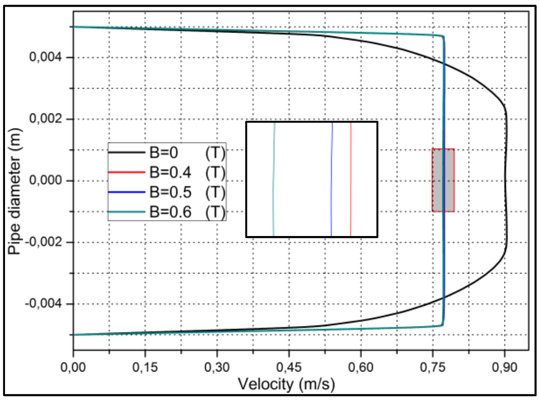

Figure 4.38. Local flow velocity under the magnetic field.

Local flow velocity profiles were compared at 0.12 m of the pipe length under the effect of magnetic field induction values that are B = 0 T, B = 0.4 T, B = 0.5 T and B = 0.6 T. Figure 4.38 shows that increase in magnetic field induction damps the local flow velocity. The flow velocity is depressed by the created Lorentz force because of the applied magnetic field and so turbulent fluctuations and velocity decreases. The hydrodynamic boundary layer thickness and average velocity is decreased by the increase of magnetic field induction. B=0 T was accepted as a reference state and achieved a statistical analysis to identify the decrease rates of local flow velocity values. Decrease rates of local velocity was specified approximately as 6.93% for B = 0.4 T, 6.95% for B = 0.5 T, and 7.12% for B = 0.6 T. In ref. [36, 39], it is discussed that velocity decreases with the increase in Hartmann number.

Externally applied normal magnetic field on electrically conductive fluid flow creates an opposite force that is against to the flow direction. So, the opposite force means the back pressure on the flow domain. Variation of static pressure through the central axis of the pipe by the appliance of magnetic field induction with the values that are B = 0 T, B = 0.4 T, B = 0.5 T, B = 0.6 T is presented in Figure 4.39.

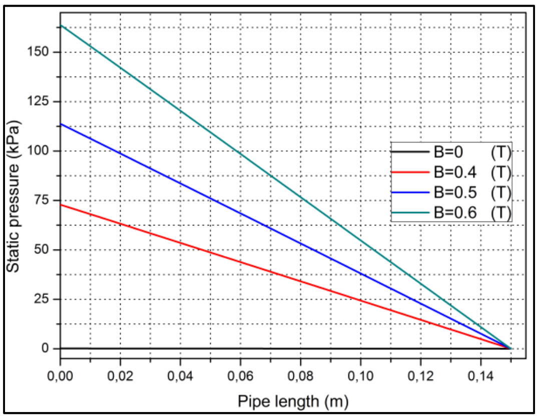

Figure 4.39. Central static pressure under the magnetic field.

Figure 4.39 displays that central static pressure was increased by the increase of magnetic field induction. Increase rates of statistic pressure are determined as about 73,376%, 114,646% and 165,086% by the application of magnetic field with values that are B = 0 T, B = 0.4 T, B = 0.5 T, B = 0.6 T. Similar case determined in ref. [44, 70] as pressure rise increases with an increase in magnetic parameter.

The dynamic pressure of flow domain was observed at 0.12 m of the pipe length and dynamic pressure is seen in Figure 4.40.

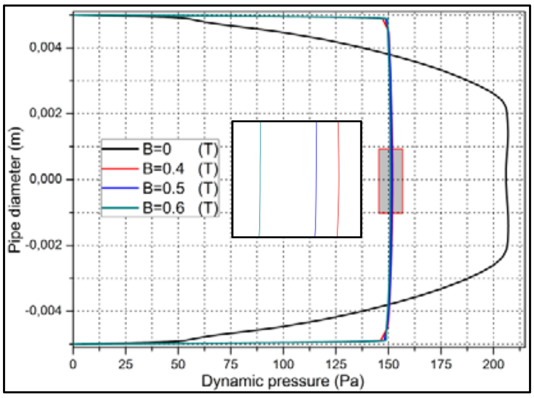

Figure 4.40. Local dynamic pressure under the magnetic field.

Figure 4.40 designates that increase in magnetic field causes the reduction of the dynamic pressure which is the dependent hydrodynamic parameter to the flow velocity. The decrease rates of dynamic pressure are 13.02%, 13.03%, 13.31% by the increase of magnetic field intensity from B = 0 T to B = 0.6 T. In ref. [31], it is concluded that increase in Lorentz force by the increase of magnetic field strength the dynamic pressure decreases.

Skin friction coefficient was observed under the effect of magnetic field at the adjacent region of the pipe wall through the model length and the obtained data is seen in Figure 4.41.

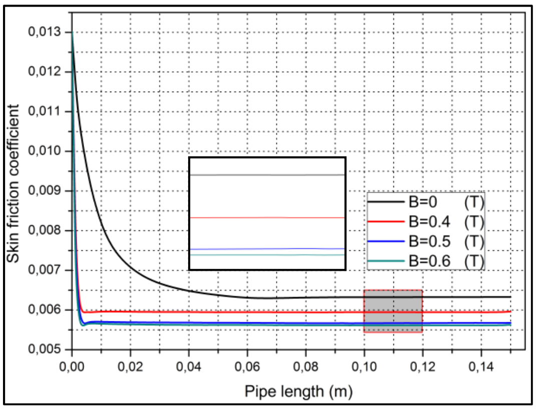

Figure 4.41. Skin friction coefficient under magnetic field.

Figure 4.41 designates that skin friction coefficient decreases by the increase of magnetic field induction. By taking of B = 0 T as a reference, achieved a statistical analysis to determine the decrease rates of skin friction coefficient by the increase of magnetic field induction. Skin friction coefficient decreases with rates that are 6.06% for B = 0.4 T, 10.44% for B = 0.5 T, and 11.35% for B = 0.6 T by the increase of constantly applied magnetic field. In ref. [100, 130], it is determined that skin friction coefficient decreases as the magnetic parameter.

Magnetic field effects the skin friction coefficient and so shearing that is between the flow lines. Shear stress under the effect of magnetic field was investigated by taking data from the adjacent region of the model wall through the pipe length and taken data is presented in Figure 4.42.

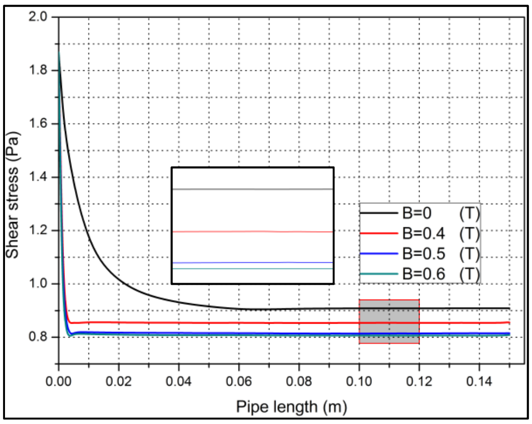

Figure 4.42. Shear stress under the magnetic field.

As seen in Figure 4.42, shear stress that is between the flow lines decreases by the increase of magnetic field induction and the decrease rates of shear stress were determined by statistically for further increase of magnetic field induction that is from B = 0.4 T to B = 0.6 T. The average value of shear stress decreases about is 10.57 % for B = 0.4 T, 14.67 % for B = 0.5 T and 15.55 % for B = 0.6 T. Shear stress decreases with the increase of the magnetic parameter in ref. [126, 141].

Variation the temperature of liquid lithium was studied by the effect of externally applied magnetic field for magnetic field induction values are B = 0 T, B = 0.4 T, B = 0.5 T, B = 0.6 T, and taken data was evaluated. Due to this examination, temperature of the liquid lithium that is at the central region of pipe through pipe length under the influence of externally applied magnetic field is visualized in Figure 4.43.

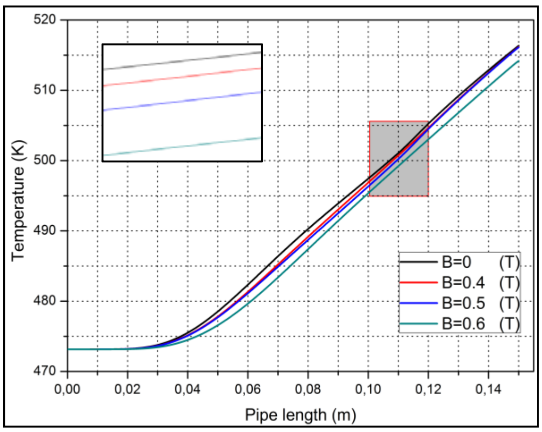

Figure 4.43. Central temperature under the magnetic field.

Liquid metal central temperature was decreased through the pipe length by the increase of magnetic field as seen in Figure 4.43. The percentage of temperature decrease rates were evaluated for the magnetic induction values that are B = 0.4 T, B = 0.5 T, B = 0.6 T by taking the B = 0 T as a reference and estimation rates that are presented in the same order as 0.10%, 0.14%, 0.35%. Studies are ref. [62, 81] from the literature summarized that temperature of the fluid flow domain decreases with the increasing values of the magnetic parameter.

Magnetic effects on the local temperature of flowing liquid lithium was studied and taken local temperature data that is from 0.12 m thermally fully developed region of the model is seen in Figure 4.44.

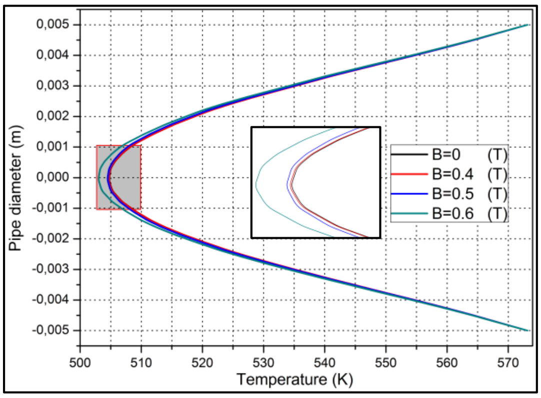

Figure 4.44. Local temperature under the magnetic field.

Figure 4.44 could be interpreted as local liquid lithium temperature decreases by the increase of magnetic field induction from B = 0.4 T to B= 0.6 T. Decrease rates were determined by statistical analyses for further increase of magnetic field induction. B = 0 T was determined as a reference state and so the decrease rates were evaluated as 0.007%, 0.05%, 0.15% in the range of applied magnetic field induction. It is concluded that in ref. [91, 109] with the increase of the Hartmann number temperature in the channel decreases.

The variation of Nusselt number was examined under the effect of perpendicularly applied magnetic field at the adjacent region of the pipe wall through the length of pipe model. Change of Nusselt number is demonstrated in Figure 4.45 by the appliance of magnetic field induction values that are B = 0 T, B = 0.4 T, B = 0.5 T, B

= 0.6 T in regard to the heating of flowing liquid lithium by a constant wall temperature.

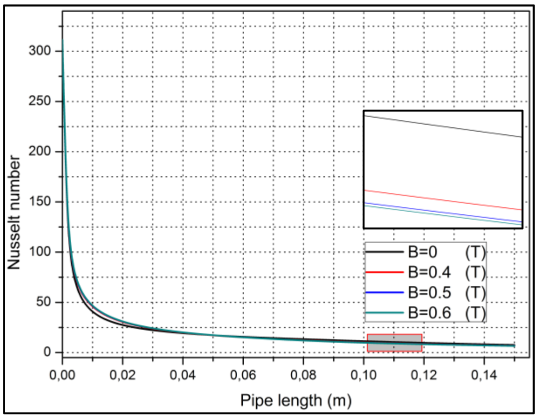

Figure 4.45. Nusselt number under the magnetic field.

As seen in Figure 4.45, Nusselt number decreases by the increase of applied magnetic field induction. By taking B = 0 T as a reference, achieved a statistical analysis to determine the decrease rates of average Nusselt number by the increase of magnetic field induction. Under the effect of magnetic field, the decrease rates are determined as 0.84% for B = 0.4 T, 1.07% for B = 0.5 T, and 1.18% for B = 0.6 T. In ref. [88, 111], it is clarified that convective heat transfer and hence the Nusselt number decreases by perpendicularly applied magnetic field due to reduction in turbulent fluctuations with increase of magnetic field. Decrease in Nusselt number means that the decreases of heat transfer. The reason of this situation is discussed in ref. [109, 120] as the magnitude of the velocity decreases for large values of magnetic parameter. However, this change of velocity is maximum in the near surface and minimum far away from the surface.

4.2.2. Duct Flow under the Imposed Magnetic Field

Rectangular duct turbulent steady state incompressible magnetoviscous flow condition was studied and the effect of magnetic field on hydrodynamic and thermophysical properties and heat transfer of liquid lithium flow was searched. The magnetic field was applied normally on the flow stream as seen in Figure 4.46.

The studied duct model with boundary conditions was illustrated in Figure 4.46.

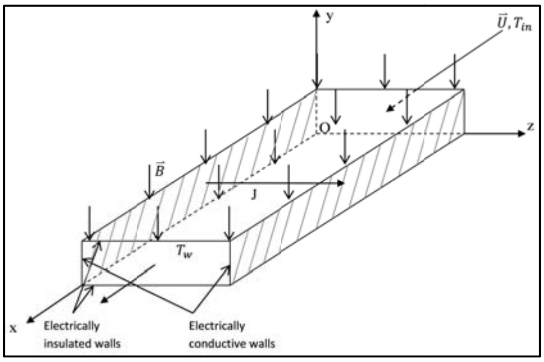

Figure 4.46. Duct model.

Local flow velocity of the liquid lithium within the effect of constantly applied magnetic field was observed by taking data from the 0.12 m of the model. In this scope, the velocity data was taken through the distance of narrow model surfaces. Local velocity data is visualized in Figure 4.47.

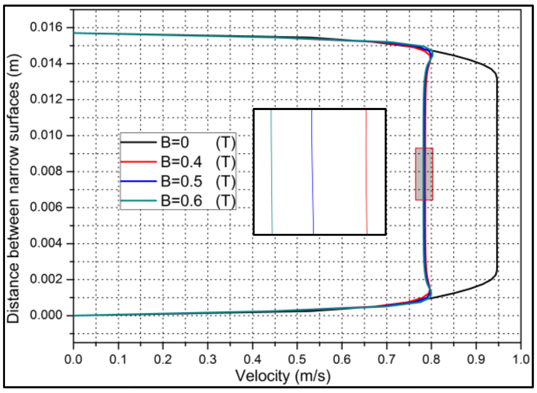

Figure 4.47. Local flow velocity under the magnetic field.

Figure 4.47 clarifies that the local flow velocity decreases by the effect of applied magnetic field. The local flow velocity behaves similar characteristics as pipe flow. The local flow velocity and turbulent fluctuations dominated by magnetic forces. Average local flow velocity calculated and seen that the average value of it was decreased by the increase of magnetic field induction that is from B = 0 T to B = 0.6 T. Decrease rates are about 14.82%, 14.87%, and 14.9% for B = 0.4 T, B = 0.5 T and B = 0.6 T. In ref. [77, 110], it is discussed that magnetic field was found to annihilate turbulence followed by flattening of the velocity profile.

Magnetic field effect on static pressure was investigated through the central axis of the model and taken data that is from the model central axis is presented in Figure 4.48.

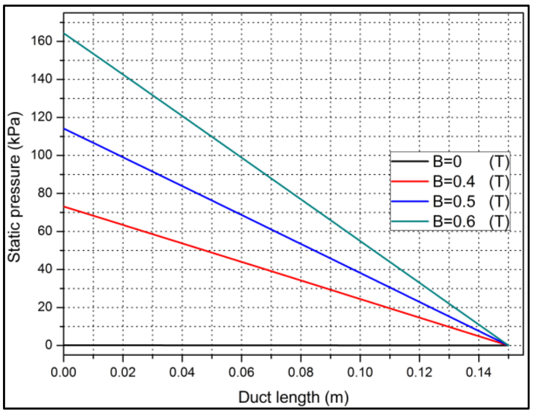

Figure 4.48. Central static pressure under the magnetic field.

Figure 4.48 shows that central static pressure of the model increases by the increase of magnetic field induction. Increase rates of the static pressure were evaluated as 59,872%, 93,532% and 134,675% for each constant value of magnetic field inductions are B = 0.4 T, B = 0.5 T and B = 0.6 T at the central region of the flow model. In ref. [95, 140], it is concluded that applied Lorentz force on to the flow produced a static pressure increase.

The local dynamic pressure was observed to determine the effect of magnetic field and is presented in Figure 4.49.

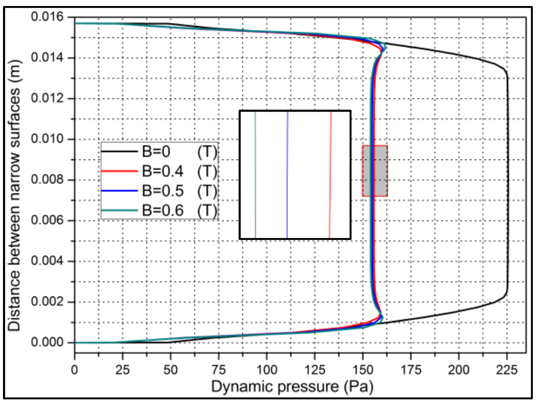

Figure 4.49. Local dynamic pressure under the magnetic field.

Figure 4.49 shows that increase in magnetic field induction affected the dynamic pressure inversely because of the created Lorentz force. The local dynamic pressure decrease rates were determined as 27.78%, 27.89%, 27.95% by the increase of magnetic field from B = 0 T to B = 0.6 T. It is known theoretically that the dynamic pressure is the directly dependent parameter to flow velocity and so decrease in flow velocity is discussed in ref. [36, 39] as decrease in velocity by the increase of Hartmann number, decreases the local dynamic pressure.

Effect of magnetic field on skin friction coefficient was evaluated and is visualized in Figure 4.50.

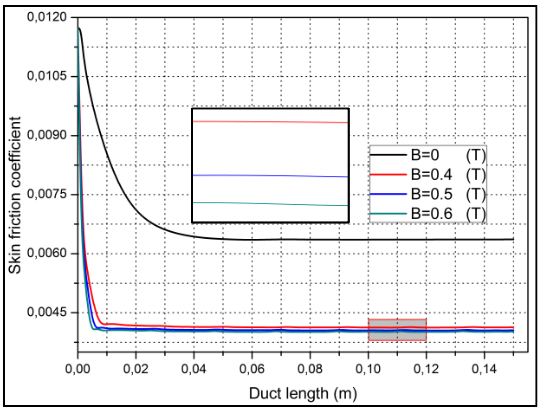

Figure 4.50. Skin friction coefficient under the magnetic field.

Figure 4.50 illustrates that increase in applied magnetic field intensity decreases the skin friction coefficient. Average value of skin friction coefficient was effected the magnetic field with variable rates. Decrease rates of skin friction coefficient were estimated as 37.28%, 38.80%, and 39.67% for each varied applied magnetic field intensity is B = 0.4 T, B = 0.5 T, and B = 0.6 T. In ref. [36, 92], it is shown that skin friction decreases with magnetic parameter.

Variation of shear stress between the flow stream lines under the influence of magnetic field was evaluated and is given in Figure 4.51.

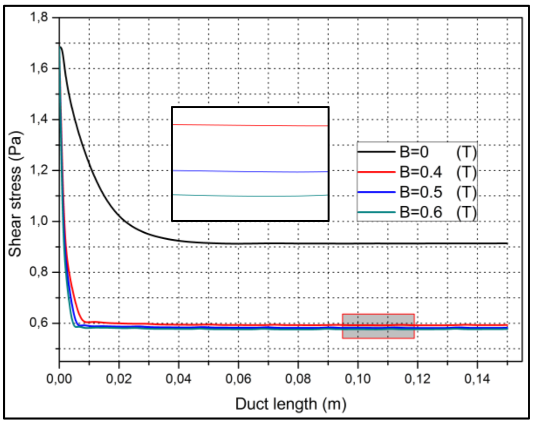

Figure 4.51. Shear stress under the magnetic field.

Figure 4.51 could be clarified with the linear relation between skin friction coefficient and shear stress. The shear stress decreases by the increase of applied magnetic field intensity. Decrease rates of average value of shear stress were determined as 37.28%, 38.8%, and 39.67%, for each constantly applied magnetic field intensity values. Results in ref. [110, 141] showed that the turbulence suppression by the magnetic field decreases the Reynolds shear stress near the wall.

Effect of magnetic field on central temperature of flowing liquid lithium was studied and taken temperature data that is from the central axis of the model through the model length is presented in Figure 4.52.

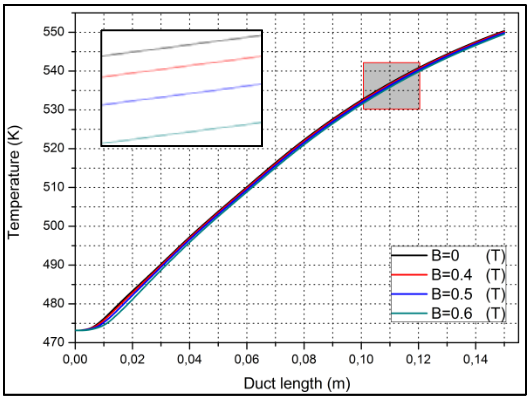

Figure 4.52. Central temperature under the magnetic field.

Central temperature of the liquid lithium was reduced by the effect of magnetic field and is presented in Figure 4.52. The reduction rates of central liquid lithium temperature are 0.05%, 0.12%, and 0.23% for applied each magnetic field intensity values are B = 0.4 T, B = 0.5 T, B = 0.6 T. Similar assessment was presented in ref. [39, 136] as magnetic field suppresses the turbulent velocity fluctuation and so temperature is decreased.

Local temperature of the flow was examined by taking local temperature data that is from the 0.12 m of thermal developed region of the model. Local liquid lithium temperature data are visualised in Figure 4.53.

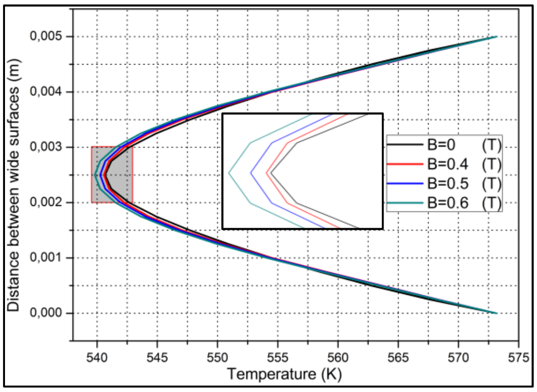

Figure 4.53. Local temperature under the magnetic field.

Figure 4.53 clarifies that application of magnetic field decreases the local temperature of the flowing liquid lithium. Average values of local temperature decrease for each step of increase of magnetic field induction with the values that are B = 0 T, B = 0.4 T, B = 0.5 T and B = 0.6 T. The decrease rates are 0.02% for B = 0.4 T, 0.03% for B = 0.5 T, and 0.08% for B = 0.6 T. Obtained results supported with the evaluation in ref. [159, 166] as temperature decreases monotonically with magnetic parameter.

Nusselt number data were taken from close region of the duct wall and variation of it was investigated through the duct length in Figure 4.54.

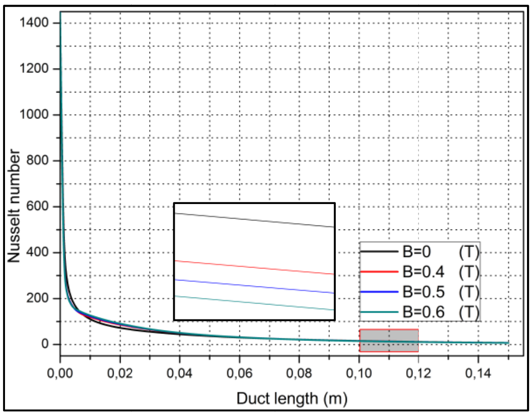

Figure 4.54. Nusselt number under the magnetic field.

Figure 4.54 designates that applied magnetic field weaken the Nusselt number. The decrease rates of Nusselt number were determined for each applied magnetic field induction values. Decrease rates are 0.52% for B = 0.4 T, 0.65% for B = 0.5 T, and 2.31% for B = 0.6 T. It could be concluded the heat transfer rate from the wall to the central axis of the model decreases by the increase of magnetic field induction. Nusselt number decrease with increase in Hartmann number in ref. [139, 153].

4.2.3. Pipe Flow under the Imposed Magnetic and Electrical Field

As seen in Figure 4.55, the pipe model was constructed with two part wall to obtain two different (+) and (-) poles. The positive and negative electric potentials were applied on these walls to create an external electrical field. Change of the poles changes the created electrical field direction from positive to negative. Magnetic field applied through the - y direction on to the pipe model. Fluid flow determined in the + x direction.

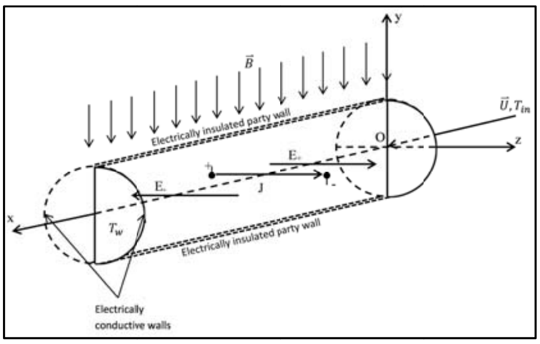

Figure 4.55. Pipe model.

The local flow velocity was examined under the effect of electrical field on flow characteristics at 0.12 m of the model and is visualised in Figure 4.56.

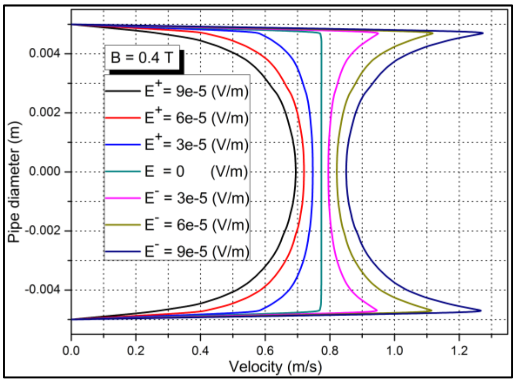

a) B = 0.4 T

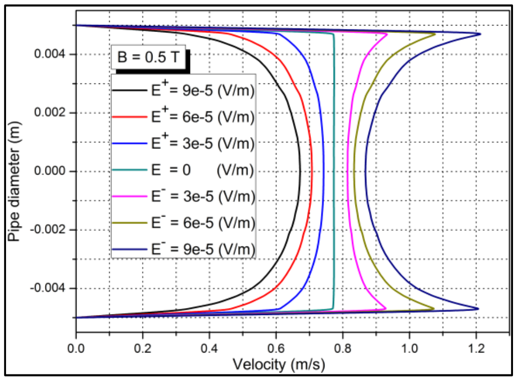

b) B = 0.5 T

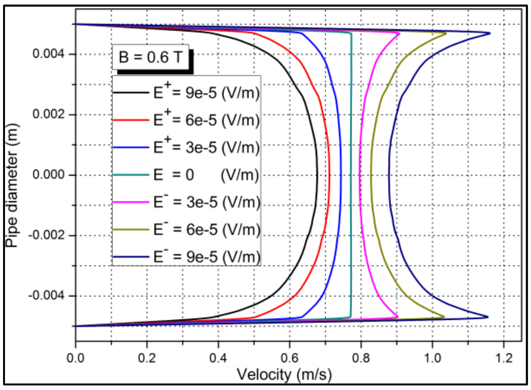

c) B = 0.6 T

Figure 4.56. Local flow velocity under the magnetic and electrical field.

It is apparent that from the Figure 4.56, the effect of magnetic field on liquid lithium flow streamlines were boosted by the increase of electrical field in positive direction (E^+). Increase of the electrical field (E^+) causes more suppression of the turbulent fluctuations and flow domain smoothness is increased and flow velocity at the close region of the pipe wall decreases, too. Changing the direction of electrical field to the opposite (E^-), the effect of magnetic field was lessened and the flow velocity and turbulent fluctuations increase and flow velocity increases at the close region of the model wall by the increase of electrical field. Similar case for turbulent flow is determined in ref. [161] as with respect to the laminar case, turbulent profiles present a dramatic decrease of the side layer velocity and a thickening of the boundary layer. For each constantly applied magnetic field value, the decrease or increase rates of local flow velocity by the variation of electrical field were estimated. The decrease rates of flow velocity are about 8.24%, 15.96%, 22.74% for B = 0.4 T and electrical field was applied in the positive direction with values that are E^+ = 3e-5 V/m, E^+ = 6e-5 V/m, E^+ = 9e-5 V/m. In other case for B = 0.4 T and electrical field was applied in the negative direction with values that are E^- = 3e-5 V/m, E^- = 6e-5 V/m, E^- = 9e-5 V/m, the velocity was increased with a rates that are 7.38%, 15.14%, 22.59%. For B = 0.5 T, the velocity decrease rates are 8.12%, 16.16%, 23.25% and increase rates that are 9.08%, 15.58% and 22.873%. For B = 0.6 T, the velocity decrease rates that are 7.17%, 14.52%, 21.27% and increase rates that are 6.74%, 14.04% and 22.21%. In ref. [164, 172], it is discussed that transverse magnetic field changes the velocity distribution in channel and suppresses turbulent pulsations.

Change of central static pressure of the fluid domain was evaluated according to demonstrated linear lines in Figure 4.57.

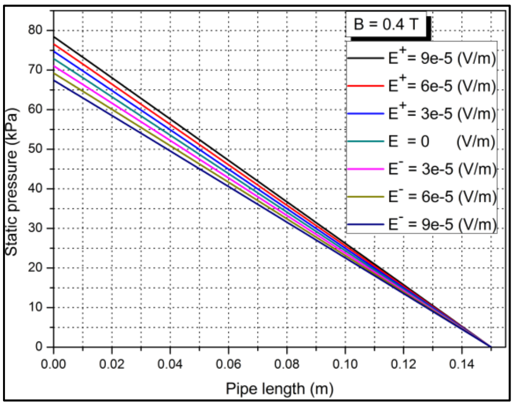

a) B = 0.4 T

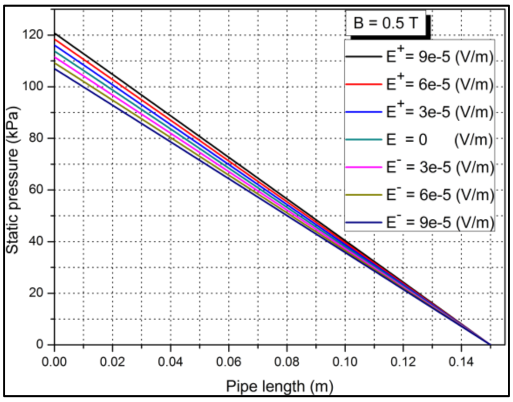

b) B = 0.5 T

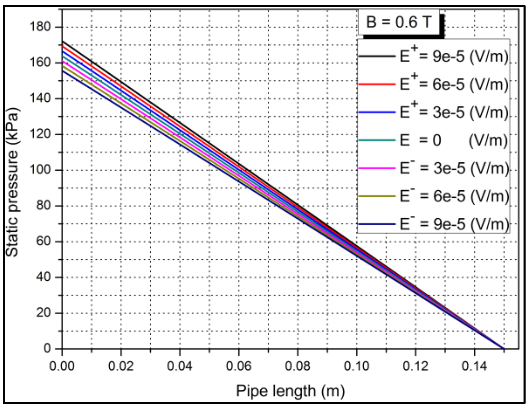

c) B = 0.6 T

Figure 4.57. Central static pressure under the magnetic and electrical field.

Figure 4.57 show that static pressure increases by the increase of electrical field (E^{+}) in positive direction. If the electrical field direction change and increases, the static pressure decreases. The increase and decrease rates were calculated statistically for each constant magnetic field values are B = 0.4 T, B = 0.5 T and B = 0.6 T and variable electrical field intensity values that are $E^{\pm}$=3e-5 V/m, $E^{\pm}$=6e-5 V/m, $E^{\pm}$=9e-5 V/m. While magnetic field was being applied with a constant value of B = 0.4 T, electrical fields were applied with values that are $E^{\pm}$=3e-5 V/m, $E^{\pm}$=6e-5 V/m, $E^{\pm}$=9e-5 V/m and the rates of increase in static pressure was determined as 2.53%, 5.07%, 7.61% and by the change of direction of electrical field the decrease rates in static pressure were determined as 2.50%, 4.99%, 7.46%. In case of application of magnetic field with value is B = 0.5 T, electrical field was applied with values that are $E^{\pm}$=3e-5 V/m, $E^{\pm}$=6e-5 V/m, $E^{\pm}$=9e-5 V/m, the positive directional application of electrical field increased the central static pressure with values that are 2.02%, 4.06%, 6.11% and reverse directional application of electrical field decreased the central static pressure with values that are 1.99%, 3.99%, 5.97%. Lastly for externally applied magnetic field is as B = 0.6 T, positive directional application of electrical field enhanced the effect of magnetic field and so central static pressure was increased with the values that are 1.68%, 3.39%, 5.10%. Application of electrical field in negative direction decreased the influence of magnetic field and the pressure was decreased with the values that are 1.67%, 3.33%, 4.97%. MHD flow decelerated by Lorentz force; and increase the static pressure in ref. [95, 140].

Figure 4.58 show the variation of local dynamic pressure at 0.12 m of the pipe length under the imposed magnetic and electrical field.

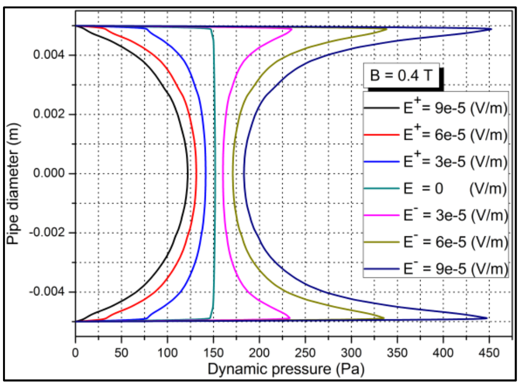

a) B = 0.4 T

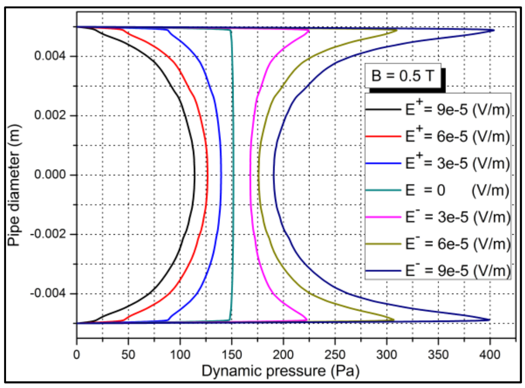

b) B = 0.5 T

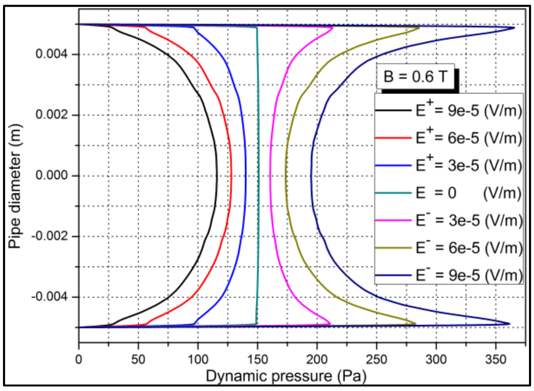

c) B = 0.6 T

Figure 4.58. Local dynamic pressure under the magnetic and electrical field.

Visualised local dynamic pressure data from the occurred analyses were given in Figure 4.58 and it is clearly seen that local dynamic pressure increase and decrease behaviour under the influence of externally applied magnetic field according to the applied electrical field direction. The graph curves showed similar characteristics as the flow velocity. Similarly, increase in positive directional electrical field decreases the dynamic pressure. Local dynamic pressure is increased by applied electrical field that is through the negative direction Decrease rates of local dynamic pressure by the increase of electrical field that is in positive direction are estimated as for each constantly applied magnetic field. For constant B = 0.4 T, the dynamic pressure decrease rates that are 16.44%, 29.72%, 39.71% and increase rates that are 17.06%, 36.92% and 57.77%. For B = 0.5 T, the dynamic pressure decrease rates that are 16.17%, 30.27%, 41.21% and increase rates that are 20.13%, 36.76% and 56.40%. For B = 0.6 T, the dynamic pressure decrease rates that are 14.38%, 27.56%, 38.39% and increase rates that are 15.01%, 32.59% and 53.37% for each step of increase of positive and negative directional electrical field intensity. Decrease in velocity means the decrease in dynamic flow pressure, decrease in flow velocity as discussed in ref. [39, 77].

Skin friction coefficient was illustrated in Figure 4.59 to have an idea about the effect of magnetic and electrical field on the hydrodynamic property is the skin friction coefficient.

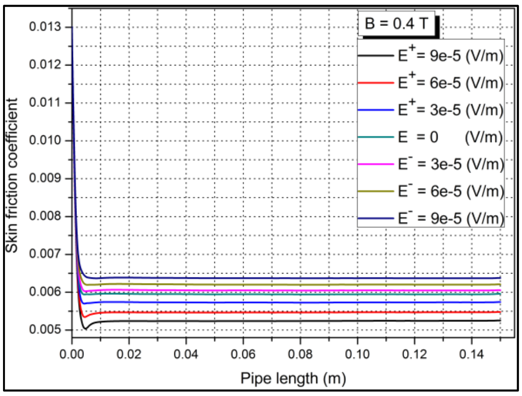

a) B = 0.4 T

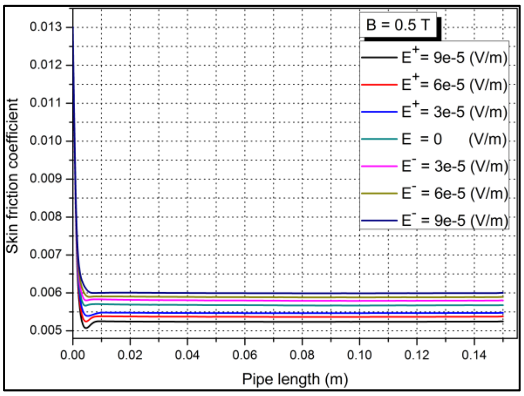

b) B = 0.5 T

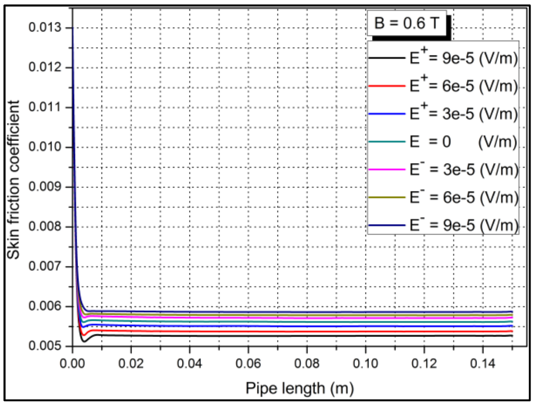

c) B = 0.6 T

Figure 4.59. Skin friction coefficient under the magnetic and electrical field.

Figure 4.59 shows that skin friction coefficient decreases by the increase of positive directional electrical field which is applied together with constant magnetic field. However, increase in negative directional electrical field increases the skin friction coefficient. For B = 0.4 T, electrical field was applied with values are $E^{\pm}$=3e-5 V/m, $E^{\pm}$=6e-5 V/m, $E^{\pm}$=9e-5 V/m and decrease rates of the friction coefficient were determined as 3.57%, 7.95%, 11.70%. Increase rates of the skin friction coefficient are 1.69%, 4.25%, 7.03% in case of redirecting the electrical field in negative direction. For B = 0.5 T, decrease rates of skin friction coefficient are in the order as 2.60%, 5.34%, 7.62% and increase rates that are 1.14%, 3.71%, 5.57% by the increase of $E^{\pm}$ = 3e-5 to $E^{\pm}$ = 9e-5. In case of application of B = 0.6 T, increase of E^{+} decreases rates the skin friction coefficient are as 1.92%, 4.29%, 6.28%. And applied E^{-} caused the increase the skin friction coefficient with rates that are 1.12%, 2.96%, 4.37%. Decrease in skin friction coefficient was concluded in ref. [92, 130] as the skin friction coefficient decreases as the magnetic parameter.

The shear stress that is between streamlines of flow domain because of imposed to magnetic and electrical field was studied and is presented in Figure 4.60.

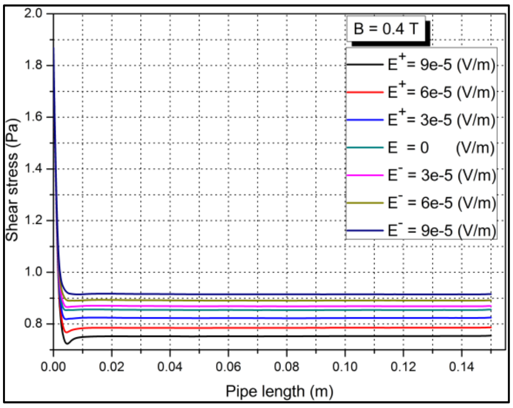

a) B = 0.4 T

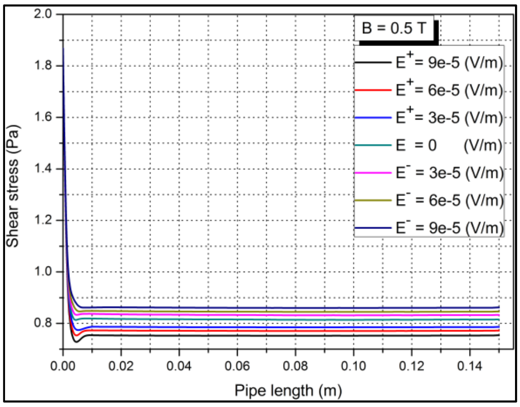

b) B = 0.5 T

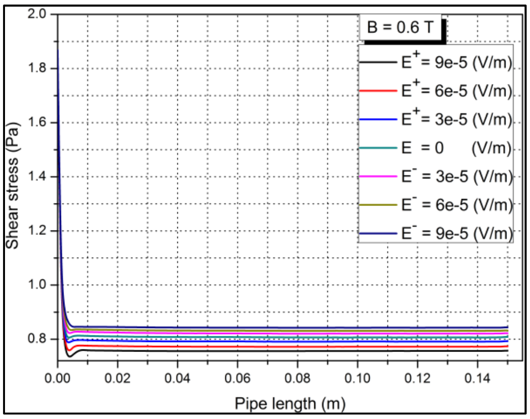

c) B = 0.6 T

Figure 4.60. Shear stress under the magnetic and electrical field.

In each case shown in Figure 4.60 could be interpreted as while applying the magnetic field constantly, increase of externally directed electrical field in positive way decreases the shear stress and shear stress increases by the change of direction and increase of electrical field. Decrease rates are determined as 3.57%, 7.95%, 11.70% by the application of electrical field in positive direction and increase rates are 1.69%, 4.25%, 7.03% by directing the electrical field in negative direction under the imposed magnetic field that is B = 0.4 T. While applying B = 0.5 T, decrease rates that are 2.60%, 5.34%, 7.62% for application and increase of electrical field in positive direction and increase rates that are 1.14%, 3.71%, 5.57% by the change of electrical field direction. Similar effect is determined for B = 0.6 T, the decrease rates of the shear stress are 1.92%, 4.29%, 6.28% and increase rates are 1.12%, 2.96%, 4.37% for negatively directed electrical field. Similar assessments about magnetic forces on shearing is seen in ref. [141, 155] as increase in magnetic field decreases shear stress.

Temperature distribution was examined while magnetic field constantly applying on flow model and electrical field was varied with the values that are $E^{\pm}$ = 3e-5 V/m, $E^{\pm}$ = 6e-5 V/m, $E^{\pm}$ = 9e-5 V/m. Central temperature distribution is shown under the influence of magnetic and electrical field in Figure 4.61 for the heating flow condition of liquid lithium in a constant wall temperature model.

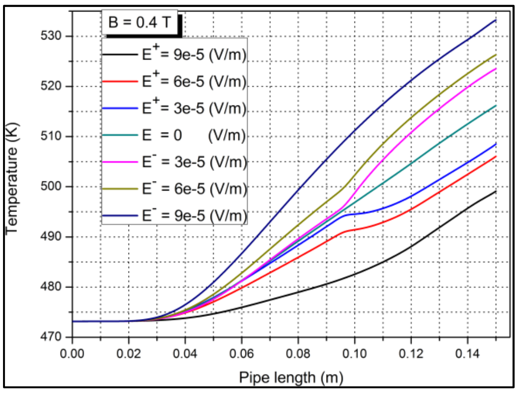

a) B = 0.4 T

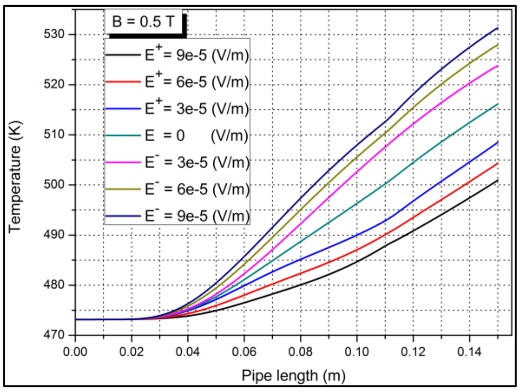

b) B = 0.5 T

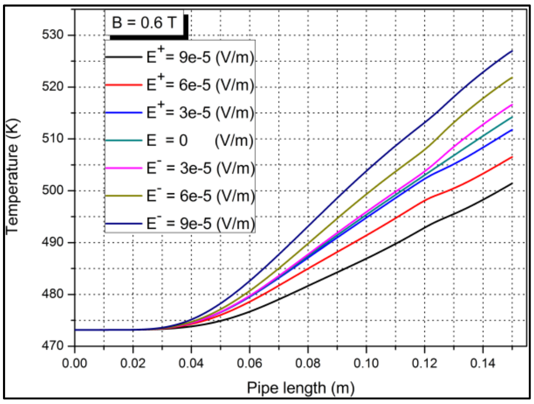

c) B = 0.6 T

Figure 4.61. Central temperature under the magnetic and electrical field.

As seen in Figure 4.61, the axial temperature values were decreased by the increase of applied E^{+} field while magnetic field was being applied constantly whereas the axial temperature values were increased by the appliance the E^{-} electrical field values. While constant magnetic field was being applied with the value is B = 0.4 T, decrease rates of temperature were evaluated in the order as 0.47%, 0.81%, 1.77% by the appliance of E^+ = 3e-5 V/m, E^+ = 6e-5 V/m, E^+ = 9e-5 V/m and the temperature values were increased as 0.43%, 0.76%, 1.73% by the appliance of E^- = 3e-5 V/m, E^- = 6e-5 V/m, E^- = 9e-5 V/m. Similarly, for B = 0.5 T, the evaluated temperature decrease rates are in the order as 0.73%, 1.15%, 1.49% by the appliance of E^+ = 3e-5 V/m, E^+ = 6e-5 V/m, E^+ = 9e-5 V/m and the temperature values were increased about 0.72%, 1.10%, 1.44% by the appliance of E^- = 3e-5 V/m, E^- = 6e-5 V/m, E^- = 9e-5 V/m. For B = 0.6 T, decrease rates of temperature values were evaluated in the order as 0.11%, 0.55%, 1.10% by the appliance of E^+ = 3e-5 V/m, E^+ = 6e-5 V/m, E^+ = 9e-5 V/m and the temperature values were increased as 0.10%, 0.52%, 1.10% by the appliance of E^- = 3e-5 V/m, E^- = 6e-5 V/m, E^- = 9e-5 V/m. Similar results were evaluated in ref. [62, 109] as temperature profiles decreases by increasing the values of magnetic field.

Temperature profile of the liquid lithium was studied at thermal fully developed region where is 0.12 m of the pipe model length and was illustrated in Figure 4.62 for the applied magnetic field induction and electrical field intensity values. For each applied constant magnetic field induction values that are B = 0 T, B = 0.4 T, B = 0.5 T, B = 0.6 T, the electrical field was applied with the values that are $E^{\pm}$ = 3e-5 V/m, $E^{\pm}$ = 6e-5 V/m, $E^{\pm}$ = 9e-5 V/m on the flow domain.

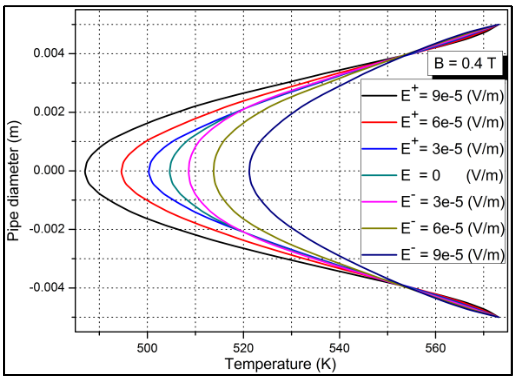

a) B = 0.4 T

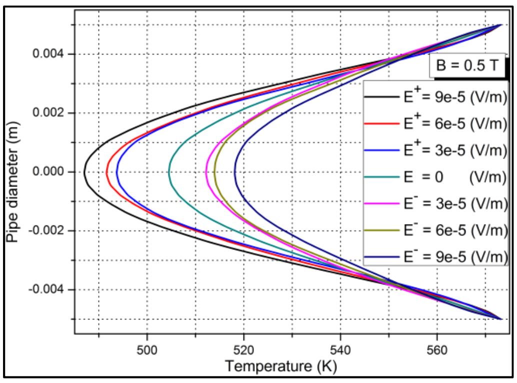

b) B = 0.5 T

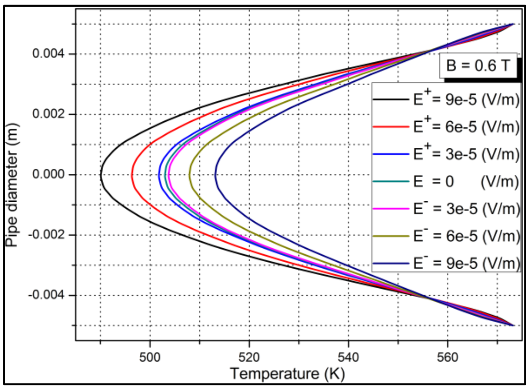

c) B = 0.6 T

Figure 4.62. Local temperature under the magnetic and electrical field.

Figure 4.62 represents the effect of applied electrical field on the local temperature of flowing liquid lithium under the influence of applied constant magnetic field. Local temperature decreases by the increase of electrical field intensity values that are E^+ = 3e-5 V/m, E^+ = 6e-5 V/m, E^+ = 9e-5 V/m while flow body is under the imposed magnetic field. For B = 0.4 T, the decrease rates of local temperature are determined as 0.16%, 0.75%, 1.60% by the increase of positive directional electrical field. Within the appliance of E^- = 3e-5 V/m, E^- = 6e-5 V/m, E^- = 9e-5 V/m, the temperature were increased as 0.14%, 0.68%, 1.52%. For applied B = 0.5 T, the temperature decrease were evaluated as 0.84%, 1.08%, 1.66% by the appliance of E^+ = 3e-5 V/m, E^+ = 6e-5 V/m, E^+ = 9e-5 V/m and the temperature were increased as 0.60%, 0.80%, 1.32% by the appliance of E^- = 3e-5 V/m, E^- = 6e-5 V/m, E^- = 9e-5 V/m. Lastly, for B = 0.6 T, the temperature reduction were evaluated as 0.11 %, 0.72%, 1.38% by the appliance of E^+ = 3e-5 V/m, E^+ = 6e-5 V/m, E^+ = 9e-5 V/m and the temperature were increased as 0.06%, 0.53%, 1.08% by the appliance of E^- = 3e-5 V/m, E^- = 6e-5 V/m, E^- = 9e-5 V/m. Variation of temperature under the imposed magnetic forces is evaluated in ref. [78, 126] as temperature decreases with magnetic parameter.

The change of Nusselt number was observed at the adjacent region of the pipe wall through the pipe length under the effect of normally applied magnetic field induction values that are as B = 0.4 T, B = 0.5 T, B = 0.6 T and electrical field intensity vales that are as $E^{\pm}$ = 3e-5 V/m, $E^{\pm}$ = 6e-5 V/m, $E^{\pm}$ = 9e-5 V/m is seen in Figure 4.63.

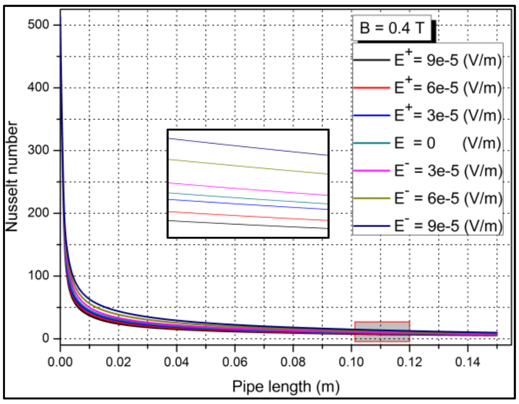

a) B = 0.4 T

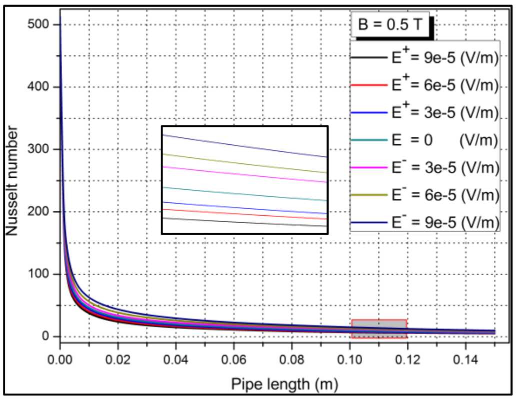

b) B = 0.5 T

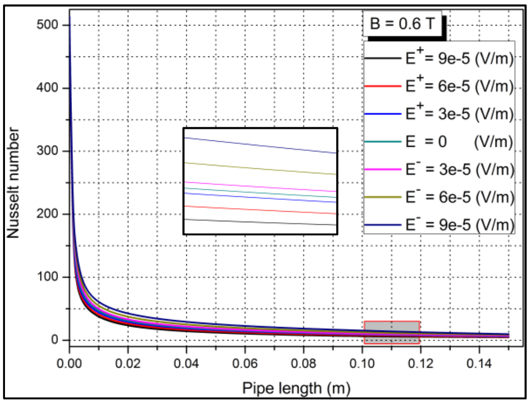

c) B = 0.6 T

Figure 4.63. Nusselt number under the magnetic and electrical field.

Figure 4.63 present that, increase in positive directional electrical field intensity (E^+), enhanced the effect of the applied magnetic field induction and so the Nusselt number was decreased. However, Nusselt number was increased by the change of electrical field direction and each step of increase of E^- value. For applied B = 0.4 T, the Nusselt number was lessened by the application of electrical field with the values that are E^+ = 3e-5 V/m, E^+ = 6e-5 V/m, E^+ = 9e-5 V/m and the rates of reduction are determined as 5.18%, 12.71%, 18.78% and Nusselt number was enhanced about 7.98%, 22.45%, 36.57% by the appliance of E^- = 3e-5 V/m, E^- = 6e-5 V/m, E^- = 9e-5 V/m. For B = 0.5 T, the decrease rates of Nusselt number were evaluated in the order as 8.06%, 14.62%, 21.08% by the appliance of E^+ = 3e-5 V/m, E^+ = 6e-5 V/m, E^+ = 9e-5 V/m and Nusselt number were increased as 11.35%, 23.07%, 36.82% by the appliance of E^- = 3e-5 V/m, E^- = 6e-5 V/m, E^- = 9e-5 V/m. For B = 0.6 T, the decrease rates were evaluated in the order as 5.12%, 13.61%, 21.57% by the increase of applied E^+ = 3e-5 V/m, E^+ = 6e-5 V/m, E^+ = 9e-5 V/m and the increase rates that are 6.09%, 18.77%, 33.78% by the appliance of E^- = 3e-5 V/m, E^- = 6e-5 V/m, E^- = 9e-5 V/m. Nusselt number decreases by reduction in turbulent fluctuations with the increase of magnetic field in ref. [88, 92].

4.2.4. Duct Flow under the Imposed Magnetic and Electrical Field

In this part of the study, influence of combined effect of magnetic and electrical on hydrodynamic, thermophysical parameters and heat transfer of liquid lithium while flowing turbulently in a constant wall temperature duct channel was investigated. Studied duct model is seen in Figure 4.64. The positive (+) and negative (-) electrical potentials were applied on the conducting walls. Magnetic field applied through the -y direction on to the duct model. Fluid flow determined in the +x direction.

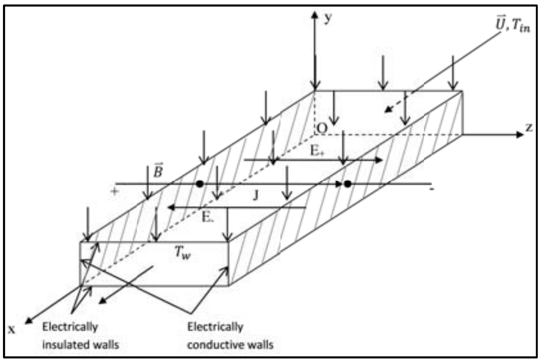

Figure 4.64. Duct model.

Combined effect of magnetic and electrical field on the flow velocity is visualised in Figure 4.65.

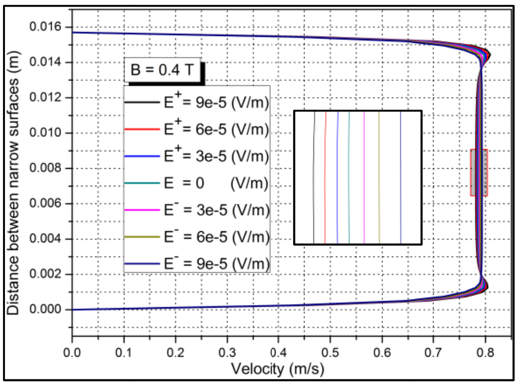

a) B = 0.4 T

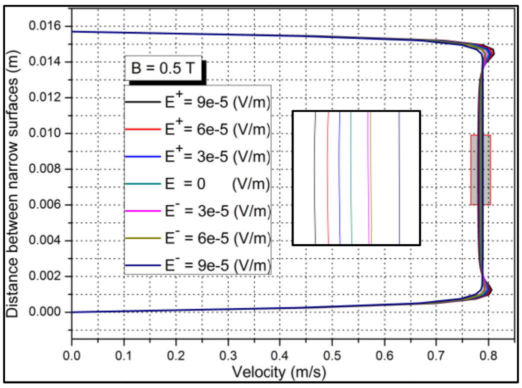

b) B = 0.5 T

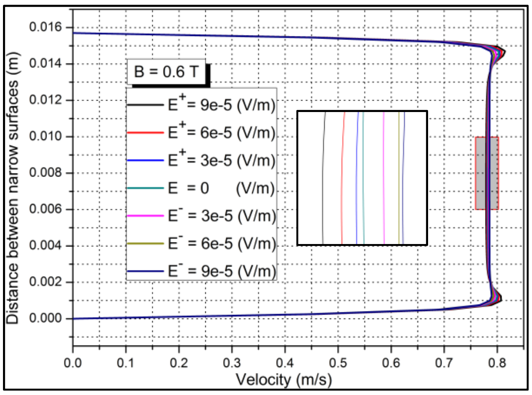

c) B = 0.6 T

Figure 4.65. Local flow velocity under the magnetic and electrical field.

Figure 4.65 illustrates that liquid lithium flow velocity decreases by the application and increase in magnetic field. The dominant effect of magnetic field on flow velocity could be boosted or lessen by the application of electrical field together with magnetic field. In case of the application of electrical field in negative direction the created Lorentz force that is in same direction with the flow velocity and shows the supporting effect to the flow. In the reverse directional application of electrical field which creates the Lorentz force in the backward direction of flow stream and causes a resistance against to flow. The decrease rates of flow velocity were determined as 0.005%, 0.01%, 0.016% when magnetic field was applied with value that is B = 0.4 T and electrical field was applied with values that are E^+ = 3e-5 V/m, E^+ = 6e-5 V/m, E^+ =9e-5 V/m. Application of electrical field in the opposite direction with values that are E^- = 3e-5 V/m, E^- = 6e-5 V/m, E^- = 9e-5 V/m enhance the flow velocity and so the increase rates are in the order as 0.007%, 0.013%, 0.026%. For B = 0.5 T, the decrease rates are evaluated as 0.004%, 0.008%, 0.013% by the increase of E^+ and increase rates that are 0.006%, 0.009%, 0.015% by the increase of E^-. For B = 0.6 T, the decrease rates that are 0.001%, 0.006%, 0.014% by the increase of E^+ and increase rates that are 0.004%, 0.007%, 0.014% by the increase of E^-. Similar flow characteristic concluded in ref. [88, 128] as increase in magnetic parameter modifies the mean flow velocity as well as turbulence reduction.

The static pressure was investigated through the centreline of the model and is seen in Figure 4.66.

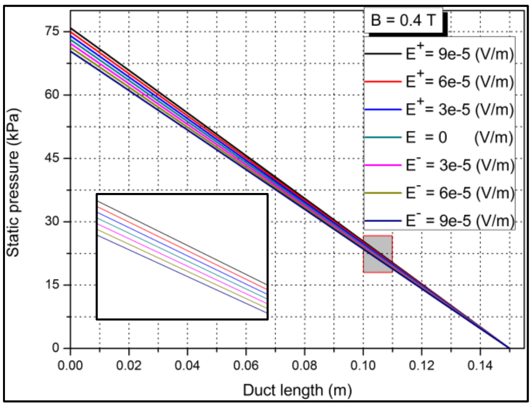

a) B = 0.4 T

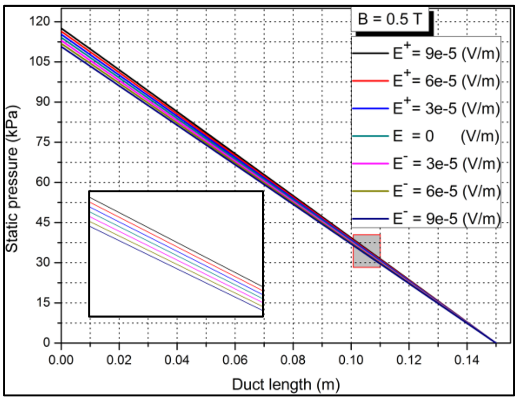

b) B = 0.5 T

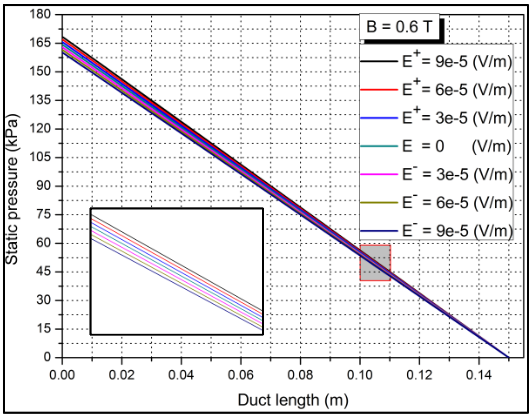

c) B = 0.6 T

Figure 4.66. Central static pressure under the magnetic and electrical field.

Figure 4.66 presents that for each values of applied magnetic field application and increase of positive directional electrical field support the magnetic forces and so the central static pressure increases. Increase in negative directional electrical field dominates the magnetic field effect and so central static pressure decreases. Increase rates are in the pressure were evaluated as 1.25%, 2.50% and 3.7% for applied magnetic field induction that is B = 0.4 T and electrical field in the positive direction. Decrease rates in the pressure are 1.25%, 2.51%, 3.75% in case of application of electrical field in negative direction. For B = 0.5 T increase rates were determined as 1.02%, 2.02% and 3.07% for each value of positive directional electrical field. Negative directional electrical field decreased the pressure with rates that are 1.01%, 2.04% and 3.09%. Lastly, positive directional electrical field increased the pressure with rates that are 0.83%, 1.66% and 2.53% and negative directional electrical field decreased the pressure with rates that are 0.83%, 1.67%, 2.54% during magnetic field imposed constantly with value of B = 0.6 T. Similar assessment about the magnetic forces effect on flow domain clarified in ref. [138] as produced greater electromagnetic force causes the higher static pressure.

Local dynamic pressure was taken into account in Figure 4.67.

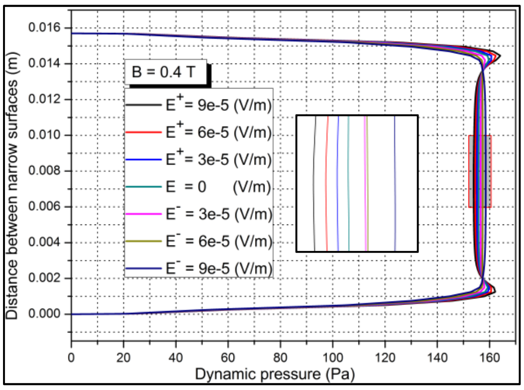

a) B = 0.4 T

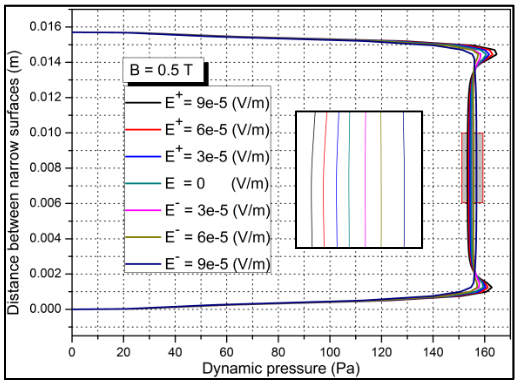

b) B = 0.5 T

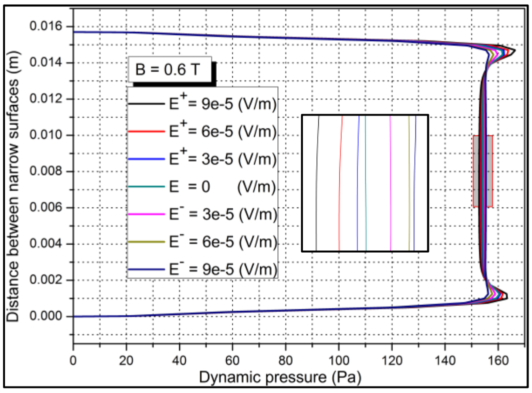

c) B = 0.6 T

Figure 4.67. Local dynamic pressure under the magnetic and electrical field.

Figure 4.67 defines that constantly applied magnetic field effect could be developed or weaken by the externally applied electrical field. Positive directional electrical field that is from E^+ = 3e-5 to E^+ = 9e-5 enhances the effect of magnetic field. The rates of enhancement are 0.026 %, 0.055%, 0.084% for constantly applied magnetic field that is B = 0.4 T, 0.021%, 0.04%, 0.063% for B = 0.5 T, and 0.008%, 0.03%, 0.056% for B = 0.6 T. Negative directional electrical field dominates the effect of constantly applied magnetic field with different rates. The rates of domination in local dynamic pressure are 0.041%, 0.086%, 0.17% for B = 0.4 T, 0.034%, 0.047%, 0.094% for B = 0.5 T, and 0.025%, 0.042%, 0.063% for B = 0.6 T. In ref. [145], it is determined that the growing Reynolds number a relative value of the intensity of velocity fluctuations decreases and tends to a constant value 3.5% at Re > 5,000 and also dynamic pressure (ρV^2) is dependent parameter to flow velocity. Decrease in flow velocity by magnetic field means the decrease in dynamic pressure.

The given Figure 4.68 demonstrates the skin friction coefficient and the variation of it by imposed magnetic and electrical field.

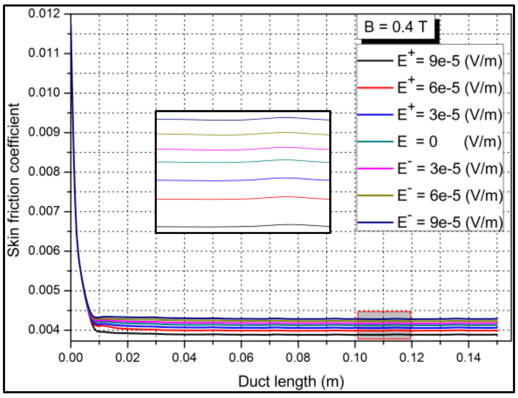

a) B = 0.4 T

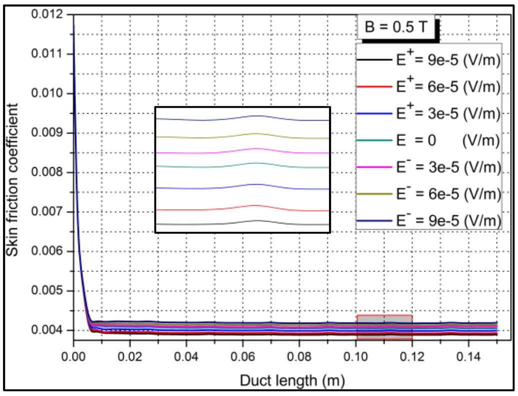

b) B = 0.5 T

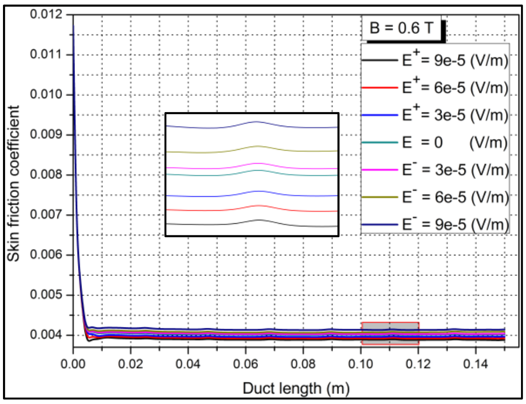

c) B = 0.6 T

Figure 4.68. Skin friction coefficient under the magnetic and electrical field.

Figure 4.68 presents that externally applied positive directional electrical field enhances the effect of constantly applied magnetic field and skin friction coefficient decreases more and more. Beside that negative directional electrical field weaken the magnetic forces and skin friction coefficient increases. Decrease rates are 1.52%, 3.13%, 5.48% for B = 0.4 T, 1.44%, 2.89%, 3.86% for B = 0.5 T, 1.28%, 2.20%, 3.12% for B = 0.6 T by the application of electrical field that is from E^+ = 3e-5 V/m to E^+ = 9e-5 V/m. Negative directional electrical field with values that are from E^- = 3e-5 to E^- = 9e-5 V/m increases the skin friction with rates that are 1.08%, 2.31%, 3.56% for B = 0.4 T, 0.86%, 1.92%, 3.13% for B = 0.5 T, and lastly 0.45%, 1.42%, 2.93% for B = 0.6 T. In ref. [92, 146], it is concluded that the decrease in turbulent skin friction is reduced by electromagnetic forces.

Relation between the shear stress and magnetic forces is visualised in Figure 4.69.

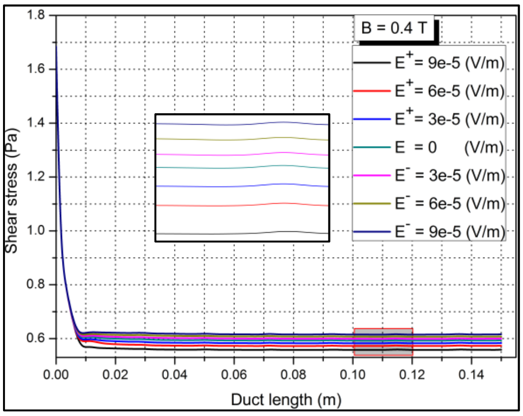

a) B = 0.4 T

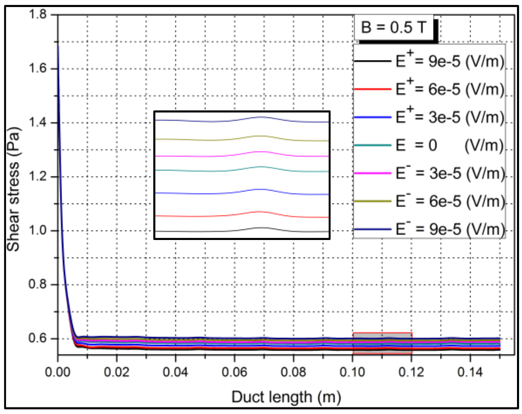

b) B = 0.5 T

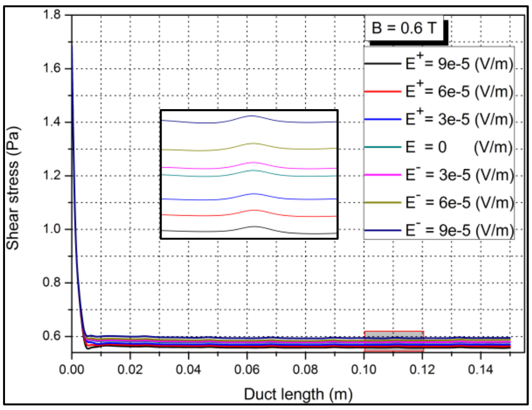

c) B = 0.6 T

Figure 4.69. Shear stress under the magnetic and electrical field.

Increase in positive directional electrical field increases the shear stress as seen in Figure 4.69. Negative directional electrical field means the increase of shearing that is between flow lines. The average values of shear stress decrease by positive directional electrical field application together with constant magnetic field. Decrease rates of the shear stress that are 1.52%, 3.12%, 5.48% for magnetic field is

B = 0.4 T, 1.44%, 2.89%, 3.86% for B = 0.5 T, 1.28%, 2.20%, 3.12% for B = 0.6 T. The increase rates of shear stress that are 1.08%, 2.31%, 3.56% for B = 0.4 T, 0.86%, 1.92%, 3.13% for B = 0.5 T, and 0.44%, 1.42%, 2.93% for B = 0.6 T by the application together with negative directional electrical field. Magnetic force influence on the shearing was clarified in ref. [131, 155] as turbulent stresses typically decay more rapidly away from the walls than predicted by mixing-length models by imposed magnetic field.

Temperature distribution through the centreline of the duct under the applied magnetics and electric field was examined for each constant value of magnetic field induction values that are B = 0.4 T, B = 0.5 T, B = 0.6 T, the electrical field intensity was applied with values that are $E^{\pm}$ = 3e-5 V/m, $E^{\pm}$ = 6e-5 V/m, $E^{\pm}$ = 9e-5 V/m. The temperature distribution is seen in Figure 4.70 for the heating flow condition of lithium with constant wall temperature.

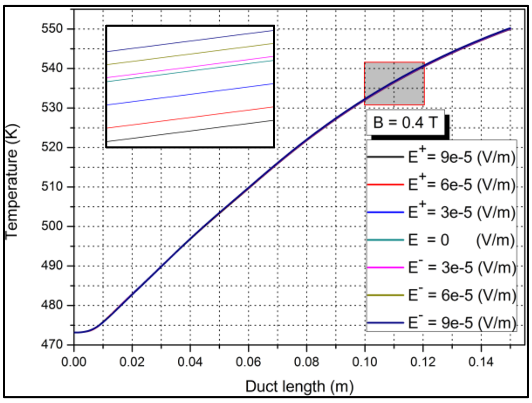

a) B = 0.4 T

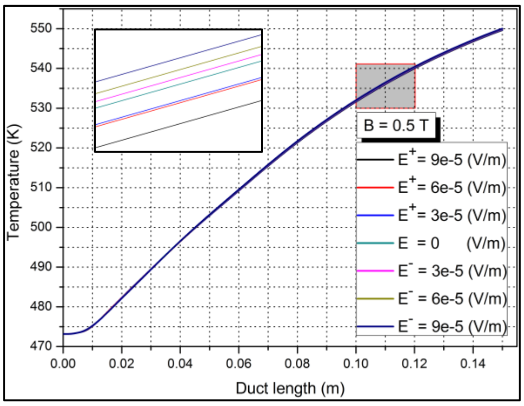

b) B = 0.5 T

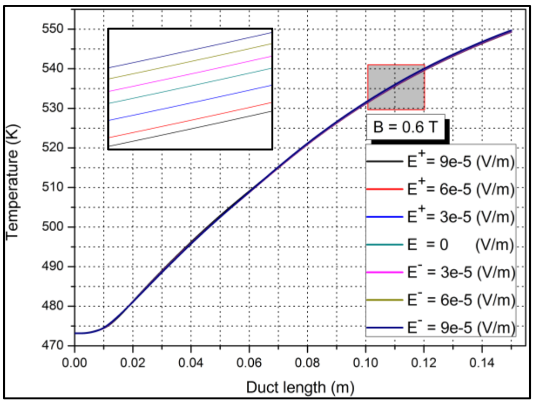

c) B = 0.6 T

Figure 4.70. Central temperature under the magnetic and electrical field.

As seen in Figure 4.70, the temperature values were decreased by the increase of applied E^+ field for each constant magnetic field induction whereas the axial temperature values were increased by the appliance the E^- electrical field values together with magnetic field. While applying B = 0.4 T, decrease rates of temperature were determined in the order as 0.006%, 0.016%, 0.025% by the appliance of E^+ = 3e-5 V/m, E^+ = 6e-5 V/m, E^+ = 9e-5 V/m and the temperature values were increased as 0.002%, 0.004%, 0.006% by the appliance of E^- = 3e-5 V/m, E^- = 6e-5 V/m, E^- = 9e-5 V/m. Similarly, while B = 0.5 T was applied together with the electrical field with the increasing values that are from E^+ = 3e-5 V/m, to E^+ = 9e-5 V/m, the decrease rates were evaluated in the order as %, 0.015%, 0.017%, 0.03% and the increase rates were determined as 0.003%, 0.007%, 0.018% by the appliance of negative directional electrical field that are E^- = 3e-5 V/m, E^- = 6e-5 V/m, E^- = 9e-5 V/m. Lastly, under the effect of B = 0.6 T, the decrease rates were specified in the order as 0.007%, 0.015%, 0.048% by the appliance of E^+ = 3e-5 V/m, E^+ = 6e-5 V/m, E^+ = 9e-5 V/m and the temperature values were increased as 0.004%, 0.009%, 0.014% by the appliance of E^- = 3e-5 V/m, E^- = 6e-5 V/m, E^- = 9e-5 V/m. Similar evaluations are seen in ref. [39, 134] as fluid temperature decrease with increasing magnetic parameter.

Temperature profile was evaluated at thermal fully developed region where is the 0.12 m of the length and is represented in Figure 4.71. For each values of applied magnetic field induction that are B = 0.4 T, B = 0.5 T, B = 0.6 T, the electrical field intensity applied with values that are $E^{\pm}$ = 3e-5 V/m, $E^{\pm}$ = 6e-5 V/m, $E^{\pm}$ = 9e-5 V/m.

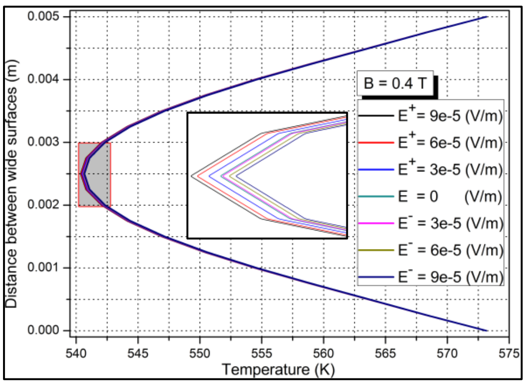

a) B = 0.4 T

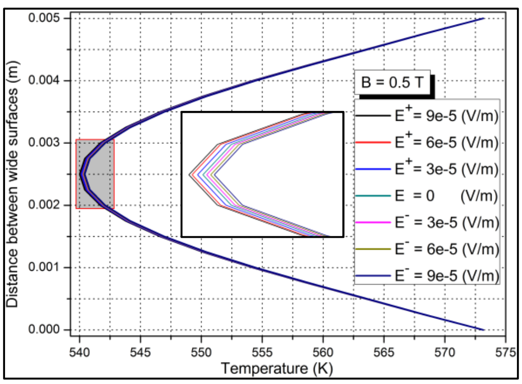

b) B = 0.5 T

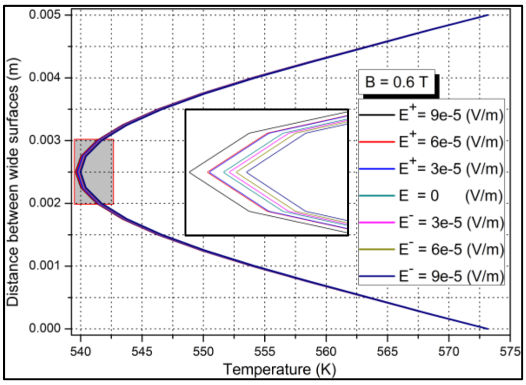

c) B = 0.6 T

Figure 4.71. Local temperature under the magnetic and electrical field.

Figure 4.71 designates the impact of the electrical field intensity on the local temperature distribution of flow domain under the influence of applied constant magnetic field induction. While magnetic field was applied with value is B = 0.4 T, the local temperature was decreased by the increase of electrical field intensity with values that are E^+ = 3e-5 V/m, E^+ = 6e-5 V/m, E^+ = 9e-5 V/m. In the same order, the decrease rates acquired as 0.008%, 0.016%, 0.02%. The increase rate of temperature were evaluated as 0.001%, 0.006%, 0.01% by the appliance of negative directional electrical field with values that are E^- = 3e-5 V/m, E^- = 6e-5 V/m, E^- = 9e-5 V/m. For constantly applied B = 0.5 T, the decrease rates were evaluated as 0.011%, 0.013%, 0.027% by the increase of electrical field intensity with values that are E^+ = 3e-5 V/m, E^+ = 6e-5 V/m, E^+ = 9e-5 V/m, and the increase rates of temperature that are 0.004%, 0.01%, 0.018% for E^- = 3e-5 V/m, E^- = 6e-5 V/m, E^- = 9e-5 V/m. During the appliance of B = 0.6 T, the decrease of temperature rates were evaluated as 0.009%, 0.018%, 0.024% by the increase the electrical field with values that are E^+ = 3e-5 V/m, E^+ = 6e-5 V/m, E^+ = 9e-5 V/m, and the temperature were increased as 0.006%, 0.013%, 0.019% by the appliance of opposite direction electrical field with values that are E^- = 3e-5 V/m, E^- = 6e-5 V/m, E^- = 9e-5 V/m. It is discussed that temperature decreases with magnetic parameter in ref. [78, 81].

The variation of Nusselt number at the adjacent region of the duct wall through the duct length was expired under the effect of normally applied magnetic field induction which are as B = 0.4 T, B = 0.5 T, B = 0.6 T and electrical field intensity values that are $E^{\pm}$ = 3e-5 V/m, $E^{\pm}$ = 6e-5 V/m, $E^{\pm}$ = 9e-5 V/m is shown in Figure 4.72.

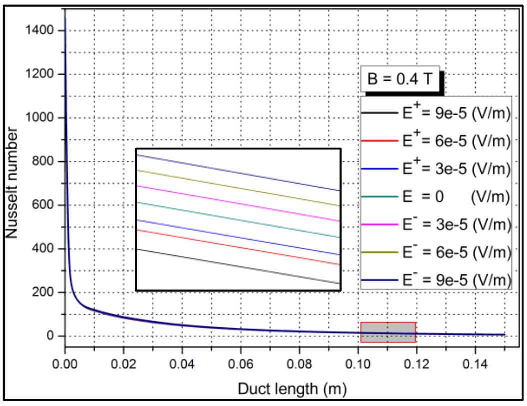

a) B = 0.4 T

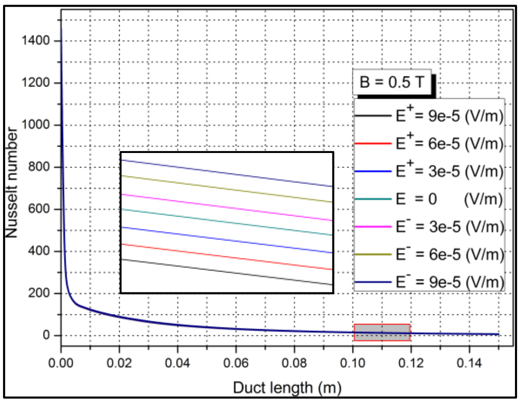

b) B = 0.5 T

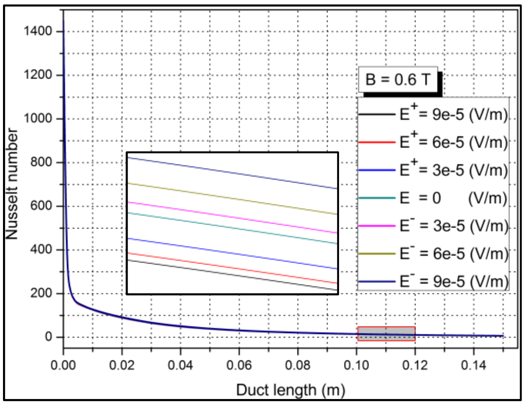

c) B = 0.6 T

Figure 4.72. Nusselt number under the magnetic and electrical field.

Figure 4.72 shows that increase in positive directional electrical field intensity enhances the influence of the applied magnetic field and so the Nusselt number decreases more for each value of E^+, but by the change of the direction of electrical field intensity to negative way increases the Nusselt number for each step of increase of E^- value. While applying the magnetic field with value is B = 0.4 T, the decrease rates of Nusselt number were determined as 0.53%, 1.07%, 1.43% for each applied electrical field with values that are E^+ = 3e-5 V/m, E^+ = 6e-5 V/m, E^+ = 9e-5 V/m and the increase rates in Nusselt number are 0.38%, 0.81%, 1.22% by the appliance in the opposite directional electrical field with vales are E^- = 3e-5 V/m, E^- = 6e-5 V/m, E^- = 9e-5 V/m. In case of application of B = 0.5 T, the decrease rates of Nusselt number are as 0.55%, 0.66%, 1.39% by the appliance of E^+ = 3e-5 V/m, E^+ = 6e-5 V/m, E^+ = 9e-5 V/m and the Nusselt number was increased with the rates that are 0.29%, 0.67%, 1.10% by the appliance of E^- = 3e-5 V/m, E^- = 6e-5 V/m, E^- = 9e-5 V/m. For B = 0.6 T, Nusselt number decreased with rates that are 0.48%, 0.86%, 1.15% by the increase of applied electrical field values that are $E^+ = 3e\text{-}5$ V/m, $E^+ = 6e\text{-}5$ V/m, $E^+ = 9e\text{-}5$ V/m, and Nusselt number was increased with rates that are 0.16%, 0.46%, 0.74% in case of application of negative directional electrical field with values are $E^- = 3e\text{-}5$ V/m, $E^- = 6e\text{-}5$ V/m, $E^- = 9e\text{-}5$ V/m. It is mentioned that Nusselt number decreases with increase of magnetic parameter in ref. [111, 139].

PART 5

CONCLUSION

Liquid lithium internal flow case was investigated under the imposed magnetic field and combined with electrical field to determine the effect of magnetic forces on the hydrodynamic, thermophysical fluid parameters and heat transfer. Steady state incompressible liquid lithium laminar and turbulent flow regimes were examined in circular pipe and rectangular duct models. Study was realized computationally by ANSYS Fluent 15.0 software MHD module. Concluded results were evaluated as given below.

1. Increase in applied magnetic field on laminar liquid lithium flow in a circular pipe or a rectangular duct model causes that;

    - Flow velocity decreases,
    - Static pressure increases,
    - Dynamic pressure reduces,
    - Skin friction coefficient rises,
    - Wall shear stress grows up,
    - Central liquid metal temperature enhanced,
    - Local flow temperature is developed,
    - Nusselt number is boosted,
    - Heat transfer on the flow domain is enhanced,

2. Increase in applied magnetic field and positive directional electrical field on laminar liquid lithium flow in a circular pipe or a rectangular duct model inspires that;

    - Flow velocity declines,

- Static pressure goes up,
- Dynamic pressure goes down,
- Skin friction coefficient swells,
- Wall shear stress grows up,
- Central liquid metal temperature is enhanced,
- Local flow temperature is augmented,
- Nusselt number is gathered,
- Heat transfer on the flow domain is progressed,

3. Increase in applied magnetic field and negative directional electrical field on laminar liquid lithium flow in a circular pipe or a rectangular duct model presented that;

- Flow velocity increases,
- Static pressure declines,
- Dynamic pressure rises,
- Skin friction coefficient reduces,
- Wall shear stress diminishes,
- Central liquid metal temperature is declined,
- Local flow temperature is reduced,
- Nusselt number is weaken,
- Heat transfer on the flow domain is dominated,

4. Increase in applied magnetic field on turbulent liquid lithium flow in a circular pipe or a rectangular duct model yield that;

- Flow velocity goes down,
- Static pressure is developed,
- Dynamic pressure declines,
- Skin friction coefficient reduces,
- Wall shear stress decreases,
- Central liquid metal temperature is lessened,

- Local flow temperature is depressed,
- Nusselt number is suppressed,
- Heat transfer on the flow domain is weaken,

5. Increase in applied magnetic field and positive directional electrical field on turbulent liquid lithium flow in a circular pipe or a rectangular duct model inspires that;

- Flow velocity reduces,
- Static pressure increases,
- Dynamic pressure lessens,
- Skin friction coefficient declines,
- Wall shear stress goes down,
- Central liquid metal temperature is weaken,
- Local flow temperature is depressed,
- Nusselt number is reduced,
- Heat transfer on the flow domain is dominated,

6. Increase in applied magnetic field and negative directional electrical field on turbulent liquid lithium flow in a circular pipe or a rectangular duct model brings out that;

- Flow velocity goes up,
- Static pressure declines,
- Dynamic pressure rises,
- Skin friction coefficient develops,
- Wall shear stress improves,
- Central liquid metal temperature is grown up,
- Local flow temperature is gained,
- Nusselt number is developed,
- Heat transfer on the flow domain is enhanced.

Discussed results are visualized in Table 3.4 for the sake of clarity.

Table 3.4. Effects of magnetic field and combined effect of magnetic field together with electrical field.

FLOW	FIELD	U (m/s)	P_s (Pa)	P_d (Pa)	C_f	τ_w (Pa)	T (K)	Nu number
LAMINAR	B (T)	↓	↑	↓	↑	↑	↑	↑
	B (T), E^+ (V/m)	↓	↑	↓	↑	↑	↑	↑
	B (T), E^- (V/m)	↑	↓	↑	↓	↓	↓	↓
TURBULENT	B (T)	↓	↑	↓	↓	↓	↓	↓
	B (T), E^+ (V/m)	↓	↑	↓	↓	↓	↓	↓
	B (T), E^- (V/m)	↑	↓	↑	↑	↑	↑	↑

Evaluated results in this thesis could be applicable in the related fields discussed below;

1. MHD electromagnetic stirring, braking and shaping processes in metallurgical processing.

2. High temperature MHD air heater technologies in heavy metal industry.

3. Pumping the conductive liquids by the magnetic forces in special systems which are as nuclear plants cooling system liquid metal pumps without needs any moving and service required parts.

4. MHD generator systems.

5. MHD mixers are the energy efficient alternatives of mechanical mixers.

6. Controlling the convective heat and mass transfer in crystallization period of metallurgical processes by magnetic forces.

7. Control of liquid metal flow and temperature during the moulding process in metal industry.

8. High temperature liquid metal lubrication by hydro magnetic forces increases bearing pressurisation and load capacities.

9. MHD valves to control the flow of liquid metals in chemical, metallurgic and nuclear industry.

10. Liquid filtration systems to prevent scale build up that is caused by dissolved minerals in all types of fluid flow lines in filtration industry.

REFERENCES

1. Kim, C.N., “A liquid metal magnetohydrodynamic duct flow with sudden contraction in a direction perpendicular to a magnetic field”, ***Comput. Fluids***, 108: 156-167 (2015).

2. Ahmed, N., and Dutta, M., “Heat transfer in an unsteady MHD flow through an infinite annulus with radiation”, ***Bound. Value Probl.***, 2015(11): 1-17 (2015).

3. Mabood, F., Khan, W.A., and Ismail, A.I.M., “MHD boundary layer flow and heat transfer of nanofluids over a nonlinear stretching sheet: A numerical study”, ***J. Magn. Magn. Mater.***, 374: 569-576 (2015).

4. Selimli, S., Recebli, Z., and Arcaklioglu, E., “Turbulent MHD duct flow thermophysical analysis”, ***3rd Int. Semp. Innov. Tech. Eng. Sci.***, Valencia, 2375-2378 (2015).

5. Mahmoudi, A., Mejri, I., Abbassi, M.A., and Omri, A., “Analysis of MHD natural convection in a nanofluid-filled open cavity with non-uniform boundary condition in the presence of uniform heat generation/absorption”, ***Powder Technol.***, 275-289 (2015).

6. Recebli, Z., Selimli, S., and Arcaklioglu, E., “Turbulent MHD pipe flow hydrodynamic analysis”, ***3rd Int. Semp. Innov. Tech. Eng. Sci.***, Valencia, 2379-2383 (2015).

7. Fakour, M., Vahabzadeh, A., Ganji, D.D., “Study of heat transfer and flow of nanofluid in permeable channel in the presence of magnetic field”, ***Propul. Power Res.***, in press: doi:10.1016/j.jppr.2015.02.005, 1-13 (2015).

8. Heidary, H., Hosseini, R., Pirmohammadi, M., and Kermani, M.J., “Numerical study of magnetic field effect on nano-fluid forced convection in a channel”, ***J. Magn. Magn. Mater.***, 374: 11-17 (2015).

9. Selimli, S., Recebli, Z., and Arcaklioglu, E., “MHD numerical analyses of hydrodynamically developing laminar liquid lithium duct flow”, ***Int. J. Hydrogen Energ.***, in press, doi:10.1016/j.ijhydene.2015.02.020: 1-7 (2015).

10. Dada, M.S., and Disu, A.B., “Heat transfer with radiation and temperature dependent heat source in MHD free convection flow in a porous medium between two vertical wavy walls”, ***J. Nigerian Math. Soc.***, in press: doi:10.1016/j.jnnms.2014.12.001, 1-16 (2015).

11. Selimli, S., Recebli, Z., and Arcaklioglu, E., “Combined effects of magnetic and electrical field on the hydrodynamic and thermophysical parameters of magnetoviscous fluid flow”, ***Int. J. Heat Mass. Tran.***, 86: 426-432 (2015).

12. Abd-Alla, A.M., and Abo-Dahab, S.M., “Magnetic field and rotation effects on peristaltic transport of a Jeffrey fluid in an asymmetric channel”, ***J. Magn. Magn. Mater.***, 374: 680-689 (2015).

13. Recebli, Z., Selimli, S., and Ozkaymak, M., “Theoretical analyses of immiscible MHD pipe flow”, ***Int. J. Hydrogen Energ.***, In press:doi:10.1016/j.ijhydene. 2015.04.010 (2015).

14. Sheikholeslami, M., and Ganji, D.D., “Nanofluid flow and heat transfer between parallel plates considering Brownian motion using DTM”, ***Comput. Method Appl. M.***, 283: 651-663 (2015).

15. Selimli, S., Recebli, Z., and Arcaklioglu, E., “Computational hydrodynamic analysis of turbulent duct flow”, ***Int. Conf. Eng. Nat. Sci.***, Skopje, 454-459 (2015).

16. Haq, R.U., Nadeem, S., Khan, Z.H., and Akbar, N.S., “Thermal radiation and slip effects on MHD stagnation point flow of nano fluid over a stretching sheet”, ***Physica E***, 65: 17-23 (2015).

17. Recebli, Z., Selimli, S., and Arcaklioglu, E., “CFD thermophysical analysis of MHD turbulent pipe flow”, ***Int. Conf. Eng. Nat. Sci.***, Skopje, 460-464 (2015).

18. Yamamoto, Y., and Kunugi, T., “Direct numerical simulation of MHD heat transfer in high Reynolds number turbulent channel flows for Prandtl number of 25”, ***Fusion Eng. Des.***, 90: 17-22 (2015).

19. Recebli, Z., Gedik, E., and Selimli, S., “Electrical field effect on three-dimensional magnetohydrodynamic pipe flow: a CFD study”, ***Prog. Comput. Fluid. Dy.***, Accepted: In press (2015).

20. Aurang, Z., and Shafie S., “Thermal diffusion and diffusion thermos effects on unsteady MHD free convection flow over a stretching surface considering Joule heating and viscous dissipation with thermal stratification, chemical reaction and Hall current”, ***J. Frankl Inst.***, 351: 1268-1287 (2014).

21. Abbasbandy, S., Naz, R., Hayat, T., and Alsaedi, A., “Numerical and analytical solutions for Falkner–Skan flow of MHD Maxwell fluid”, ***Appl. Math. Comput.***, 242: 569-575 (2014).

22. Alam, M.K., Siddiqui, A.M., Rahim, M.T., Islam, S., Avital, E.J., and Williams, J.J.R., “Thin film flow of magnetohydrodynamic (MHD) pseudo-plastic fluid on vertical wall”, ***Appl. Math. Comput.***, 245: 544-556 (2014).

23. Sirivinas, S., Reddy, A.S., Ramamohan, T.R., and Shukla, A.K., “Influence of heat transfer on MHD flow in a pipe with expanding or contracting permeable wall”, ***Ain Shams Eng. J.***, 5: 817-830 (2014).

24. Theuri, U., and Makinde, O.D., "Thermodynamic analysis of variable viscosity MHD unsteady generalized Couette flow with permeable walls", ***Appl. Comput. Math.***, 3(1): 1-8 (2014).

25. Jiang, C., Feng, W., Zhong, H., Zeng, J., and Zhu, Q, "Effects of a magnetic quadrupole field on thermomagnetic convection of air in a porous square enclosure", ***J. Magn. Magn. Mater.***, 357: 53–60 (2014).

26. Cao, Z., Xu, J., Sun, D., Xie, J., Xing, F., Chen, Q., and Wang, X., "Numerical simulation of modulated heat transfer tube in laminar flow regime", ***Int. J. Therm. Sci.***, 75: 171-183 (2014).

27. Chutia, M., and Deka, P.N., "Numerical study on steady magnetohydrodynamics (MHD) flow and heat transfer in a heated rectangular electrically insulated duct under the action of strong oblique transverse magnetic field", ***Int. J. Comput. Appl.***, 86(15): 27-34 (2014).

28. Selimli, S., and Recebli, Z., "MHD steady state turbulent liquid metal duct flow convective heat transfer analyses", ***Int. Symp. Conv. Heat Mass Trans.***, Kusadasi, 1-11 (2014).

29. Khan, M.S., Karim, I., and Islam, M.S., "Possessions of chemical reaction on MHD heat and mass transfer nanofluid flow on a continuously moving surface", ***Am. Chem. Sci. J.***, 4(3): 401-415 (2014).

30. Sahin, A., Zueco, J., and Lopez, O., "Numerical modeling of MHD convective heat and mass transfer in presence of first-order chemical reaction and thermal radiation", ***Chem. Eng. Comm.***, 201(3): 419–436 (2014).

31. Sarma, D., Deka, P.N., and Kakaty, S.C., "Numerical study of liquid metal MHD flow through a square duct", ***Asian J. Eng. Maths***, 3(2): 15-19 (2014).

32. Raju, K.V.S., Reddy, T.S., Raju, M.C., Narayana, P.V.S., and Venkataramana, S., "MHD convective flow through porous medium in a horizontal channel with insulated and impermeable bottom wall in the presence of viscous dissipation and Joule heating", Ain Shams Eng. J., 5: 543-551 (2014).

33. Selimli, S., Recebli, Z., and Arcaklioglu, E., "Changes of thermo-physical behaviours of liquid lithium laminar steady state pipe flow under the externally applied magnetics and electrical field", ***Int. Conf. Adv. Tech. Sci.***, Antalya, 991-995 (2014).

34. Mabood, F., Khan, W.A., and Ismail, A.I.M., "MHD flow over exponential radiating stretching sheet using homotopy analysis method", in press: doi:10.1016/j.jksues.2014.06.001: 1-7 (2014).

35. Malvandi, A., and Ganji, D.D., "Magnetohydrodynamic mixed convective flow of Al_2O_3–water nanofluid inside a vertical microtube", ***J. Magn. Magn. Mater.***, 369: 132-141 (2014).

36. Gebre, D.H., Makinde, O.D., and Kinyanjui, M., "Analysis of turbulent Hydromagnetic flow with Radiative heat over a moving vertical plate in a Rotating System", ***Appl. Comput. Math.***, 3(3): 100-109 (2014).

37. Rashad, A.M., "Effects of radiation and variable viscosity on unsteady MHD flow of a rotating fluid from stretching surface in porous medium", ***J. Egypt. Math. Soc.***, 22: 134-142 (2014).

38. Recebli, Z., Selimli, S., and Arcaklioglu, E., "Combine effect of magnetic and electrical field on heat transfer within the steady state liquid lithium duct flow", ***Int. Conf. Adv. Tech. Sci.***, Antalya, 980-984 (2014).

39. Mosayebidorcheh, S., Sheikholeslami, M., Hatami, M., and Ganji, D.D., "Analysis of turbulent MHD Couette nanofluid flow and heat transfer using

hybrid DTM–FDM", ***Particuology***, in press doi:10.1016/j.partic.2014.07.004, 1-8 (2014).

40. Olajuwon, B.I., Oahimire, J.I., and Ferdow, M., "Effect of thermal radiation and Hall current on heat and mass transfer of unsteady MHD flow of a viscoelastic micropolar fluid through a porous medium", ***Eng.Sci. Tech. Int. J.***, 17: 185-193 (2014).

41. Selimli, S., Recebli, Z., and Arcaklioglu, E., "MHD numerical analyses of hydrodynamically developing laminar liquid lithium duct flow", ***4th Int. Conf. Nucl. Renew. Energ. Resour.***, Antalya, 1-5 (2014).

42. Alimohamadi, H., Niri, V.D., Sarmadi, P., and Ashjaee, M., "Improvement of heat transfer performances of biomagnetic flow in a rectangular duct under different types of magnetic fields", ***Int. J. Tech Enh. Emerg. Eng. Res.***, 2(8): 44-48 (2014).

43. Recebli, Z., Selimli, S., and Ozkaymak, M., "Theoretical Analyses of Immiscible MHD Pipe Flow", ***4th Int. Conf. Nucl. Renew. Energ. Resour.***, Antalya, 1-4 (2014).

44. Akram, S., Nadeem, S., and Hussain, A., "Effects of heat and mass transfer on peristaltic flow of a Bingham fluid in the presence of inclined magnetic field and channel with different wave forms", ***J. Magn. Magn. Mater.***, 362: 184-192 (2014).

45. Recebli, Z., and Selimli, S., "Convectional heat transfer numerical analysis of MHD steady state laminar lithium pipe flow", ***Int. Symp. Conv. Heat Mass Trans.***, Kusadasi, 1-9 (2014).

46. Adhikari, A., and Sanyal, D.C., "Heat transfer on MHD viscous flow over a stretching sheet with prescribed heat flux", ***Bull. Int. Math. Virtual Inst.***, 3: 35-47 (2013).

47. Ashraf, M., and Batool, K., "MHD flow and heat transfer of a micropolar fluid over a stretchable disk", ***J. Theor. Appl. Mech.***, 51(1): 25-38 (2013).

48. Jat, R.N., and Chand G., "MHD flow and heat transfer over an exponentially stretching sheet with viscous dissipation and radiation effects", ***Appl. Math. Sci.***, 7(4): 167 -180 (2013).

49. Mansour, M.A., Bakier, A.Y., and Bakeir, M.A.Y., "MHD natural convection in the localized heat sources of an inclined trapezoidal nanofluid-filled enclosure", ***Am. J. Eng. Res.***, 2(9): 140-161 (2013).

50. Nyabuto, R., Sigey, J.K., Okelo, J.A., and Okwoyo, J.M., "Magneto-hydrodynamics analysis of free convection flow between two horizontal parallel infinite plates subjected to constant heat flux", ***SIJ Trans. Comp. Networks & Commun. Eng.***, 1(4): 79-83 (2013).

51. Ozturk A., "MHD slip flow between parallel plates heated with a constant heat flux", ***J. Ther. Sci. Tech.***, 33(1): 11-20 (2013).

52. Recebli, Z., Selimli, S., and Gedik E., "Three dimensional numerical analysis of magnetic field effect on convective heat transfer during the MHD steady state laminar flow of liquid lithium in a cylindrical pipe", ***Comput. Fluids***, 88: 410–417, (2013).

53. Uddin, M.J., Khan, W.A., and Ismail, A.I.M., "MHD forced convective laminar boundary layer flow from a convectively heated moving vertical plate with radiation and transpiration effect", ***Plos One***, 8(5): 1-10 (2013).

54. Vidyasagar, G., Ramana, B., and Raddy, P.B.A., "MHD convective heat and mass transfer flow over a permeable stretching surface with suction and internal heat generation/absorption", ***Int. J. Adv. Eng. Tech.***, 4(1): 41-45 (2013).

55. Zhang L., Ouyang J., and Zhang X., "The variational multiscale element free Galerkin method for MHD flows at high Hartmann numbers", ***Comput. Phys. Commun.***, 184(4): 1106–1118 (2013).

56. Ahmed, S.E., Mansour, M.A., and Mahdy, A., "MHD mixed convection in an inclined lid-driven cavity with opposing thermal buoyancy force: Effect of non-uniform heating on both sidewalls", ***Nucl. Eng. Des.***, 265: 938-948 (2013).

57. Sezgin, M.T., Bozkaya, C., and Turk, O, "BEM and FEM based numerical simulations for biomagnetic fluid flow", ***Eng. Anal. Bound. Elem.***, 37: 1127-1135 (2013).

58. Prasad, K.V., Datti, P.S., and Vajravelu, K., "MHD mixed convection flow over a permeable non-isothermal wedge", ***J. King Saud Univ. Sci.***, 25:313-324 (2013).

59. Nadeem, S., Haq, R.U., Akbar, N.S., and Khan, Z.H., "MHD three-dimensional Casson fluid flow past a porous linearly stretching sheet", ***Alexandria Eng. J.***, 52: 577-582 (2013).

60. Ibrahim, W., and Shankar, B., "MHD boundary layer flow and heat transfer of a nanofluid past a permeable stretching sheet with velocity, thermal and solutal slip boundary conditions", ***Comput. Fluids***, 1-10 (2013).

61. Hayat, T., Shafiq, A., Alsaedi, A., and Awais M., "MHD axisymmetric flow of third grade fluid between stretching sheets with heat transfer", ***Comput. Fluids***, 86: 103-108 (2013).

62. Ellahi, R., "The effects of MHD and temperature dependent viscosity on the flow of non-Newtonian nanofluid in a pipe: Analytical solutions", ***Appl. Math. Model.***, 37: 1451-1467 (2013).

63. Gururaj, A.D.M., and Pavithra, C., "Nonlinear MHD boundary layer flow of a liquid metal with heat transfer over a porous stretching surface with nonlinear radiation effects", ***Adv. Appl. Sci. Res.***, 4(2): 77-92 (2013).

64. Sahoo, S.N., "Heat and mass transfer effect on MHD flow of a viscoelastic fluid through a porous medium bounded by an oscillating porous plate in slip flow regime", ***Int. Jo. Chem. Eng.***, 2013: 1-8 (2013).

65. Salehi, E, Alizadeh, R., and Darvish, A., "Laminar MHD mixed convection flow of newtonian fluid between vertical parallel plates channel", ***Proc. 2013 Int. Conf. Mech. Fl. Heat Elasticity Electromagnet Field***, Venice, 21-23 (2013).

66. Jafar, K., Nazar, R., Ishak, A., and Pop, I., "MHD boundary layer flow due to a moving wedge in a parallel stream with the induced magnetic field", ***Bound. Value Probl.***, 20: 1-14 (2013).

67. Alammar, K., Vilagines, R., Shariff, M., Kaneesamkandi, Z., and Abdullah, S., "Simulation of fully-developed average turbulent MHD pipe flow with heat transfer", ***Fluid Heat Trans.***, 7: 2619-2622 (2012).

68. Ashraf, M., and Rashid, M., "MHD boundary layer stagnation point flow and heat transfer of a micropolar fluid towards a heated shrinking sheet with radiation and heat generation", ***World Appl. Sci. J.***, 16(10): 1338-1351 (2012).

69. Attia, H.A., and Abdeen, M.A.M., "Unsteady MHD flow and heat transfer between parallel porous plates with exponential decaying pressure gradient", ***Kragujevac J. Sci.***, 34: 15-22 (2012).

70. Gedik, E., Kurt, H., Recebli, Z., and Balan, C., "Two-dimensional CFD simulation of magneto rheological fluid between two fixed parallel plates applied external magnetic field", ***Comput. Fluids***, 63: 128-134 (2012).

71. Lakshmi, M.P., Reddy, N.B., and Poornima, T., "MHD boundary layer flow of heat and mass transfer over a moving vertical plate in a porous medium with suction and viscous dissipation", ***Int. J. Eng. Res. Appl.***, 2(5): 149-159 (2012).

72. Li, Y., and Tian, Z.F., "An exponential compact difference scheme for solving 2D steady magnetohydrodynamic (MHD) duct flow problems", ***J. Comput. Phys.***, 231(16), 5443-5468 (2012).

73. Makinde, O.D., "Computational modelling of mhd unsteady flow and heat transfer toward a flat plate with Navier slip and Newtonian heating", ***Braz. J. Chem. Eng.***, 29(1): 159-166 (2012).

74. Rushikumar, B., and Gangadhar, K., "MHD free convection flow between two parallel porous walls with varying temperature", ***Int. J. Eng.***, 3: 67-72, (2012).

75. Ibrahim, W., and Shanker, B., "Unsteady MHD boundary-layer flow and heat transfer due to stretching sheet in the presence of heat source or sink", ***Comput. Fluids***, 70: 21-28 (2012).

76. Abbassi, H., "Numerical analyses of the effect of Lorentz force on electrically conducting fluid flow around an obstacle", ***Progr. Comput. Fluid Dynam. Int. J.***, 12(6): 427-432 (2012).

77. Dey, P.K., and Zikanov, O., "Turbulence and transport of passive scalar in magnetohydrodynamic channel flows with different orientations of magnetic field", ***Int. J. Heat Fluid Fl.***, 36: 101-117 (2012).

78. Miyazaki, K., Inoue, H., Kimoto, T., Yamashita, S., Inoue, S., and Yamaoka, N., "Heat transfer and temperature fluctuation of lithium flowing under transverse magnetic field", ***J. Nucl. Sci. Technol.***, 23: 582-593 (1986).

79. Aminossadati S.M., Raisi A., and Ghasemi B. "Effects of magnetic field on nanofluid forced convection in a partially heated microchannel", ***Int. J. Nonlin. Mech.***, 46(10): 1373 - 1382 (2011).

80. Aydin, O., and Kaya, A., "MHD mixed convection from a vertical slender cylinder", ***Commun. Nonlinear Sci.***, 16(4), 1863-1873 (2011).

81. Chamka, A.J., and Ahmed, S.E., "Unsteady MHD heat and mass transfer by mixed convection flow in the forward stagnation region of a rotating sphere in the presence of chemical reaction and heat source", ***Proceedings of the World Congress on Engineering***, London, 133-138 (2011).

82. Hayat, T., Awais, M., Qasim, M., and Hendi, A.A., "Effects of mass transfer on the stagnation point flow of an upper-convected Maxwell (UCM) fluid", ***Int. J. Heat Mass Tran.***, 54(15-16): 3777-3782 (2011).

83. Ishak, A., Nazar, R., Arifin, N.M., Ali, F.M., and Pop, I., "MHD stagnation-point flow towards a stretching sheet with prescribed surface heat flux", ***Sains Malays.***, 40(10): 1193-1199 (2011).

84. Yacob, N.A., and Ishak, A., "MHD flow of a micropolar fluid towards a vertical permeable plate with prescribed surface heat flux", ***Chem. Eng. Res. Des.***, 89: 2291-2297 (2011).

85. Kaya A., "The effect of conjugate heat transfer on MHD mixed convection about a vertical slender hollow cylinder", ***Commun. Nonlinear Sci.***, 16(4): 1905–1916, (2011).

86. Makinde, O.D., and Chinyoka, T., "Numerical study of unsteady hydromagnetic Generalized Couette flow of a reactive third-grade fluid with asymmetric convective cooling", ***Comput. Math. Appl.***, 61(4): 1167-1179 (2011).

87. Makinde, O.D., and Onyejekwe, O.O., "A numerical study of MHD generalized Couette flow and heat transfer with variable viscosity and electrical conductivity", ***J. Magn. Magn. Mater.***, 323(22): 2757-2763 (2011).

88. Rao, J.S., and Sankar, H., "Numerical simulation of MHD effects on convective heat transfer characteristics of flow of liquid metal in annular tube", ***Fusion Eng. Des.***, 86(2-3): 183-191 (2011).

89. Yazdi, M.H., Abdullah, S., Hashim, I., and Sopian, K., "Effects of viscous dissipation on the slip MHD flow and heat transfer past a permeable surface with convective boundary conditions", ***Energies***, 4(12): 2273-2294 (2011).

90. Hussam, W.K., Thompson, M.C., and Sheard, G.J., "Dynamics and heat transfer in a quasi-two-dimensional MHD flow past a circular cylinder in a duct at high Hartmann number", ***Int. J. Heat Mass Tran.***, 54: 1091-1100 (2011).

91. Malekzadeh, A., Heydarinasab, A., and Jahangiri, M., "Magnetic field effect on laminar heat transfer in a pipe for thermal entry region", ***J. Mech. Sci. Technol.***, 25(4): 877-884 (2011).

92. Yamamoto, Y., and Kunugi, T., "Developments in Heat Transfer 1st ed.", ***Intech***, Rijeka, 637-648 (2011).

93. Yomamoto, Y., and Kunugi, T., "Direct Numerical Simulation of MHD Turbulent Flows with High-Pr Heat Transfer", ***Prog. Nucl. Sci. Tech.***, 2: 550-555 (2011).

94. Malekzadeh, A., Heydarinasab, A., and Dabir, B., "Magnetic field effect on fluid flow characteristics in a pipe for laminar flow", ***J. Mech. Sci. Technol.***, 25(2): 333-339 (2011).

95. Murakami, T., and Okuno, Y., “Experiment and simulation of MHD power generation using convexly divergent channel”, ***42nd AIAA Plasmadynamics Lasers Conf.***, Honolulu, 1-7 (2011).

96. Ahmed, S., and Batin, A., “Analytical model of MHD mixed convective radiating fluid with viscous dissipative heat”, ***Int. J. Eng. Sci. Technol.***, 2(9): 4902-4911 (2010).

97. Ellahi, R., Hayat, T., Mahomed, F.M., and Zeeshan, A., “Analytic solutions for MHD flow in an annulus”, ***Commun. Nonlinear Sci. Numer. Simul.***, 15(5): 1224-1227 (2010).

98. Gavili, A., Lajvardi, M., and Sabbaghzadeh, J., “The effect of magnetic field gradient on ferro fluids heat transfer in a two-dimensional enclosure”, ***J. Comput. Theor. Nanos.***, 7(8): 1425-1435 (2010).

99. Hayat, T., Sajjad, R., and Asghar S., “Series solution for MHD channel flow of a Jeffery fluid”, ***Commun. Nonlinear Sci. Numer. Simul.***, 15(9): 2400-2406 (2010).

100. Hayat, T., Abbas, Z., Pop, I., and Asghar, S., “Effects of radiation and magnetic field on the mixed convection stagnation-point flow over a vertical stretching sheet in a porous medium”, ***Int. J. Heat Mass Tran.***, 53(1-3): 466-474 (2010).

101. Huang, H., and Li, B., “Heat transfer enhancement of MHD flow by conducting strips on the insulating wall”, ***J. Heat Transf.***, 133(2): 89-94 (2010).

102. Loganathan, P., Ganesan, P., and Iranian, D., “Effects of thermal conductivity on unsteady MHD free convective flow over a semi-infinite vertical plate”, ***Int. J. Eng. Sci. Techol.***, 2(11): 6257-6268 (2010).

103. Makinde, O.D., "Similarity solution of hydro magnetic heat and mass transfer over a vertical plate with a convective surface boundary condition", ***Int. J. Phys. Sci.***, 5(6): 700-710 (2010).

104. Mohebujjaman, M., Khaleque, T.S., and Samad, M.A., "MHD heat transfer mixed convection flow along a vertical stretching sheet in presence of magnetic field with heat generation", ***Int. J. Basic Appl. Sci.***, 10(2): 71-80 (2010).

105. Motozawa, M., Chang, J., Sawada, T., and Kawaguchi, Y., "Effect of magnetic field on heat transfer in rectangular duct flow of a magnetic fluid", ***Phys Procedia***, 9: 190-193 (2010).

106. Kumari, M., Pop, I., and Nath, G., "Transient MHD stagnation flow of a non-Newtonian fluid due to impulsive motion from rest", ***Int. J. Nonlin. Mech.***, 45: 463-473 (2010).

107. Muzychka, Y.S., Walsh, E., and Walsh, P., "Simple models for laminar thermally developing slug flow in noncircular ducts and channels", ***J. Heat Transf.***, 132(11): 38-48 (2010).

108. Zueco, J., Eguia, P., Granada, E., Miguez, J.L., and Beg, O.A., "An electrical network for the numerical solution of transient MHD Couette flow of a dusty fluid: Effects of variable properties and hall current", ***Int. Commun. Heat Mass***, 37: 1432-1439 (2010).

109. Zijovin, S.M., Nikodijevic, D.D., Blagojevic, B.D., and Savic, S.R., "MHD flow and heat transfer of two immiscible fluids between moving plates", ***T. Can. Soc. Mech. Eng.***, 34(3-4): 351-372 (2010).

110. Chaudhary R., Vanka S.P., and Thomas, B.G., "Direct numerical simulations of magnetic field effects on turbulent flow in a square duct", ***Cont. Cast. Rep.***, Urbana, USA, June 7, 2010.

111. Mahmoud, M., and Shimaa, W., “Effects of slip and heat generation/absorption on MHD mixed convection flow of a micropolar fluid over a heated stretching surface”, ***Math. Prob. Eng.***, 2010: 1-20 (2010).

112. Abbasbandy, S., and Hayat, T., “Solution of the MHD Falkner-Skan flow by homotopy analysis method”, ***Commun. Nonlinear Sci.***, 14(9-10): 3591-3598 (2009).

113. Abelman, S., Momoniata, E., and Hayat, T., “Steady MHD flow of a third grade fluid in a rotating frame and porous space”, Nonlinear Anal-Real, 10(6): 3322-3328 (2009).

114. Atik, K., and Recebli, Z., “A numerical examination of the effects of magnetic and electric fields on convection heat transfer”, ***JEA***, 14(1): 1-10 (2009).

115. Dehghan M., and Mirzaei D. “Meshless local boundary integral equation (LBIE) method for the unsteady magneto hydrodynamic (MHD) flow in rectangular and circular pipes”, ***Comput. Phys. Commun.***, 180(9): 1458–1466 (2009).

116. Grigoriadis, D.E.G., Kassinos, S.C., and Votyakov, E.V., “Immersed boundary method for the MHD flows of liquid metals”, ***J. Comput. Phys.***, 228(3): 903-920 (2009).

117. Samad, M.A., and Mohebujjaman, M., “MHD heat and mass transfer free convection flow along a vertical stretching sheet in presence of magnetic field with heat generation”, ***Res. J. Appl. Sci. Eng. Technol.***, 1(3): 98-106 (2009).

118. Srinivas S, Gayathri R, and Kothandapani M., “The influence of slip conditions wall properties and heat transfer on MHD peristaltic transport” ***Comput. Phys. Commun.***, 180(11): 2115–2122 (2009).

119. Khedr, M.E.M., Chamka, A.J., and Bayomi, M., "MHD flow of a micropolar fluid past a stretched permeable surface with heat generation or absorption", ***Nonlin. Anal. Model. Cont.***, 14(1): 27-40 (2009).

120. Hayat, T., Abbas, Z., and Ali, N., "MHD flow and mass transfer of a upper-convected Maxwell fluid past a porous shrinking sheet with chemical reaction species" ***Phys. Lett. A***, 372(26): 4698-4704 (2008).

121. Hayat, T., Saif, S., and Abbas, Z., "The influence of heat transfer in an MHD second grade fluid film over an unsteady stretching sheet", ***Phys. Lett. A***, 372(30): 5037-5045 (2008).

122. Misra, J.C., Shit, G.C., and Rath, H.J., "Flow and heat transfer of a MHD viscoelastic fluid in a channel with stretching walls: some applications to haemodynamics", ***Comput. Fluids***, 37(1): 1-11 (2008).

123. Rahman, M.M., Mamun, A.A., Azim, M.A., and Alim, M.A., "Effects of temperature dependent thermal conductivity on magnetohydrodynamic (MHD) free convection flow along a vertical flat plate with heat conduction", ***Nonlinear Anal. Model. Control,*** 13(4): 513–524, (2008).

124. Recebli, Z., Atik, K., and Sekmen, P., "A numerical examination of the effects of magnetic and electric fields on convection heat transfer with variable physical property fluid", ***PAJES***, 14(1): 41-47 (2008).

125. Ishak, A., Nazar, R., and Pop, I., "Magnetohydrodynamic (MHD) flow and heat transfer due to a stretching cylinder", ***Energ. Convers. Manage.***, 49: 3265-3269 (2008).

126. Khan, M., Ali, S.H., Hayat, T., and Fetecau, C., "MHD flows of a second grade fluid between two side walls perpendicular to a plate through a porous medium", ***Int. J. Nonlin. Mech.***, 43: 302-319 (2008).

127. Yamamoto, Y., Kunugi, T., Satake, S., and Smolentsev, S., "DNS and k–ε model simulation of MHD turbulent channel flows with heat transfer", ***Fusion Eng. Des.***, 83: 1309-1312 (2008).

128. Takeuchi, J., Satake, S., Morley, N.B., Kunugi, T., Yokomine, T., and Abdou, M.A., "Experimental study of MHD effects on turbulent flow of Flibe simulant fluid in circular pipe", ***Fusion Eng. Des.***, 83: 1082-1086 (2008).

129. Abbasi, H., and Nassrallah, S.B., "MHD flow and heat transfer in a backward-facing step", ***Int. Commun. Heat Mass***, 34(2): 231-237 (2007).

130. Sajid, M., Hayat, T., and Asghar, S., "Non-similar analytic solution for MHD flow and heat transfer in a third-order fluid over a stretching sheet", ***Int. J. Heat Mass Tran.***, 50(9-10): 1723-1736 (2007).

131. Boeck, T., Krasnov, D., and Zienicke, E., "Numerical study of turbulent magnetohydrodynamic channel flow", ***J. Fluid Mech.***, 572: 179-188 (2007).

132. Satake, M., Yuki, K., Chiba, S., and Hashizume, H., "Numerical analysis of MHD flow structure behind a square rod", ***Fusion Eng. Des.***, 81: 525-532 (2006).

133. Yokomine, T., Takeuchi, J., Nakaharai, H., Satake, S., Kunugi, T., Morley, N.B., Abdou, M.A., "Zikanov, O., and Thess, A., "Experimental investigation of turbulent heat transfer of high Prandtl number fluid flow under strong magnetic field", ***Fusion Sci. Technol.***, 52: 625-629 (2007).

134. Huang, H., and Fang Y., "MHD effect on heat transfer in liquid metal free surface flow around a cylinder", ***Eng. Appl. Comp. Fluid Mech.***, 1(2): 88-95 (2007).

135. Jalil, J.M., and Al-Tae'y, K.A., "MHD turbulent natural convection in a liquid metal filed square enclosure", ***Emirates J. Eng. Res.***, 12(2): 31-40 (2007).

136. Nakaharai, H., Takeuchi, J., Yokomine, T., Kunugi, T., Satake, S., Morley, N.B., and Abdou, M.A., "The influence of a magnetic field on turbulent heat transfer of a high Prandtl number fluid", EXP. ***Therm. Fluid Sci.***, 32: 23-28 (2007).

137. Jordan, J.Z., "Network simulation method applied to radiation and viscous dissipation effects on MHD unsteady free convection over vertical porous plate", ***Appl. Math. Model.***, 31: 2019-2033 (2007).

138. Guo-yan, Z., Yan, P., Ling-zhi, Z., Ran, L., and Ci-wen, S., "Analytical study on flow process of floating-oil recovery device from oil-contaminated seawater by MHD method", ***J. Hydrodyn.***, 19: 195-200 (2007).

139. Jalil, J.M., Murtadha, T.K., and Altae'y, K.A., "Three-dimensional computation of turbulent natural convection in the presence of magnetic field", ***J. Indian Inst. Sci.***, 86: 705-721 (2006).

140. Nishihara, M., "Low-temperature supersonic flow control using repetitively pulsed MHD force", PhD Thesis, ***Graduate School of the Ohio State University***, Ohio, 110-112 (2006).

141. Kobayashi, H., "Large eddy simulation of magnetohydrodynamic turbulent channel flows with local subgrid-scale model based on coherent structures", ***Phys. Fluids***, 18(4): http://dx.doi.org/10.1063/1.2194967 (2006).

142. Racabovadiloglu, Z., and Atik, K., "A numeric solution to the effect of magnetic field on heat convection", ***KSU J. Eng. Sci.***, 8(2): 43-47 (2005).

143. Zniber, K., Oubarra, A., and Lahjomri, J., "Analytical solution to the problem of heat transfer in an MHD flow inside a channel with prescribed sinusoidal wall heat flux", ***Energ. Convers. Manage.***, 46(7-8): 1147-1163 (2005).

144. Attia, H.A., and Ahmed, M.E.S., "Circular Pipe MHD Flow of a Dusty Bingham Fluid", ***Tamkang J Sci. Eng.***, 8(4): 257-265 (2005).

145. Andreev, O., Kolesnikov, Y., and Thess, A., "MHD-channel flow of liquid metal under inhomogeneous magnetic field – part 1: experiment", ***Joint 15th Riga 6th Pamir Int. Conf. Fund. Appl. MHD***, Rigas Jurmala, 185-190 (2005).

146. Pang, J., and Choi, K.S., "Turbulent drag reduction by Lorentz force oscillation", ***Phys. Fluids***, 16(5): http://dx.doi.org/10.1063/1.1689711 (2004).

147. Ganesan, P., and Palani, G., "Finite difference analysis of unsteady natural convection MHD flow past an inclined plate with variable surface heat and mass flux", ***Int. J. Heat Mass Tran.***, 47: 4449-4457 (2004).

148. Postelnicu, A., Influence of a magnetic field on heat and mass transfer by natural convection from vertical surfaces in porous media considering Soret and Dufour effects, ***Int. J. Heat Mass Tran***., vol. 47, pp. 1467-1472, (2004).

149. Chamkha, A.J., Mujtaba, M., Quadri, A., and Issa, C., "Thermal radiation effects on MHD forced convection flow adjacent to a non-isothermal wedge in the presence of a heat source or sink", ***Heat Mass Transfer***, 39(4): 305–312, (2003).

150. Lahjomri, J., Zniber, K., Oubarra, A., and Alemany, A., "Heat transfer by laminar Hartmann's flow in thermal entrance region with uniform wall heat flux: the Graetz problem extended", ***Energ. Convers. Manage.***, 44(1): 11-34 (2003).

151. Ke, Y., Wang, H.Y., and Wu, Y.C., "MHD simulation of the liquid metal/helium gas dual-cooled waste transmutation blanket for FDS", ***Fusion Eng. Des.***, 69: 431-435 (2003).

152. Uda, N., Yamaoka, N., Horiike, H., and Miyazaki, K., "Heat transfer enhancement in lithium annular flow under transverse magnetic field", ***Energ. Convers. Manage.***, 43(3): 441-447 (2002).

153. Smolentsev, S., Abdou, M., Morley, N., Ying, A., and Kunugi, T., "Application of the ''K–e'' model to open channel flows in a magnetic field", ***Int. J. Eng. Sci.***, 40: 693-711 (2002).

154. Lahjomri, J., Oubarra, A., and Alemany, A., "Heat transfer by laminar Hartmann flow in thermal entrance region with a step change in wall temperatures: the Graetz problem extended", ***Int. J. Heat Mass Tran.***, 45: 1127-1148 (2002).

155. Lee, D., and Choi, H., "Magnetohydrodynamic turbulent flow in channel at low magnetic Reynolds number", ***J. Fluid Mech.***, 439: 367-394 (2001).

156. Umeda N., and Takahashi, M., "Numerical analysis for heat transfer enhancement of a lithium flow under a transverse magnetic field", ***Fusion Eng. Des.***, 51–52, 899 – 907 (2000).

157. Yih, K.A., "MHD forced convection flow adjacent to a non-isothermal wedge", ***Int. Commun. Heat Mass***, 26(6): 819-827, (1999).

158. Takahashi, M., Aritomi, M., Inoue, A., and Matsuzaki, M., "MHD pressure drop and heat transfer of lithium single-phase flow in a rectangular channel under transverse magnetic field", Fusion Engineering and Design 42(1-4), 365-372 (1998).

159. Yovanovich, M.M., and Muzychka, Y.S., "Modeling Nusselt numbers for thermally developing laminar flow in non-circular ducts", ***7th AIAA/ASME Jnt Thermophys Heat Transfer Conf.***, Albuquerque, 1-12 (1998).

160. Zikanov, O., and Thess, A., "Direct numerical simulation of forced MHD turbulence at low magnetic Reynolds number", ***J. Fluid Mech.***, 358: 299-333 (1998).

161. Cuevas, S., Picologlou, B.F., Walker, J.S., Talmage, G., and Hua, T.Q., " Heat transfer in laminar and turbulent liquid-metal MHD flows in square ducts with thin conducting or insulating walls", ***Int. J. Eng. Sci.***, 35(5): 505-514 (1997).

162. Ji, H.C., and Gardner, R.A., "Numerical analysis of turbulent pipe flow in a transverse magnetic field", ***Int. J. Heat Mass Tran.***, 40(8): 1839-1851 (1997).

163. Hua, T.Q., and Walker, J.S., "MHD flow in rectangular ducts with inclined non-uniform transverse magnetic field", ***Fusion Eng. Des.***, 27: 703-710 (1995).

164. Kirillov, I.R., Reed, C.B., Barleon, L., and Miyazaki, K., "Present understanding of MHD and heat transfer phenomena for liquid metal blankets", ***Fusion Eng. Des.***, 27: 553-569 (1995).

165. Branover, H., Eidelman, A., and Nagorny, M., "Use of turbulence modification for heat transfer enhancement in liquid metal blankets", ***Fusion Eng. Des.***, 27: 719-724 (1995).

166. Branover, H., and Unger, Y., "Progress in Turbulence Research Vol. 162", Seebass, A.R., ***Amer Inst of Aeronautics***, Reston, 21-102 (1994).

167. Takase, K., and Hasan, M.Z., "Heat transfer in MHD laminar flow through a rectangular channel in the plasma facing components of fusion reactors", ***Fusion Eng.***, 2: 1206-1209, (1993).

168. Lee, S., Yovanovich, M.M., and Jafarpur, K., "Effects of geometry and orientation on laminar natural convection from isothermal bodies", ***J. Thermophys***, 5(2): 208-216 (1991).

169. Kumari, M., Takhar, H.S., and Nath, G., "MHD flow and heat transfer over a stretching surface with prescribed wall temperature or heat flux", ***Heat Mass Transfer***, 25(6): 331-336 (1990).

170. Sukoriansky, S., Klaiman, D., and Branover, H., "MHD enhancement of heat transfer and its relevance to fusion reactor blanket design", ***Fusion Eng. Des.***, 8: 277-282 (1989).

171. Soundalgekar, V.M., and Takhar, H.S., "On MHD flow and heat transfer over a semi-infinite plate under transverse magnetic field", ***Nucl. Eng. Des.***, 42(2): 233-236 (1977).

172. Gardner, R.A., and Lykoudis, P.S., "Magneto-fluid-mechanic pipe flow in a transverse magnetic field part 2, Heat transfer", ***J. Fluid Mech.***, 48(1): 129-141 (1971).

173. Hwang, U.P., Fan, L.T., and Hwang, C.L., "Compressible laminar MHD flow inside a flat duct with heat transfer", ***AIAA J.***, 5(12): 2113-2121 (1967).

174. Vinchurkar, S., and Longest, P.W., "Evaluation of hexahedral, prismatic and hybrid mesh styles for simulating respiratory aerosol dynamics", ***Comput. Fluids***, 37(3): 317-331 (2008).

175. Biswas, R., and Strawn, R.C., "Tetrahedral and hexahedral mesh adaptation for CFD problems", ***Appl. Numer. Math.***, 26(1-2): 135-151 (1998).

176. Williams, R.K., Coleman, G.L., and Yarbrough, D.W., "An evaluation of some thermodynamic and transport properties of solid and liquid lithium over the temperature range 200-1700 K", ***ORNL Report***, ***Tennessee***, 1-31 (1988).

177. Davison, H.W., “Compilation of thermo physical properties of liquid lithium”, ***NASA Report***, ***Washington***, 1-21 (1968).

AUTOBIOGRAPHY

Selcuk SELIMLI was born in Kayseri, 1986. He graduated from Kocasinan Foreign Language High School in 2005. Then, continued his study in Gaziantep University Mechanical Engineering Department until graduation in 2010. Since 2011, he has been a research assistant at Energy Systems Engineering Department, Karabuk University. He hold a Master's degree in Energy Systems Engineering by the approval of the thesis is entitled as ‘‘*Recuperator design for industrial reheating furnace*’’ in June 2012. He has been graduated for the degree of Doctor of Philosophy in Mechanical Engineering by the approval of the dissertation is entitled as "*Computational hydrodynamic and heat transfer analysis of magnetohydrodynamic internal flow*".

ADRESS INFORMATION

Address : 100. Yıl Mah. Teknoloji Fakultesi
Enerji Sistemleri Mühendisligi Karabuk Universitesi

Phone : (370) 433 8210

Fax : (370) 433 8204

E-mail : selcukselimli@karabuk.edu.tr